

# REVIEWS OF MODERN PHYSICS

VOLUME 40, NUMBER 3

JULY 1968

## Spectral Distribution of Atomic Oscillator Strengths\*

U. FANO†

*Department of Physics, University of Chicago, Chicago, Illinois*

J. W. COOPER

*National Bureau of Standards, Washington, D.C.*

Information on the spectrum of oscillator strength for neutral atoms in their ground states is surveyed with particular regard to recent progress in the far uv-soft x-ray range and to the theoretical interpretation of data from experiments and from numerical calculations. The analysis brings out numerous aspects of atomic mechanics and problems that remain unsolved. An effort is made to interconnect different theoretical approaches within the framework of the theory of atomic spectra.

### CONTENTS

1. Introduction . . . . .	441	5.4. Consistency of Approximate Oscillator Strengths . . . . .	478
2. Properties of the Oscillator Strength . . . . .	443	5.5. Survey of Existing Calculations . . . . .	479
2.1. Polarizability of Atoms . . . . .	444	6. Effect of Intrachannel Interaction upon the Resonance	
2.2. Dielectric and Optical Constants: Photoabsorption		near Threshold . . . . .	481
Cross Section . . . . .	445	6.1. The Influence of Excitation Transfer . . . . .	481
2.3. Time Correlations . . . . .	446	6.2. Direct Calculations . . . . .	483
2.4. Spectral Distribution and Its Moments . . . . .	446	6.3. Plasma-type Treatment . . . . .	486
2.5. Sum Rules: Optical and Related Constants . . . . .	449	7. Core Relaxation and Double Excitations . . . . .	488
2.6. Role of Polarizability in the Collisions of Fast		7.1. The "Sudden" Approximation . . . . .	488
Charged Particles . . . . .	451	7.2. Summary of Experimental Evidence on Double	
3. Experimental Aspects . . . . .	452	Transitions . . . . .	491
3.1. Spectral Line Sources . . . . .	453	8. Effects of Interchannel Interactions . . . . .	493
3.2. Sources with Continuous Spectrum . . . . .	453	8.1. Profile of Lines Broadened by Autoionization . . . . .	493
3.3. Absorption Spectroscopy . . . . .	453	8.2. Gross Effects of Spectral Repulsion . . . . .	496
3.4. Detectors . . . . .	454	8.3. Strong Coupling . . . . .	498
3.5. Subsidiary Experiments . . . . .	454	8.4. Radial Correlations in the Ground State . . . . .	499
4. Experimental Data and Independent-Electron Calculations . . . . .	455	8.5. The Random Phase Approximation . . . . .	500
4.1. Survey of Experimental Evidence . . . . .	455	9. Unsolved Problems . . . . .	503
4.2. Single-Electron Model . . . . .	460		
4.3. Hydrogenic Calculations . . . . .	461		
4.4. Average Electric Field and Centrifugal Repulsion . .	463		
4.5. Resonance near Threshold . . . . .	465		
4.6. Nonresonant Absorption . . . . .	468		
4.7. Depression and Apparent Shift of Absorption Edges .	469		
4.8. Variation of Spectra Along the Periodic System . . .	470		
4.9. Sum Rules for the Single-Electron Model . . . . .	472		
5. Many-Body Formulation . . . . .	473		
5.1. Slater-Determinant Wave Functions . . . . .	473		
5.2. Sum Rules in the Many-Body Formulation . . . . .	474		
5.3. Successive Approximation Procedure . . . . .	476		

\* This work was reported in part as an invited paper by J. W. Cooper at the 1965 American Physical Society Meeting in Washington, D.C. It formed the basis of a course in Atomic Physics at the University of Chicago in the Winter Quarter of 1967 and of a brief published note (Fa66).

† Consultant and formerly Senior Research Fellow at the National Bureau of Standards. Supported in part by U. S. Atomic Energy Commission Contract COO-1674-11.

### 1. INTRODUCTION

The absorption coefficient of electromagnetic radiation in the continuous spectrum of atoms (and molecules) characterizes the radiation penetration and its action upon matter. For sufficiently low radiation frequencies, this coefficient is proportional to the spectral density of oscillator strength for the relevant atom at the relevant frequency; the oscillator strength is a dynamical parameter which bears on numerous phenomena as outlined in Sec. 2. The restriction to "low" radiation frequencies, assumed throughout this article, implies that the wavelength is much larger than the atomic structure responsible for the absorption, and that accordingly the photon momentum and the attendant Compton scattering are negligible. These conditions obtain for photon energies below a few keV in the

lightest elements and below 50 keV in most atoms. They also ensure that relativity effects are unimportant.

In the x-ray range of the spectrum, say, above 1- to 10-keV photon energy or below 1- to 10-Å wavelength, basic studies of the absorption coefficient have been carried out in the early days of atomic physics and are being refined steadily (see, e.g., WG57, McG59, HB66, SP67). These studies show that x-ray absorption proceeds, in the main, in accordance with a hydrogen-like model because it stems from inner shell electrons. Each of these electrons is influenced primarily by the Coulomb field of the nucleus; furthermore, its repulsion by the other electrons can be represented fairly adequately by "inner" and "outer" screening corrections to the nuclear field which do not change its Coulomb character. The contribution of inner electrons to photoionization is also more easily measured than that of outer electrons; being affected weakly by the state of aggregation of matter, it need not be observed in the state of atomic vapor.

The electrons of each shell (or, rather, subshell) of an atom contribute directly to its photoionization only when the photon energy exceeds the threshold for ionization of that subshell. According to the hydrogen-like approximation, this contribution *decreases monotonically* from the threshold up, as the photon energy increases. Thereby the plots of absorption coefficient versus photon energy acquire a familiar saw-tooth shape, each "tooth" representing the contribution of the electrons from one inner subshell. (The steep edge of a tooth corresponds to the absorption threshold, the gentler slope to the monotonic decrease toward higher photon energies.) Each absorption edge is complicated by a fine structure due to indirect photoionization, that is, to excitation of an inner electron to a discrete outer level, followed by Auger effect. However, this structure can readily be accounted for (see, e.g., Ba59a, Wa65) as long as the hydrogen-like approximation is applicable.

At lower photon energies, the hydrogen-like model of photoionization breaks down progressively (except for the H atom itself, of course) for the following reasons. First, the net average field due to nuclear and electronic charges departs sharply from the Coulomb law in the outer portion of atoms which is the primary seat for the absorption of lower-energy photons. Second, departures from the independent electron approximation, such as exchange effects and two-electron jumps, are no longer negligible in the outer regions as compared to the effects of a central potential. These various departures have in fact proved responsible for conspicuous phenomena.

As late as 1960, evidence on photoionization in the energy range from 1000 eV to the proximity of the lowest threshold was quite fragmentary and provided no picture of the relevant physical circumstances. Tentative tabulations of absorption coefficients were based on extrapolation of the hydrogen-like approxima-

tion (Vi48, Le53a) which turned out to be inadequate. Sources of radiation and other techniques adequate for systematic experimental studies in this range had not been developed.

Rapid progress has now been achieved, as atomic physics started again pushing in new directions, partly in response to needs of space and plasma physics. Even though the results of this work are in many respects preliminary or incomplete, they provide an initial description and interpretation of atomic properties in the energy range from the lowest ionization threshold to the point where the hydrogen-like approximation becomes a dependable guide.

A survey of this recent work has been undertaken to present available information from a single point of view. In the course of this survey opportunities arose to extend the theoretical analysis and interpretation of data and to develop formalisms that connect different theoretical approaches. This effort also pointed up unsolved questions that seem suitable for investigation in the next several years. The material thus accumulated constitutes the present report.

Some remarks may be made at the outset on the context of our subject. Whereas the measurement of photoabsorption coefficients constitutes a direct measurement of oscillator strengths, important evidence on these strengths is also provided by other studies; the combined evidence will be considered here. Much of the experimentation on photoabsorption has aimed at observing features characteristic of solid-state structure or properties of atmospheric gases, rather than at studying single atoms *per se*. Our emphasis will be on *single neutral atoms*. Therefore, data obtained on solids and on molecular gases will have to be examined for relevance to their constituent atoms; conversely, improved knowledge of the behavior of isolated atoms should provide a firmer basis for identifying the influence of the state of aggregation on the observable properties of matter.

This article has the primary purpose of describing the gross features of the oscillator strength spectrum for atoms throughout the periodic system, the extent and the sources of our data on this subject, and their interpretation in terms of atomic mechanics. Emphasis will be placed on the newly explored range of the spectrum. Since the continuous spectrum includes the bulk of the oscillator strength, except for H, the discrete spectrum will usually be regarded as an appendage of the continuum regardless of its practical importance.

As a subsidiary task the article indicates connections between the oscillator strengths and other atomic properties. Some of these properties are of interest to other fields of physics and some pertain to the internal dynamics of atoms. The latter subject has been advancing rapidly just because the absorption of photons with energy above  $\sim 20$  eV and similar energy transfers in particle collisions have permitted the study of two-electron transitions and of other electron-interaction

processes which unfreeze an increased number of intraatomic degrees of freedom. The set of properties to be considered is in fact so broad that this article touches to some extent a substantial portion of atomic dynamics.

Section 2 reviews the connections of the oscillator strengths of atoms with electric, magnetic, and other properties of low-density monoatomic gases and with dynamical properties of each atom such as the time-dependent autocorrelation between electron positions and the mean kinetic energy of electrons. (The more complex relationships with properties of condensed matter are not considered.) Section 3 outlines the main experimental developments that have permitted extensive measurements of photoabsorption in new spectral ranges and indicates collateral experiments which bear on the mechanism of photoabsorption.

Section 4 describes and analyzes much of the experimental evidence in the context of an independent-electron model, in which the electrons of each shell are governed by a central but *non-Coulomb* force. The characteristics of this force, and especially its interplay with the centrifugal force, give rise to notable departures from hydrogen-like behavior. One of these is the occurrence of quasiresonances, which cause precipitous drops of absorption coefficients with increasing photon energy, followed by subsidiary low maxima. Another is a depression of absorption near the threshold for each subshell, an effect which increases with the orbital angular momentum.

Section 5 formulates the complete many-body calculation of oscillator strengths in a manner that incorporates an independent-electron calculation as an initial step and permits one to assess and take into account various possible improvements in succession. Each successive step would involve in effect the diagonalization of a submatrix of the infinite-dimensional energy matrix. However, this approach remains largely undeveloped. It may be contrasted with the straightforward method of obtaining for *each photon energy* a pair of "best" approximate wave functions for the initial and final state of the atom, usually by separate Hartree-Fock calculations; the straightforward method leads more rapidly at a fair approximation to any desired value of the oscillator strength but it does not keep in sight the consistency requirements over the whole spectrum or the influence of various physical mechanisms.

Section 6 deals with an effect of electron exchange forces which influences the spectrum considerably and has been evaluated primarily for Ar in the 15–35-eV range; it also describes plasma-type approaches to this effect. Section 7 deals with a side effect of photoabsorption by an electron, namely, with the readjustment of the other electrons in the atom including the possible excitation or ionization of a second electron.

Finally, Sec. 8 describes effects of channel interaction such as the line profiles attendant to autoionization and the spectral repulsion between channels with

different thresholds, which depresses absorption edges further and occasionally even inverts them. These effects generally have a minor influence on the gross distribution of oscillator strengths, but exceptions might occur. Data obtained from the observation of one interaction effect have a bearing on another one; e.g., the profile of an autoionization line provides an index of the spectral repulsion between channels. Our knowledge of this field is mostly quite tentative and spotty, yet its study appears very promising.

Two major works have appeared recently whose content has much in common with the present article but whose intent is largely complementary to ours. G. V. Marr's "Photoionization Processes in Gases" (Ma67b) is a textbook which describes theoretical and experimental information on the yield of these processes, primarily for lower photon energies. Biberman and Norman's review of "Continuous Spectra of Atomic Gases and Plasmas" (BN67) is concerned primarily with providing data relevant to plasma workers but contains also a thorough analysis of current theoretical methods of calculation. Previous surveys are referred to in these two works and will be mentioned in this article only where they are immediately relevant (see also Mu67).

Some remarks may be added on the connection of our subject with collision theory. If one regards the action of radiation as a photon-atom collision process, the whole treatment of radiation absorption and scattering reduces to an application of the general theory of scattering. The general formalism of scattering theory involves certain complexities because of the coupling of alternative final states, degenerate and near-degenerate in energy. In the case of radiation processes these complexities can be bypassed insofar as the photon-atom interaction is weak and therefore amenable to a more familiar perturbation treatment. However, the complexities arise anyhow in the treatment of the atom itself when it absorbs sufficient energy to open up alternative channels of photoionization or when its many-body properties become important. A formulation of radiation absorption and refractivity from the point of view of scattering theory has been presented recently by Shore (Sh67). Here we shall follow the ordinary theory of atomic spectra more closely and utilize collision theory only where necessary.

## 2. PROPERTIES OF THE OSCILLATOR STRENGTH<sup>1</sup>

The concept of oscillator strength stems from the late 19th century model of the electrical and optical behavior of matter. Electrons were supposed to lie at equilibrium positions within atoms and to react elastically to weak disturbances. Thus they would perform forced oscillations when exposed to electromagnetic radiation. The amplitude and phase of these oscillations

<sup>1</sup> This section may be complemented by Chap. 1 of (Le60).

would depend on the characteristic (angular) frequency of free oscillation of each electron  $\omega_s$ , on its (weak) damping constant  $\gamma_s$ , and on the radiation frequency  $\omega$  according to a simple law of mechanics.

Actually, electrons do not have fixed equilibrium positions within atoms but, rather, a statistical distribution of positions, indicated by  $|\psi|^2$ , which is fixed under equilibrium conditions but is distorted quasi-elastically by weak disturbances. This distribution can perform free oscillations with a spectrum of frequencies far more numerous than the number of electrons in an atom. Therefore to each spectral frequency  $\omega_s$  corresponds a portion of the integrated  $|\psi|^2$ , which is generally represented by an irrational number rather than by an integer and which is called the oscillator strength  $f_s$  of the atom at that frequency. To frequencies  $\omega_s$  of the continuous spectrum corresponds, more appropriately, a spectral density of oscillator strength,  $df/d\omega_s$ .

The classical model was not developed sufficiently to determine the spectral frequencies  $\omega_s$  and the corresponding numbers of electrons  $f_s$ . However, quantum mechanics defines the  $\omega_s$  and  $f_s$  in terms of the eigenvalues and eigenfunctions of the Schrödinger equation. Thus their calculation constitutes a well-defined mathematical task, but one that can only be accomplished approximately for many-electron atoms. The development of suitable approximations depends in practice on hints drawn from experimental evidence.

### 2.1. Polarizability of Atoms

In the classical model one may consider an electron that experiences a displacement  $z$  from its equilibrium position under the influence of an electric field  $E_0 \exp(-i\omega t)$  directed along  $z$ . If the electron is also subject to an elastic force  $-m\omega_s^2 z$  and to a frictional force  $-m\gamma_s dz/dt$ , its displacement is

$$z = (e/m)[E_0/(\omega_s^2 - \omega^2 - i\gamma_s\omega)] \exp(-i\omega t). \quad (2.1)$$

The polarizability of this electron, i.e., its dipole moment  $ez$  per unit field strength is

$$\alpha(\omega) = ez/E_0 \exp(-i\omega t) = (e^2/m)(\omega_s^2 - \omega^2 - i\gamma_s\omega)^{-1}. \quad (2.1a)$$

The concept of a complex field  $E_0 \exp(-i\omega t)$  is, of course, a mathematical artifice; one is actually interested in its real part  $E_0 \cos \omega t$  and in the displacement induced by it, which is the mean of (2.1) and of its complex conjugate. The complex character of  $\alpha(\omega)$  serves to represent by a single number the phase lag and the magnitude of the displacement  $z$  with respect to the field oscillation. One can then write

$$ez = \frac{1}{2}[\alpha(\omega) E_0 \exp(-i\omega t) + \alpha^*(\omega) E_0 \exp(i\omega t)], \quad (2.1b)$$

with  $\alpha$  given by (2.1a) and  $\alpha^*$  its complex conjugate. This formula is better suited to quantum-mechanical interpretation.

A dilute gas, containing  $\mathfrak{N}$  atoms per unit volume and  $f_s$  oscillators of frequency  $\omega_s$  per atom, has the susceptibility

$$\chi_e(\omega) = \mathfrak{N}\alpha(\omega) = \mathfrak{N}(e^2/m) \sum_s [f_s/(\omega_s^2 - \omega^2 - i\gamma_s\omega)]. \quad (2.2)$$

Since we are interested in the properties of isolated atoms, all formulas will be derived to *lowest order* in  $\mathfrak{N}$ .

To obtain the corresponding result by a quantum treatment of atoms one may assume that a macroscopic oscillating field  $E_0 \cos \omega t$  is applied to each atomic electron of a dilute gas. If  $z_j$  indicates the  $z$  component of the position of the  $j$ th electron of an atom with respect to its nucleus, the assumption amounts to adding a term  $-e \sum_j z_j E_0 \cos \omega t$  to the Hamiltonian of each atom. This addition causes the unperturbed ground-state wave function  $\psi_0$  to be replaced by a superposition of all the unperturbed wave functions  $\psi_0, \psi_1, \dots, \psi_s \dots$  with coefficients calculated to lowest order in  $E_0$  by first-order perturbation theory. In the calculation it is expedient to add to each unperturbed energy eigenvalue an imaginary part which represents the decay of any atomic excitation due to collisions or to radiation emission; e.g., if the energy level of the  $s$ th eigenstate lies at  $E_s = \hbar\omega_s$  above that of the ground state, the corresponding eigenvalue is indicated by  $E_s - i\hbar\gamma_s/2$ . Details of the calculation are described in textbooks, see, for example, pp. 390–391 of (Sl51).<sup>2</sup>

Having calculated the perturbed ground-state wave function, one finds that the mean dipole moment of a unit volume of gas does not vanish but is represented by

$$\mathfrak{N}e \langle \sum_j z_j \rangle = \frac{1}{2} [\chi_e(\omega) E_0 \exp(-i\omega t) + \chi_e^*(\omega) E_0 \exp(i\omega t)]. \quad (2.2a)$$

Here  $\chi_e$  is the same as (2.2) provided one defines

$$f_s (2m\omega_s/\hbar) |(z)_s|^2 = (2mE_s/\hbar^2) |(z)_s|^2, \quad (2.3)$$

where

$$(z)_s = \int \psi_s^* \sum_j z_j \psi_0 d\tau \quad (2.4)$$

and  $d\tau$  is the volume element of all electron coordinates.

<sup>2</sup> Representing the perturbed wave function by  $\Sigma_s a_s(t) \psi_s$ , one calculates the coefficients  $a_s(t)$  by integrating a first-order differential equation in  $da_s(t)/dt$  with the initial condition  $a_s(0) = 0$  for  $s \neq 0$ . Terms with a factor  $\exp(-\gamma_s t/2)$  are disregarded for sufficiently large values of  $t$ . The treatment of (Sl51) does not introduce the  $\gamma_s$  for simplicity but then meets some difficulty in justifying the correct final results on the basis of the correct initial conditions.

One of the two factors  $(z)_s$  in (2.3) originates from a matrix element of the perturbed Hamiltonian and the other from the calculation of the mean dipole.

Modern techniques such as that of Feynman quoted in Sec. 2.3 make it unnecessary to treat the external field classically and to represent the decay of atomic excitation by adding an imaginary part to the energy eigenvalues. They enable one to treat by a single Hamiltonian a complete quantum system, which consists of the incident field, of the atom, and of additional field and matter variables that provide an "excitation sink," with appropriate interactions. The imaginary element in (2.2) is then seen to originate from boundary conditions of the "outgoing wave" type which are appropriately imposed on the state of the excitation sink (see, e.g., Fa64).

The classical and quantum definitions of  $f_s$  given above appear to depend on the mutual orientation of the  $z$  axis and of the atom, specifically of its states  $\psi_0$  and  $\psi_s$ . In fact, the  $\sum_s$  in (2.2) includes all states of equal energy  $E_s = \hbar\omega_s$  and different orientation. Moreover, the ground state  $\psi_0$  may be isotropic, in which case the polarizability is actually orientation-independent, or one may deal with atoms of random orientation, in which case averaging of  $f_s$  over all states  $\psi_0$  of different orientation is implied. In this article we shall assume throughout that averaging over the orientations of  $\psi_0$  and  $\psi_s$  has in fact been performed. [The process of averaging and its influence on the properties of oscillator strengths are discussed in Secs. 59–60 of BS57, where the averaged strengths are indicated by  $\tilde{f}$ .]

We are interested here primarily in ionization processes, that is, in states  $\psi_s$  of the continuous spectrum. In this event, the function  $\psi_s$  is understood to be normalized "per unit energy range" and the quantity (2.3) is properly indicated by  $df/dE_s = \hbar^{-1}df/d\omega_s$ . The summation symbol  $\sum_s$  in (2.2) is understood to include an integration over the continuous spectrum and is more properly represented by

$$\sum_s = \sum_s^{\text{disc.}} + \int_I^\infty \hbar d\omega_s, \quad (2.5)$$

where  $I$  is the lowest ionization threshold. [The contribution of autoionizing discrete levels, which lie above  $I$ , may be regarded as part of the continuous spectrum (see Sec. 8.1) and thus included in the second term of (2.5).]

Alternative expressions of the oscillator strength  $f_s$  exist, in terms of matrix elements of the electron velocity or momentum, acceleration, etc. These expressions are derived from (2.3) and (2.4) by means of operator transformations, based on the fact that  $E_s$  is the difference of the energy eigenvalues of the Schrödinger equation with Hamiltonian operator  $H$  corresponding to the wavefunctions  $\psi_s$  and  $\psi_0$ . Thus we

have

$$\begin{aligned} E_s(z)_s &= \int [\psi_s^* H \sum_j z_j \psi_0 - \psi_s^* \sum_j z_j H \psi_0] d\tau \\ &= \int \psi_s^* [H \sum_j z_j - \sum_j z_j H] \psi_0 d\tau \\ &= -i\hbar \int \psi_s^* \sum_j v_{jz} \psi_0 d\tau \\ &= -i\hbar (v_z)_s \\ &= -(\hbar^2/m) \int \psi_s^* \sum_j (\partial \psi_0 / \partial z_j) d\tau \\ &= -i(\hbar/m) (p_z)_s, \end{aligned} \quad (2.6)$$

where we have utilized the operator equation that defines the velocity  $\mathbf{v}$ ,  $-i\hbar\mathbf{v} = H\mathbf{r} - \mathbf{r}H$ , or, alternatively, the differential expression  $H = -(\hbar^2/2m) \sum_j \partial^2 / \partial x_j^2 + \dots$ . Substitution of (2.6) in (2.3) yields

$$\begin{aligned} f_s &= -(2i/\hbar) (z)_s^* (p_z)_s \\ &= (i/\hbar) [(p_z)_s^* (z)_s - (z)_s^* (p_z)_s]. \end{aligned} \quad (2.7)$$

Utilizing the squared modulus of (2.6), one finds instead

$$f_s = 4 |(p_z)_s|^2 / 2mE_s. \quad (2.8)$$

A further transformation analogous to (2.6) is

$$\begin{aligned} E_s(p_z)_s &= \int \psi_s^* [H \sum_j p_{jz} - \sum_j p_{jz} H] \psi_0 d\tau \\ &= -i\hbar m \int \psi_s^* \sum_j a_{jz} \psi_0 d\tau \\ &= -i\hbar m (a_z)_s \\ &= i\hbar \int \psi_s^* \sum_j (\partial V / \partial z_j) \psi_0 d\tau \\ &= i\hbar (\partial V / \partial z)_s, \end{aligned} \quad (2.9)$$

where  $a_j$  is the acceleration of the  $j$ th electron and  $-\partial V / \partial z_j$  the  $z$  component of the force applied to it by the nucleus and the other electrons. Substitution in (2.8) yields finally

$$\begin{aligned} f_s &= (2i\hbar/mE_s^2) (p_z)_s^* (\partial V / \partial z)_s \\ &= (i\hbar/mE_s^2) [(p_z)_s^* (\partial V / \partial z)_s - (\partial V / \partial z)_s^* (p_z)_s] \\ &= 4\hbar^2 |(\partial V / \partial z)_s|^2 / 2mE_s^3. \end{aligned} \quad (2.10)$$

## 2.2. Dielectric and Optical Constants: Photoabsorption Cross Section

For a nonmagnetic material of low density  $\mathfrak{N}$ , the dielectric constant equals the square of the complex

refractive index and is related to the susceptibility (2.2) by

$$\epsilon = (n + ik)^2 = 1 + 4\pi\chi_e(\omega). \quad (2.11)$$

The absorption coefficient of electromagnetic radiation is then

$$\begin{aligned} \mu &= 2(\omega/c)\kappa = 2(\omega/c) \operatorname{Im}(\epsilon)^{1/2} \\ &= 4\pi(\omega/c) \operatorname{Im}[\chi_e(\omega)], \end{aligned} \quad (2.12)$$

where the last equality holds again to lowest order in  $\mathfrak{N}$ .

One sees from (2.2) that  $\operatorname{Im}[\chi_e(\omega)]$  is appreciable only within spectral intervals of order  $\gamma_s$  about each discrete frequency  $\omega_s$ , as well as throughout the continuous spectrum of  $\omega_s$ . In the continuum one can generally assume that the spectral density  $df/d\omega_s$  is practically constant over intervals  $\sim \gamma_s$  so that it can be replaced by  $df/d\omega$  in the calculation of  $\operatorname{Im}\chi_e$  from (2.2); the sum (actually, integral) over  $\omega_s$  reduces then to an arctangent and yields

$$\begin{aligned} \mu(\omega) &= (2\pi^2 e^2/mc)\mathfrak{N}df/d\omega \\ &= (\pi e^2 h/mc)\mathfrak{N}df/dE \\ &= 1.098 \times 10^{-16} \text{ cm}^2 \text{ eV } \mathfrak{N}df/dE. \end{aligned} \quad (2.13)$$

Therefore, the photoionization cross section is

$$\begin{aligned} \sigma(\omega) &= \mu(\omega)/\mathfrak{N} \\ &= (\pi e^2 h/mc)(df/dE) \\ &= 1.098 \times 10^{-16} \text{ cm}^2 \text{ eV } (df/dE), \end{aligned} \quad (2.14)$$

a relation that enables us to treat the photoabsorption cross section and the spectral density of oscillator strength as synonymous. The quantum theory of the interaction of radiation with an atom yields (2.14) directly, with the definition (2.8), through the calculation of the probability of transition of the atom to a continuum state, without any reference to macroscopic properties or to the mean dipole moment induced by a macroscopic oscillating field (see, e.g., BS57, p. 303, Be64, Chap. 12).

Other optical constants, derived from the polarizability or refractive index, can of course be expressed in terms of oscillator strengths as detailed in Sec. 2.5.

### 2.3. Time Correlations

We have stated that the oscillator strengths represent the aptitude of atomic electrons to perform oscillations of different frequencies. In this context one may also consider how the mean electric dipole moment of an atom varies in time following an initial disturbance. (This moment vanishes for any atom in its unperturbed ground state because of symmetry under reflection at the nucleus.) For example, one may think of having applied an impulsive displacement to all atomic electrons at an initial time  $t=0$  and calculate the expected mean dipole moment at later times  $t$ . The frequency spectrum

(Fourier transform) of these dipole variations is, in essence, the spectrum of the oscillator strength.

Without resorting to a new calculation one can transform analytically the quantum-mechanical definition of oscillator strength (2.3) into the Fourier transform of a correlation<sup>3</sup> between electron positions, or velocities, at different times, utilizing a general procedure of quantum mechanics (AP48; see e.g., Ki63, Sl63). One finds

$$\begin{aligned} \frac{df}{d\omega} &= \frac{2m\omega}{\hbar} \int_{-\infty}^{\infty} dt \exp(-i\omega t) \sum_{jk} \langle z_j z_k(t) \rangle_0 \\ &= \frac{i}{\hbar} \int_{-\infty}^{\infty} dt \exp(-i\omega t) \sum_{jk} \langle p_{kz}(-t) z_j - z_j p_{kz}(t) \rangle_0, \end{aligned} \quad (2.15)$$

where

$$\langle z_j z_k(t) \rangle_0 = \int \psi_0 z_j \exp(iHt/\hbar) z_k \exp(-iHt/\hbar) \psi_0 d\tau, \quad (2.16)$$

$H$  is the full Hamiltonian of the atom and  $z_k(t)$  and  $p_{kz}(t)$  are operators in the Heisenberg representation as seen explicitly in (2.16).

Notice that these formulas do not involve excited or ionized states explicitly but take into account the complexity of atomic dynamics implicitly through the structure of  $z_k(t)$  or  $p_{kz}(t)$ . The correlation formulas may be of help in interpreting the properties of the oscillator strength distribution in terms of dynamic pictures.

Alternatively, one can obtain the expression of  $\chi_e$  in terms of the Fourier integral (2.15) directly by calculating (2.2a) through the perturbation approach of Feynman (Fe51) instead of those of Rayleigh-Schrödinger or Dirac. To this end one represents the coordinate  $z_j$  as the Heisenberg operator

$$\exp[i(H - eE \sum_k z_k)t] z_j \exp[-i(H - eE \sum_k z_k)t], \quad (2.17)$$

where  $H$  is the free atom Hamiltonian and  $E$  the electric field operator, and expands it into powers of  $E$  to first order. Upon substitution into the left side of (2.2a), this quantity depends on atomic variables through the correlation (2.16) and on the field through the mean value  $\langle E \rangle$  which is  $E_0 \cos \omega t$  according to the formulation of our problem. The expression of  $\chi_e$  in terms of (2.15) follows.

### 2.4. Spectral Distribution and Its Moments

The plot of the spectral density of oscillator strength,  $df/dE$ , against the photon energy  $E$  represents the absorption spectrum or the spectrum of the photo-

<sup>3</sup> One calls correlation the mean value of a product of two, or more, variables. The mean value is taken here over the ground state  $\psi_0$ . One of the two variables may be regarded as a perturbation, the other as the monitor of the resulting disturbance.

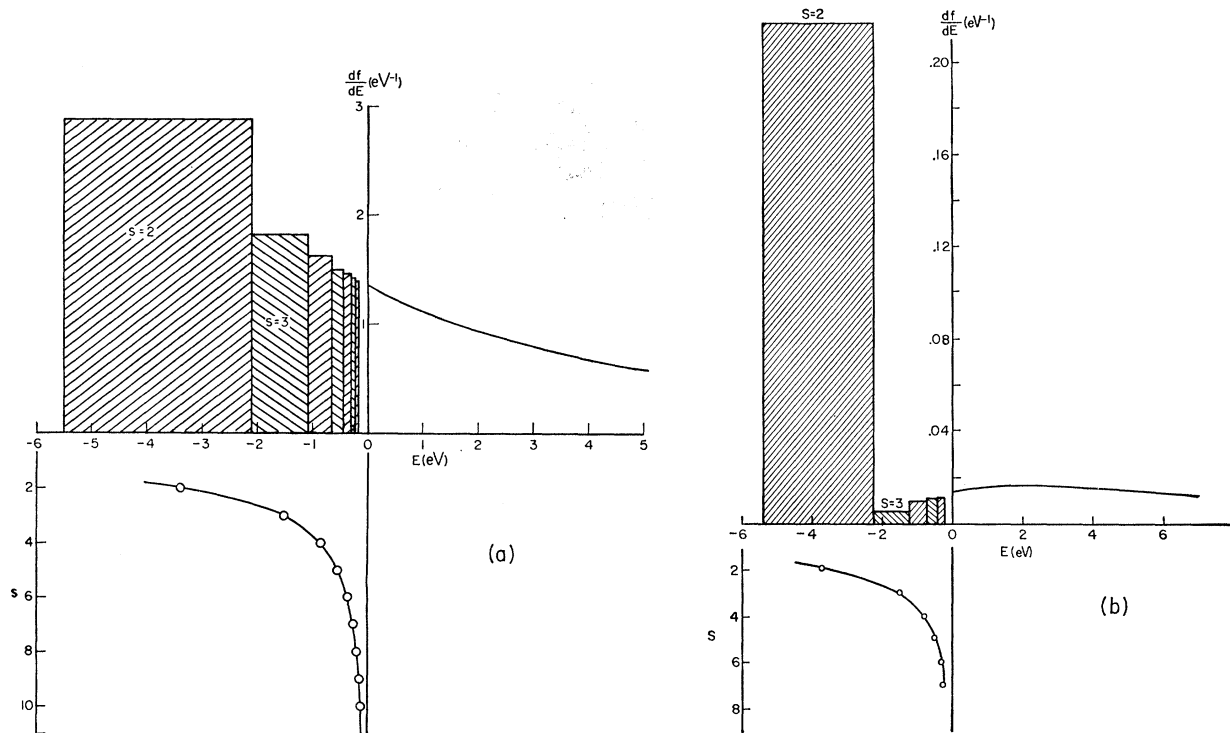


FIG. 1. Oscillator strength distribution in the discrete and part of the continuous spectra of: (a) H (theory) (b) Li (experiments, Fi31, HC67). The plot of  $E_s$  vs  $s$  in the lower part of the figure relates to the construction of the histogram. See Sec. 4.5 for interpretation of Li spectrum. (Courtesy A.R.P. Rau.)

ionization cross section, to within a proportionality constant, owing to (2.13) and (2.14). The strengths  $f_s$  of discrete transitions can be included in this plot in the form of a histogram, i.e., of a set of rectangular blocks whose respective areas are equal to the  $f_s$  and whose bases are laid about the corresponding energies  $E_s$  (Fig. 1).

That the discrete absorption spectrum of an atom may be regarded as an appendage of the continuum was indicated in Sec. 1 on the grounds that the discrete spectrum contains a minor fraction of the total oscillator strength. More intrinsically, however, the discrete spectrum itself consists normally of one or a few Rydberg series of lines whose frequencies and oscillator strengths are distributed regularly and relate closely to corresponding properties of the continuum. These features of the discrete spectrum derive from the circumstances affecting any electron that has received from photoabsorption sufficient energy to move outwards from the rest of the atom. The electron is held back primarily by Coulomb attraction as though it belonged to a hydrogen atom; whether it will remain bound in a Rydberg level or escape in a continuum state depends on the comparison of its total and potential energies far outside the rest of the atom, a comparison incidental to the initial process of photoabsorption.

Figure 1(a) displays the position and oscillator strengths of the discrete spectrum of H together with

the adjoining continuum, in a manner applicable to the Rydberg series of other atoms except for fine structure details and for localized irregularities to be mentioned in Sec. 8. The quantum defect method (Se58, Se66, see also Sec. 4.3), which provides a detailed formulation of the qualitative arguments indicated above, suggests the following procedure for constructing the histogram so as to point up the relevant regularities. Plot each observed transition energy  $E_s$  against the number  $s$  of the corresponding line in its Rydberg series and draw a smooth line through these points. [This curve should fit approximately the equation  $E_s = I - I_H/(s - \sigma)^2$ , where  $I$  is the relevant ionization threshold and  $\sigma$  a constant quantum defect; for atomic hydrogen  $I = I_H$  and  $\sigma = 0$ .] The base of the histogram block that represents the oscillator strength  $f_s$  should equal the slope of the curve,  $dE_s/ds$ , at  $s$ .<sup>4</sup> The tops of the blocks in the histogram, whose heights equal  $f_s ds/dE$ , should then form a staircase which constitutes an extrapolation of the continuous spectrum below the ionization threshold.

The discrete absorption spectra of alkaline atoms consist, in the main, of a single Rydberg series and can be represented in the manner of Fig. 1. Figure 1(b) shows

<sup>4</sup> An alternative suggestion presented in Sec. 4 of FC65 is faulty in defining the mean density of oscillator strength in a discrete spectrum as the ratio of the strength of each line to the mean of its distances from the adjacent lines. This mean distance should be replaced by the derivative  $dE_s/ds$ .

the spectrum of Li as an example; the occurrence of a minimum in the histogram of the discrete spectrum is discussed in Sec. 4.5. For other atoms one finds normally two or more Rydberg series converging to the threshold, or thresholds, of adjoining continua. [Different thresholds of continuous spectra correspond to photoabsorption processes that leave the residual ion in different energy levels.] Separate histograms similar to those in Fig. 1 may be constructed for different Rydberg series. The staircase formed by each histogram extrapolates beyond the series limit into the contribution of the corresponding continuum to the total distribution of oscillator strength. In principle, the whole continuous spectrum could be resolved into the contributions of different processes that correspond to different allocations of energy and angular momentum between the residual ion and the escaping electron. In practice this analysis would require, from the experimental point of view, procedures more refined than those for measuring only the absorption of light (see Sec. 3.5). At this time, the extrapolation of discrete series can provide some relevant information.

For purposes of qualitative analysis, one occasionally constructs graphs of the integral spectrum of oscillator strengths in which each abscissa represents a photon energy  $E$  and the corresponding ordinate the sum of all oscillator strengths corresponding to energies smaller than  $E$  (see, e.g., Fig. 13). The curve in such a graph increases monotonically with a finite nonzero slope in the continuous spectrum and with a vertical step in correspondence to each line of the discrete spectrum, these steps being separated by flat segments. (The considerations required for choosing the width of histogram blocks in the discrete spectrum of Fig. 1 are unnecessary here.) The final ordinate reached by the integral plot at  $E = \infty$  is fixed by the sum rule (2.23), so that the plot shows at a glance what fraction of the oscillator strength lies below each energy  $E$ . On the other hand, any uncertainty or error in the lower energy portions of the spectrum affects the entire integral curve at higher energies.

Proceeding now to some general descriptive considerations concerning the spectral distribution of oscillator strengths, one may recall that distribution functions are often characterized conveniently by their moments. We indicate the moments of the strength distribution  $df/dE$  by

$$S_r = \sum_s E_s^r f_s = \sum_s E_s^r f_s + \int_I^\infty E^r (df/dE) dE, \quad (2.18)$$

where the symbol  $\sum_s$  is understood in the sense of (2.2) and (2.5). The zeroth moment  $S_0$  represents the area under the plot of Fig. 1. It equals the number  $N$  of electrons in the atom, owing to the familiar Thomas-Reiche-Kuhn sum rule which underpins the validity of the classical model of electron oscillations. Many of the moments  $S_r$ , as well as related averages over the

distribution, can be expressed in terms of theoretical or experimental properties of the atom in its ground state, as will be detailed in Sec. 2.5.

Here we recall that moments of any distribution that extends to infinity may be infinite unless the distribution tail converges to zero sufficiently fast. According to nonrelativistic mechanics of the atom—whose validity is assumed throughout this article<sup>5</sup>—the spectral density of oscillator strength decreases for large  $E_s$  as

$$df/dE \sim E^{-7/2} \quad (2.19)$$

(KS57, RF67), so that  $S_r$  becomes infinite for  $r$  integer and  $> 2$ .

Knowledge of a finite set of moments  $S_r$  does not suffice to reconstruct the entire distribution of oscillator strength<sup>6</sup> but provides nevertheless information of interest. Consider, in particular the ratios

$$S_{r+1}/S_r = \sum_s E_s (E_s^r f_s) / \sum_s (E_s^r f_s), \quad (2.20)$$

which may be regarded as mean values of  $E_s$  averaged over distributions that are increasingly weighted toward high values of  $E_s$  as  $r$  increases. Since the  $f_s$  and  $E_s$  are nonnegative, the ratios (2.20) should be increasing—or, at least, nondecreasing—functions of  $r$ . That is, one must have

$$\frac{S_{r+1}}{S_r} / \frac{S_r}{S_{r-1}} = \frac{S_{r+1} S_{r-1}}{S_r^2} \geq 1. \quad (2.21)$$

This “ratio of ratios” can equal unity only for a distribution concentrated entirely at a single energy  $E_s$ , that is, for a harmonic oscillator. [In this event all ratios (2.20) are equal to  $E_s$ .] Therefore the excess of (2.21) over unity indicates how broad is the distribution.

For purposes of orientation we give in Table I some values of  $S_r$  and of the ratios (2.20) and (2.21) for atomic H, obtained from the formulas of Sec. 2.5. Note that the H electron is subjected to a Coulomb force which decreases with increasing distance from the

TABLE I. Moments and moment ratios for the H atom ( $I_H = 13.6$  eV).

$r$	-2 <sup>a</sup>	-1	0	1	2
$S_r$	$(9/8) I_H^{-2}$	$I_H^{-1}$	1	$\frac{4}{3} I_H$	$(16/3) I_H^2$
$S_{r+1}/S_r$	$(8/9) I_H$	$I_H$	$\frac{4}{3} I_H$	$4 I_H$	$\infty$
$S_{r+1} S_{r-1} / S_r^2$		$(9/8)$	$\frac{4}{3}$	3	$\infty$

<sup>a</sup> The  $S_{-2}$  value can be calculated analytically for H only, see MS48.

<sup>5</sup> In fact, atomic electrons acquire speeds comparable to  $c$  within a small volume around the nucleus. Absorption of radiation within this volume—which occurs only for high photon energies—is boosted by various relativistic effects, including pair production. As a result, even  $S_0$  becomes infinite.

<sup>6</sup> The distribution could be reconstructed from its Laplace transform  $\phi(p) = \sum_s \exp(-p E_s) f_s$ . The moments  $S_r$  are coefficients of the Taylor expansion of  $\phi(p)$  into powers of  $p$ .

nucleus, whereas the force on a harmonic oscillator increases with increasing distance.

Values of the  $S_r$  and of their ratios, obtained from the direct measurement of oscillator strengths and from the other theoretical and experimental approaches described in Sec. 2.5, are increasingly used to test the internal consistency of different sources of information and to interpolate among their results (DL57, PL64, ML65). Data on this subject are shown in Table II. We shall make extensive use of arguments concerning the moments  $S_r$ .

### 2.5. Sum Rules: Optical and Related Constants

As mentioned above, numerous moments and other properties of the oscillator strength spectrum of an atom can be related to theoretical or experimental properties of the atom in its ground state. These relationships are known under the general name of "sum rules."

Four of these sum rules, including that of Thomas-Reiche-Kuhn which sets  $S_0=N$ , are derived as general theorems of quantum mechanics in standard references (see, e.g., BS57, Secs. 62 and 61a). They are:

$$\begin{aligned} S_{-1} &= (2m/\hbar^2) \sum_{j,k}^N \langle z_j z_k \rangle_0 \\ &= (2m/\hbar^2) \langle (\sum_j^N z_j)^2 \rangle_0 \\ &= (2m/3\hbar^2) \langle |\sum_j^N \mathbf{r}_j|^2 \rangle_0, \end{aligned} \quad (2.22)$$

$$S_0 = N, \quad (2.23)$$

$$\begin{aligned} S_1 &= 2m \sum_{j,k}^N \langle v_{jz} v_{kz} \rangle_0 \\ &= 4 \langle (\sum_j^N p_{jz})^2 / 2m \rangle_0 \\ &= (4/3) \langle |\sum_j^N \mathbf{p}_j|^2 / 2m \rangle_0, \end{aligned} \quad (2.24)$$

$$\begin{aligned} S_2 &= (\hbar^2/m) \sum_j^N \langle \partial^2 V / \partial z_j^2 \rangle_0 \\ &= (4\pi/3) Z(e^2 \hbar^2/m) \langle \sum_j^N \delta(\mathbf{r}_j) \rangle_0. \end{aligned} \quad (2.25)$$

Here, notations are the same as in Sec. 2.3, including those for ground-state averages; further,

$$\sum_j^N \delta(\mathbf{r}_j)$$

is a sum of Dirac  $\delta$  functions whose mean value is the electron density at the nucleus. Average orientation of the atom is assumed in the formulas.

These sum rules follow, respectively, from the several expressions of  $f_s$  in Sec. 2.1. Specifically one chooses that expression which will not include  $E_s$  explicitly after multiplication by  $E_s^{-r}$ . Thus we utilize (2.3) to calculate

$$S_{-1} = \sum_s E_s^{-1} f_s = (2m/\hbar^2) \sum_s |(z)_s|^2. \quad (2.22')$$

Recalling the definition (2.4) of  $(z)_s$ , we see that the sum over all the excited states  $s$  reduces to a matrix multiplication,

$$\begin{aligned} \sum_s |(z)_s|^2 &= \sum_j \int \psi_0^* \sum_j z_j' \psi_s d\tau' \int \psi_s^* \sum_j z_j \psi_0 d\tau \\ &= \int \psi_0^* (\sum_j z_j)^2 \psi_0 d\tau = \langle (\sum_j z_j)^2 \rangle_0. \end{aligned} \quad (2.22'')$$

The values of  $S_0$ ,  $S_1$ , and  $S_2$  are obtained in analogous manner. In calculating the last expression of (2.25) one should notice that the electron-electron potential  $\sum_{i>j} e^2 / |\mathbf{r}_i - \mathbf{r}_j|$  yields no net contribution to  $\langle \sum_j \partial^2 V / \partial z_j^2 \rangle_0$ , as shown by Vinti (Vi32). For further details see (BS57, Sec. 62). Alternatively one could utilize the correlation formulas of Sec. 2.3, considering that summation over the states  $s$  is equivalent to integration over  $\omega$  in (2.15) and that  $\int d\omega \exp(-i\omega t) = 2\pi\delta(t)$ .

Notice that  $S_{-1}$  and  $S_1$  (but not  $S_0$  and  $S_2$ ) depend on the mean products of variables of *different electrons*, namely, on the two-electron correlations  $\langle z_j z_k \rangle_0$  and  $\langle p_{jz} p_{kz} \rangle_0$  with  $j \neq k$ . An explicit connection is thereby established between the spectrum of oscillator strength and electron-electron correlations in the ground state. If these correlations were negligible,  $S_{-1}$  and  $S_1$  would be proportional, respectively, to other well-known properties of the atom, namely, its diamagnetic susceptibility

$$\chi_m = -\frac{e^2}{6mc^2} \sum_j^N \langle \mathbf{r}_j^2 \rangle_0, \quad (2.26)$$

and the mean kinetic energy of its electrons

$$\langle K \rangle_0 = \sum_j^N \langle p_j^2 / 2m \rangle_0. \quad (2.27)$$

(Owing to the virial theorem,  $\langle K \rangle_0$  equals the total binding energy of the atom.)

Knowledge of the ground-state wave functions of an atom, much easier to achieve than for the excited states, permits one to evaluate the moments  $S_{-1}$ ,  $S_1$ , and  $S_2$ . However this information has limited relevance, for atoms other than H and He, until one can estimate the separate contributions of different atomic shells. Accordingly, any discussion of data on these moments is deferred until Chap. 4.

The negative even moments  $S_{-2r}$  are related to the light scattering and refracting properties of the atom.

TABLE II. Moments and moment ratios for the rare gases estimated from various experimental data and calculations drawn from the literature (In 67).

$r$		-2	-1	0	1	2
$S_r/I_{\text{H}}^r$	He (Theory)	0.346 <sup>a</sup>	0.752 <sup>b</sup>	2	8.17 <sup>b</sup>	121 <sup>b</sup>
	He (exp)	0.349	0.754	1.99	8.36	127
	Ne	0.667	1.95	10	320	$1.10 \times 10^5$
	Ar	2.77	5.3	18	$1.15 \times 10^3$	$1.16 \times 10^6$
	Kr	4.18	7.5	36	$5.3 \times 10^3$	$1.9 \times 10^7$
	Xe	6.82	10.3	54	$1.3 \times 10^4$	$1.0 \times 10^8$
$S_{r+1}/S_r I_{\text{H}}$	He (Theory)	2.17	2.66	4.09	14.8	$\infty$
	Ne	2.94	5.13	32	344	$\infty$
	Ar	1.91	3.40	64	$1.0 \times 10^3$	$\infty$
	Kr	1.79	4.80	147	$3.6 \times 10^3$	$\infty$
	Xe	1.51	5.24	240	$7.7 \times 10^3$	$\infty$
$S_{r+1} S_{r-1} / S_r^2$	He (Theory)		1.23	1.54	3.62	
	Ne		1.75	6.2	11	
	Ar		1.78	19	16	
	Kr		2.68	30.6	24.7	
	Xe		3.47	46	32	

<sup>a</sup> Value from (Sc61).<sup>b</sup> Values from (Pe59).

Setting  $\omega=0$  in (2.2) yields the static polarizability

$$\alpha(0)=\mathfrak{N}(e^2/m)\sum_s\omega_s^{-2}f_s=\mathfrak{N}(e^2/m)\hbar^2S_{-2}. \quad (2.28)$$

Thus  $S_{-2}$  can be determined by polarizability experiments, which we consider here, as before, in the low density limit, i.e., to lowest order in  $\mathfrak{N}$ . More generally, the moments  $S_{-2r}$  appear as coefficients of the low-frequency power expansion of the refractive index  $n^2(\omega)$ ,

$$\begin{aligned} n^2(\omega) &= 1 + (4\pi\mathfrak{N}e^2\hbar^2/m)\sum_{r=1}^{\infty} S_{-2r}(\hbar\omega)^{2(r-1)} \\ &= 1 + (4\pi\mathfrak{N}e^2\hbar^2/m)\sum_{r=1}^{\infty} S_{-2r}(hc/\lambda)^{2(r-1)}. \end{aligned} \quad (2.29)$$

Fitting this expansion to experimental data on  $n^2$  provides values of the  $S_{-2r}$ , which may help one in constructing the distribution of  $f_s$ . Moreover, the derivative of  $n^2(\omega)$  with respect to  $\omega$  determines the optical rotatory power induced by a magnetic field (Faraday effect). For spherically symmetric ( $S$  state) atoms the rate of rotation is

$$d\alpha/dz = VH = (4\pi\mathfrak{N}e^2\hbar^2/2m^2c^2)H\sum_{r=2}^{\infty}(r-1)S_{-2r}(\hbar\omega)^{2(r-1)}, \quad (2.30)$$

where  $V$  is the Verdet constant and  $H$  the magnetic field strength in the direction of light propagation. Measurement of the Verdet constant often affords a more accurate determination of  $S_{-4}$ ,  $S_{-6}$ , etc., than measurements of the refractive index.

Besides the moments  $S_r$ , four differently weighted averages of  $\ln E_s$  over the oscillator strength distribu-

tion are relevant to specific physical phenomena, namely,

$$\ln I_{-1} = \sum_s E_s^{-1} (\ln E_s) f_s / S_{-1}, \quad (2.31)$$

$$\ln I = \sum_s (\ln E_s) f_s / N, \quad (2.32)$$

$$\ln I_1 = \sum_s E_s (\ln E_s) f_s / S_1, \quad (2.33)$$

$$\ln I_2 = \sum_s E_s^2 (\ln E_s) f_s / S_2. \quad (2.34)$$

The first three of these concern, respectively, the cross section for grazing collisions of fast charged particles with atoms (IKP67), the mean energy transfer in these collisions, and its mean fluctuation (Fa63, pp. 14 and 42); the oscillator strength is involved here because the passage of a fast charge with low momentum transfer has essentially the same effect as electromagnetic radiation, as discussed in the next section. The fourth one,  $I_2$  also called  $K_0$ , concerns the Lamb shift of atomic energy levels, that is, a correction due the virtual process of emission and reabsorption of electromagnetic radiation by atomic electrons (BS57). Notice that if one defines a smooth function  $S(x)$ , such that it equals one of the  $S_r$  whenever  $x$  equals the integer  $r$ , he can regard the expressions (2.31) to (2.34) as special cases of

$$\ln I_r = [d \ln S(x)/dx]_{x=r}. \quad (2.35)$$

This formula can be useful for purposes of numerical evaluation (Pe59, Da60, DS60, BD65).

Notice also that the sum rules considered in this section provide no information about whether and how the total oscillator strength of an atom can be traced back to separate contributions from the electrons in the

various shells or subshells. The very concept of atomic shells stems from approximate models of atomic mechanics. Additional and more informative sum rules can be formulated within the framework of such approximations. Such rules will be discussed in the several relevant sections of this article, but they do not constitute at this time a clearly coherent system.

### 2.6. Role of Polarizability in the Collisions of Fast Charged Particles

When a fast charged particle passes in the proximity of an atom, but at some distance from it, the atom experiences an electric field which is rather uniform in space and sharply pulsed in time. The response of the atom to this disturbance depends on its time-dependent polarizability or on the Fourier transform thereof,  $\alpha(\omega)$ , as discussed in Secs. 2.1 and 2.3. Insofar as the field pulse can be regarded as infinitely sharp in time, its Fourier components of all frequencies have equal intensity. Under this condition, the probability of

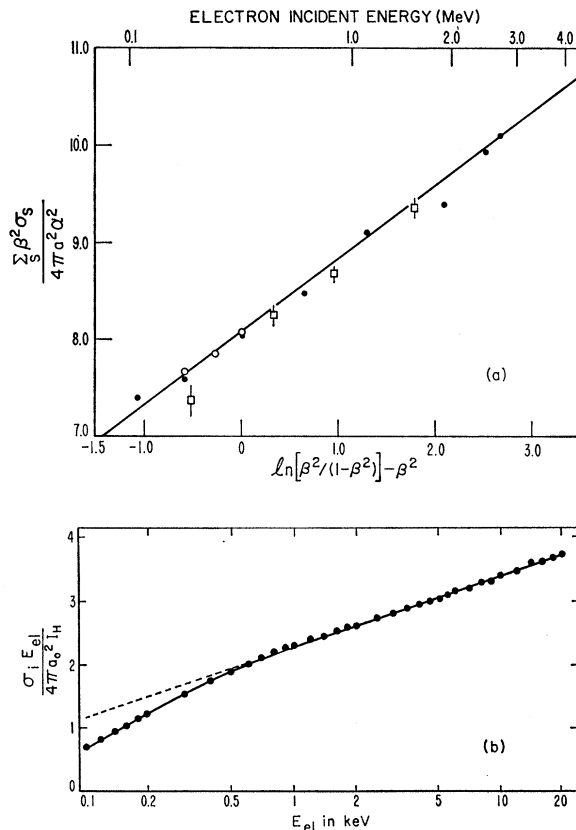


FIG. 2. Plots of the He ionization cross sections by particle collisions in the relativistic and nonrelativistic energy regions. (a)  $\Sigma_s \beta^2 \sigma_s / 4\pi a_0^2 \alpha^2$  (Eq. 2.39) for slightly impure He ionized by electron ( $\square$  MCC53,  $\bullet$  RP68) and positron ( $\circ$  RP68) impact. The theoretical curve corresponds to  $S_{-1} = 0.752 I_H^{-1}$  (IKP67). (b) Total ionization by electron impact in the nonrelativistic energy range (Sc65). Curve corresponds to Eq. (2.38) and its slope to Eq. (2.40).

absorption of an energy  $\hbar\omega$  by an atom is simply proportional to the Fourier component of the induced dipole moment which is  $90^\circ$  out of phase with the disturbance, i.e., to the imaginary part of its polarizability  $\text{Im } \alpha(\omega)$ .

These considerations suffice to surmise that the observation of the spectrum of energy transfers in collisions may serve to measure  $\text{Im } \alpha(\omega)$  and thereby the spectrum of oscillator strength in accordance with (2.2). However, it takes a rather detailed analysis of the quantum theory of inelastic collisions to derive the quantitative relationships which make this measurement not only possible but convenient. In a classical analysis one classifies the inelastic collisions of a particle with an atom according to the "impact parameter" which, when large, is essentially the distance of closest approach. A quantum analysis replaces this parameter, which is in fact unobservable, by the momentum  $\mathbf{q}$  transferred in the collision, which is a function of the energy loss and deflection of the incident particle, or by  $Q = q^2/2m$  where  $m$  is the mass of an atomic electron. Small values of  $\mathbf{q}$  or  $Q$  correspond to the large values of the impact parameter, that is to the kind of collision in which the atomic response is characterized by its polarizability.

The cross section for inelastic collisions of fast charged particles can be calculated adequately to lowest order in the particle-atom interaction. As described in another review article (Fa63), the cross section for excitation of an atom to its  $s$ th state, differential in the parameter  $Q$ , is represented by

$$\frac{d\sigma_s}{dQ} = \frac{2\pi z^2 e^4}{mv^2} \left\{ \frac{|F_s(\mathbf{q})|^2}{[Q^2(1+Q/2mc^2)^2]} + \frac{|\mathbf{g}_s \cdot \mathbf{G}_s(\mathbf{q})|^2}{[Q(1+Q/2mc^2) - E_s^2/2mc^2]^2} \right\} \left\{ 1 + \frac{Q}{mc^2} \right\} \quad (2.36)$$

$$\sim \frac{2\pi z^2 e^4 f_s}{mv^2 E_s} \left\{ \frac{1}{Q(1+Q/2mc^2)^2} + \frac{\beta_s^2 E_s^2/2mc^2}{[Q(1+Q/2mc^2) - E_s^2/2mc^2]^2} \right\} \left\{ 1 + \frac{Q}{mc^2} \right\}. \quad (2.37)$$

Equation (2.36) corresponds to (16) of (Fa63), whereas (2.37) is derived from it by utilizing the low- $Q$  approximation forms of  $F_s$  and  $\mathbf{G}_s$  from (22) and (23) of (Fa63). The charge and velocity of the incident particle are represented by  $ze$  and  $v$ , whereas  $\mathbf{g}_s$  represents the component of the velocity vector  $\mathbf{g} = \mathbf{v}/c$  on the plane perpendicular to  $\mathbf{q}$ .<sup>7</sup> Equation (2.36) simplifies considerably in the nonrelativistic

<sup>7</sup> A factor  $Z$  has been deleted in the transfer from (Fa63) because of a different normalization of the oscillator strengths [see note 9 of (Fa63)]. Exchange effects, which occur in electron collisions with atoms, were not relevant to (Fa63) and are disregarded here because they are negligible in the low- $Q$  approximation.

limit, but we cannot afford this simplification because high values of  $v$  are relevant to our application.

Equation (2.37) permits a direct determination of  $f_s$  because  $d\sigma_s/dQ$  can be measured by collecting only particles scattered within a differential solid angle. Measurements are usually made for zero-angle scattering which corresponds to the minimum value of  $Q$ ,  $Q_{\min}$ . The measured cross section per unit solid angle is easily converted to  $d\sigma/dQ$ ; often the relativistic terms in (2.37) are negligible. On the other hand, measurements have often been carried out at moderately low incident energies ( $\lesssim 1000$  eV) for which the low- $Q$  approximation formula<sup>8</sup>  $|F_s|^2 \sim Q f_s/E_s$  does not quite hold, even at  $Q=Q_{\min}=E_s^2/2mv^2$ . In this event  $|F_s(q)|^2$  is determined using (2.36) for a few values of  $Q$  and then  $f_s/E_s$  is obtained by extrapolation of  $|F_s(q)|^2/Q$  to  $Q=0$ ; this approach has been applied extensively by Lassettre and co-workers (LKS64, LBSK64, SL64, SL64a).

An alternative procedure enables one to obtain  $f_s$  from simpler and more accurate measurements of the variation of the total cross section  $\sigma_s$  as a function of the impact velocity  $v=\beta c$ , except for relativistic values of  $E_s$ . Notice that, in the integration over  $Q$  of the "exact" formula (2.36), the impact velocity appears only through multiplicative factors, except for its influence upon the range of integration. The integration near the upper limit  $Q_{\max}$  yields no appreciable contribution, unless  $E_s$  is very large, because the integrand converges to zero rapidly. The integration near the lower limit  $Q_{\min}=E_s^2/2mv^2$ <sup>8</sup> yields an increasing contribution as  $v$  increases, but this contribution can be calculated analytically, since the simpler approximate form (2.37) is applicable here. The calculation, outlined by Eqs. 24, 25, and 32 of (Fa63), yields

$$\sigma_s = \frac{2\pi z^2 e^4}{mv^2} \left\{ \frac{f_s}{E_s} \left[ \ln \frac{\beta^2}{1-\beta^2} - \beta^2 \right] + C_s \right\}, \quad (2.38)$$

where  $C_s$  is independent of  $\beta$  and irrelevant for our purposes.

According to this formula, a plot of the ratio

$$\sigma_s / [2\pi z^2 e^4 / I_H m v^2] = \beta^2 \sigma_s / 4\pi a^2 \alpha^2 \quad (2.39)$$

(where  $a=5.29 \times 10^{-8}$  cm,  $\alpha=1/137$ , and  $I_H=13.6$  eV) against  $\ln [\beta^2/(1-\beta^2)] - \beta^2$  should yield a straight line whose slope gives the value of  $f_s/(E_s/I_H) = |(z)_s|^2/a^2$ . This procedure has been applied successfully to the sum of  $\sigma_s$  over all states that lead to ionization, for various substances, especially by Platzman and co-workers (MP57, IKP67) and in (Sc65). Results for He are shown in Fig. 2. The plots approach a straight line, as expected, for increasing values of the velocity of an incident electron, thus demonstrating the range of conditions under which the assumptions underlying the derivation of (2.38) are adequately fulfilled.

<sup>8</sup> See Eq. 18 of (Fa63); the relativistic terms mentioned in this reference are negligible for our application.

Notice, however, that electron collision experiments of this type—i.e., without analysis of the electrons after collision—actually seldom determine the probability of transition to a definite excited state  $s$  and thereby the corresponding ratio  $f_s/E_s$ . (At best this happens when one measures the fluorescence from excited atoms, but even here photoemission cascades complicate the interpretation.) Usually one observes some end effect  $\alpha$ , e.g., ionization or even the fluorescence from a residual ion, which may follow excitation to different states  $s$  with different probabilities  $\eta_{sa}$ . The experiment then measures the quantity

$$\sum_s (f_s/E_s) \eta_{sa} \quad (2.40)$$

rather than a specific  $f_s/E_s$ . This circumstance complicates the interpretation of experiments, but electron collision experiments retain notable advantages of simplicity and accuracy. Notice also that in special cases  $\eta_{sa}$  may have a simple dependence on  $s$ , in which case the measurement of (2.40) acquires particular interest; specifically, Platzman has pointed out that  $\eta_{sa}=1$  for the production of ionization in slightly impure helium, whether  $s$  belongs to the discrete or to the continuous spectrum, so that (2.40) coincides with the momentum  $S_{-1}$  defined in Sec. 2.4.

### 3. EXPERIMENTAL ASPECTS

This section consists of brief notes and data concerning the technical developments and the technical limitations which have conditioned recent measurements of oscillator strength distributions and which seem relevant to foreseeable further progress. With regard to the direct measurement of absorption coefficients we consider separately the characteristics of radiation sources and detectors and the procedures of spectral analysis and absorption. A final section deals with subsidiary experiments that provide more detailed information on absorption processes. Other methods of measurement will be discussed only incidentally. Reference to more detailed descriptions of experimental methods will be relied upon insofar as possible.

Progress in the measurement of absorption coefficients between 10 and 1000 eV has been limited primarily by the total effort required to overcome a number of difficulties, rather than by any single major obstacle. Each of the techniques utilized in recent years existed in some form in the 1930's, except for synchrotron light sources. However, the practical utilization of various techniques and the possibility of combining them effectively have been enhanced greatly by progress on counting devices and on their associated electronics, by the availability of powerful pumps and by greater familiarity with vacuum techniques.

Synchrotron light, whose continuous spectrum extends far into the vacuum ultraviolet, was first observed in the 1940's. Its application to absorption spectroscopy had a brief trial in the 1950's, and has been carried out

rather extensively since 1963. This development has played an important role but has not actually provided most of the data reviewed in the present article.

A review of the history and methods of far ultraviolet spectroscopy was published by Tousey in 1962 (To62). For the approach from soft x-ray spectroscopy, see (Sa57, To57, LRS60, Lu61). For the measurement of oscillator strength distributions by inelastic electron scattering see (Ku68).

### 3.1. Spectral Line Sources

The traditional radiation sources of absorption spectroscopy have spectra with numerous strong lines. Optical-type sources utilize gas discharges in which atoms are separated from any chemical combination, and are excited and ionized, often multiply ionized. Their external excited electrons emit line spectra when dropping to lower levels. The emission from multiply ionized atoms extends throughout our spectral range of interest. X-ray sources with line spectra rely on the ejection of inner atomic electrons by electron bombardment, generally of a solid target, followed by emission of x rays of characteristic well-known wavelengths when the inner shell vacancies are filled by outer electrons in a radiative process.

The spectra of gas discharges generally consist of very large numbers of lines, often a fraction of an angstrom apart. X-ray spectra consist of fewer lines. In either case, a spectral distribution of intensity shows the lines superposed on a continuum, and part of the continuum may consist of stray radiation. Absorption measurements are made for discrete wavelengths in the middle of individual lines. Therefore these measurements cannot cover the whole spectrum continuously and do not yield an adequate analysis of fine structures in the absorption spectra. A typical source intensity is  $10^6$  photons/spark Å in the center of a line at  $\sim 200$  Å emerging from a  $1 \times 0.0025$ -cm slit.

The gas discharges of interest to us operate in successive pulses. Reproducibility, at least of the average intensity and spectral distribution, over successive sets of pulses no longer appears to cause concern, to an accuracy of a few percent.

### 3.2. Sources with Continuous Spectrum

Discharges in the noble gases produce continua of usable intensity in the region of the lowest ionization thresholds, above 600 Å in wavelength ( $\lesssim 20$  eV). The intensities have been increased by high performance differential pumping at the slit through which the light emerges from the source (TJL58, NHH62). Other discharges have also been improved to yield usable continua in approximately the same range (Ga66). The light originates not only from gas or vapor atoms but also from material removed from container walls. Discharges yielding continua that extend to much higher photon energies have been reported (BRV61)

but not yet utilized extensively. [Note added in proof: Professor W. R. S. Garton kindly informs us that such discharges have now been utilized up to 100 eV photon energy.]

The "synchrotron light" from high-energy electron accelerators provides a continuum of smooth, rather uniform spectral density up to a limit whose photon energy increases with the cube of the electron energy. The light beam is naturally well collimated. It must be piped out from a high vacuum through a slit and effective differential pumping must be maintained throughout, with care to prevent contamination of the accelerator by noxious substances. The light beam intensity from an accelerator of moderately high energy ( $\sim 180$  MeV) amounts to  $\sim 5 \times 10^8$  photons/sec Å for 40-eV photons emerging through a  $1 \times 0.1$ -cm slit. Some exploratory work on absorption spectroscopy was done at Cornell with a 300-MeV synchrotron (TH56), but extensive applications began only in 1963 with a 180-MeV accelerator at the U.S. National Bureau of Standards. For technical details on this source, see (CM65, MEC67). Other accelerators have been utilized since 1965, particularly at Frascati (JM66), Tokyo (Sa66a) and Hamburg (HK67).

The bremsstrahlung spectra produced by electron bombardment of solid targets, long familiar in x-ray physics, are convenient for absorption spectroscopy but have a low yield of radiation below 1000 eV. However, Lukirskii and collaborators have recently succeeded in utilizing this type of source down to  $\sim 60$  eV (LZ63, LZB64) by exploiting improved techniques, sacrificing resolving power and counting over extended periods. In the region of 50 Å (argon L edge) a counting rate of  $\sim 60$  sec $^{-1}$  was obtained over a spectral band of 0.094 Å. The source absorbed 0.6 kW; application of substantially higher power is conceivable.

### 3.3. Absorption Spectroscopy

The spectroscopic portion of an absorption experiment in the 20–500-eV range necessarily presents non-trivial problems owing to the combination of optical and vacuum requirements. Commercial instruments are becoming available at this time for the major portion of the range, where one uses gratings ruled especially for grazing incidence. Crystal diffraction using stearate or other large-cell materials has not yet achieved high resolution for lack of sufficiently perfect crystals. A resolving power of approximately 1 part in 2000 has been achieved in the synchrotron light spectrograph (MC65). Additional mechanical problems arise when one attaches a spectrograph to an accelerator that dissipates a large amount of ac power.

The vacuum requirement may be of the order of  $10^{-6}$  mm Hg, to accommodate windowless photomultipliers and to minimize absorption by contaminant substances. In a spectrometer with a ruled grating, approximately 10% of the incident photons at 200 Å are diffracted into

the first-order spectrum. Crystal spectrometers have a lower efficiency.

The absorbing sample is necessarily in gas or vapor form for the study of absorption by single atoms. Cross sections from  $\sim 0.1$  to  $\sim 100$  Mb ( $10^{-19}$  to  $10^{-16}$  cm $^2$ ) are considered here, so that the sample may range from  $10^{-8}$  to  $10^{-4}$  moles/cm $^2$ . The sample may be placed between source and grating, between grating and detector, or it may fill the grating chamber itself as in (MC65). This last arrangement is simplest but it allows the gas to penetrate everywhere, except for differential pumping at the entrance and exit slit, and it requires the sample to be at a very low pressure which is more difficult to measure accurately. Arrangements with contained samples require the use of exceedingly thin windows (LZ63, ET64) or of slits with a high-pressure gradient to be maintained by differential pumping. Samson (Sa64) inserted the sample between two ionization chambers that served as monitor and detector, respectively. This last arrangement has increased the measurement accuracy and permitted the use of a thicker sample but it requires a higher radiation intensity.

Since most elements are metallic, samples of their vapors to serve as absorbers can exist only at high temperatures or in the form of atomic beams. Vapor samples often contain a fraction in molecular form, which complicates the analysis of data (HC65). These circumstances, combined with the other necessary characteristics of absorbing samples, has thus far severely restricted the range of elements accessible to investigation in vapor form. Progress has been made recently in this direction by utilizing a shock wave to vaporize a solid deposit on a thin window and simultaneously triggering a light source (see particularly Ga66, p. 121). A number of absorption spectra have been obtained for elements in the form of metallic films. The gross features thus observed in the spectral range above  $\sim 100$  eV are probably characteristic of the individual atoms rather than of their state of aggregation.

Analogous remarks may be made concerning the elements that occur in the form of molecular gases, notably H<sub>2</sub>, N<sub>2</sub>, and O<sub>2</sub>. Data on these elements are often presented in a form that attributes half of the molecular absorption to each atom. This procedure involves inaccuracies that are poorly known but may be serious; for a preliminary discussion of this subject see (CF66).

#### 3.4. Detectors

Photographic detection is simple and can proceed at low intensities with long exposure times. It permits an easy inspection of absorption spectra. On the other hand, it does not lend itself well to extensive quantitative measurement of absorption coefficients, because the calibration of plate densities is laborious and inaccurate. Accuracies of about 10% in the absorption coefficient

have been achieved but are difficult to exceed. Faster photographic plates suitable for our spectral range have been developed recently, as discussed in (MEC67).

Electric detection and measurement of radiation is inherently flexible and accurate and can be very sensitive, but it requires an additional effort on subsidiary apparatus. Photon absorption in solid cathodes or in gas molecules can serve as a counter trigger. Initial amplification can be provided by a standard electron multiplier arrangement or by a gas discharge as in Geiger counters. Measurements can proceed by photon counting or by current integration.

Most of the electric detectors must operate either at high vacuum or, on the contrary, at pressures higher than the rest of the system. Maintaining the necessary pressure differential by a window presents a problem with radiations that are very strongly absorbed. The availability of powerful pumps makes it easier to maintain large pressure differentials through entrance slits or pinholes.

For a review of electric detectors see (To62).

#### 3.5. Subsidiary Experiments

Experiments observing the products of photoionization can determine the magnitude and relative phase of probability amplitudes for atomic transitions from the ground state to different ionized states. Such experiments may involve the photoelectron, the residual ion or possibly both of them in coincidence, although coincidence experiments have not yet been performed.

Measurements of the spectra of photoelectrons determine the relative probability that the residual ion has been left in any level of its discrete or continuous spectrum. Some experiments of this type have been performed recently using electric (FMcDV67, BET67, Sa67) or magnetic (TM66, Ca67) spectrometers. To determine the relative transition probability and phase of different degenerate channels, one requires the angular distribution of photoelectrons (CZ67, Li67); progress is also being made on this type of observation (BET67). All these experiments have to overcome the difficulties attendant to the limited intensity of sources and to any measurements on low energy electrons.

Experiments on the residual ion may determine its charge—i.e., the probability of double or multiple photoionization—or its state of excitation by measuring the spectrum and intensity of subsequent emission of radiation. Charge measurements have been performed by means of a mass spectrometer (CK65, Ca67). Measurements of fluorescence by the ion have been performed thus far only following ionization by electron bombardment (StJL64, HW63, HK66, MdH67) and can be interpreted in terms of photoionization as indicated in Sec. 2.6. Quantitative measurements of fluorescent radiation, especially in the vacuum ultraviolet, hinge on an adequate analysis of detection efficiency involving effective solid angles and anisotropy of emission.

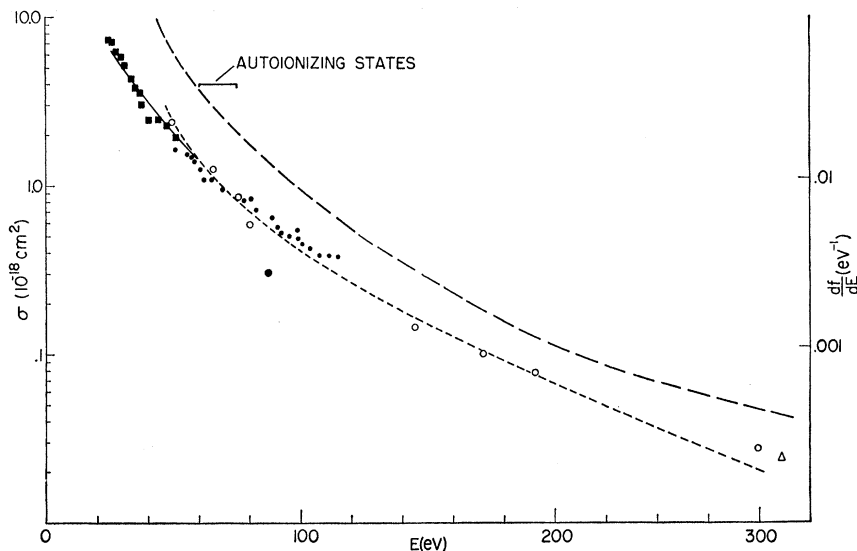


FIG. 3. Absorption spectrum of He: Experimental points: ■ Sa66, ● LTE65, ○ LBZ64, △ DS31. Theoretical calculations: — Hydrogenic approximation, — BMcV65, - - - BK67.

#### 4. EXPERIMENTAL DATA AND INDEPENDENT-ELECTRON CALCULATIONS

Section 4 presents the main evidence on the distribution of oscillator strengths. The available experimental data are displayed graphically together with the results of comparatively simple calculations which provide a semiquantitative interpretation of their gross features. Since these calculations can now be extended to all elements and to their entire spectra, theoretical results will also be presented which have not yet been subjected to direct experimental test. Certain systematic discrepancies between theoretical and experimental data emerge in this chapter and the finer features of the experimental data are not dwelt upon. The progress achieved thus far toward resolving these discrepancies and toward providing a fuller and more dependable treatment of the distribution of oscillator strengths forms the subject of later chapters.

##### 4.1. Survey of Experimental Evidence

In the intermediate range of energies, which is the primary subject of this paper, only the five noble gases He, Ne, Ar, Kr, and Xe have been studied systematically. Their absorption spectra, which have been treated in considerable detail in another recent review (Sa66), are shown in Figs. 3-7. These data provide the main basis for theoretical analysis and generalization to other elements. Thus Figs. 4-7 have been plotted on a double logarithmic scale to emphasize the over-all spectral dependence and show the agreement with or departure from various theoretical models.

Below 100 eV the absorption spectrum has been studied in detail for each gas at closely spaced intervals in  $E$  by various investigators (see Sa66). We show in the figures only a representative sampling of the available data in this spectral range. Departures from the hydro-

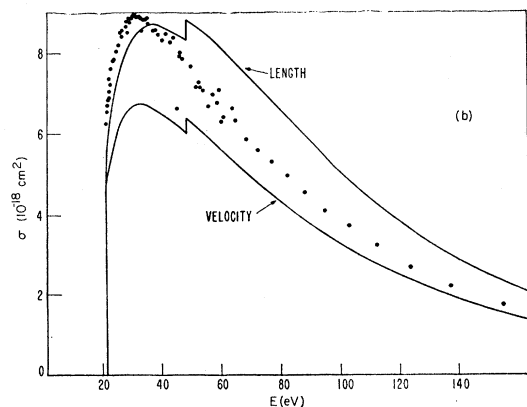
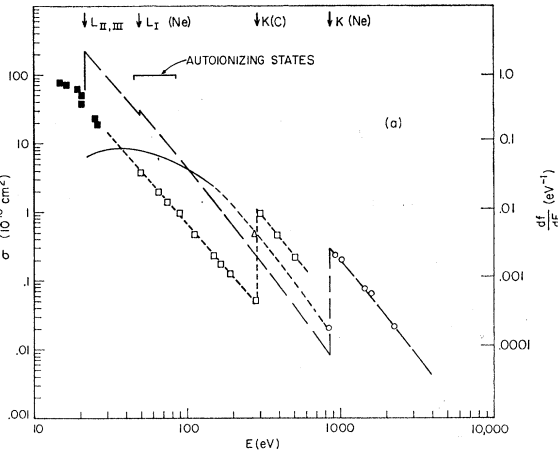


FIG. 4. (a) Absorption spectra of Ne and CH<sub>4</sub>. Ne: — Sa66, □ DS31, ○ Be58; CH<sub>4</sub>: ■ WWW55, □ LBZ64. — Hydrogenic approximation. (b) Comparison of experimental data (Sa66) with a "best wave-function" calculation (HL67) (see Sec. 5.5).

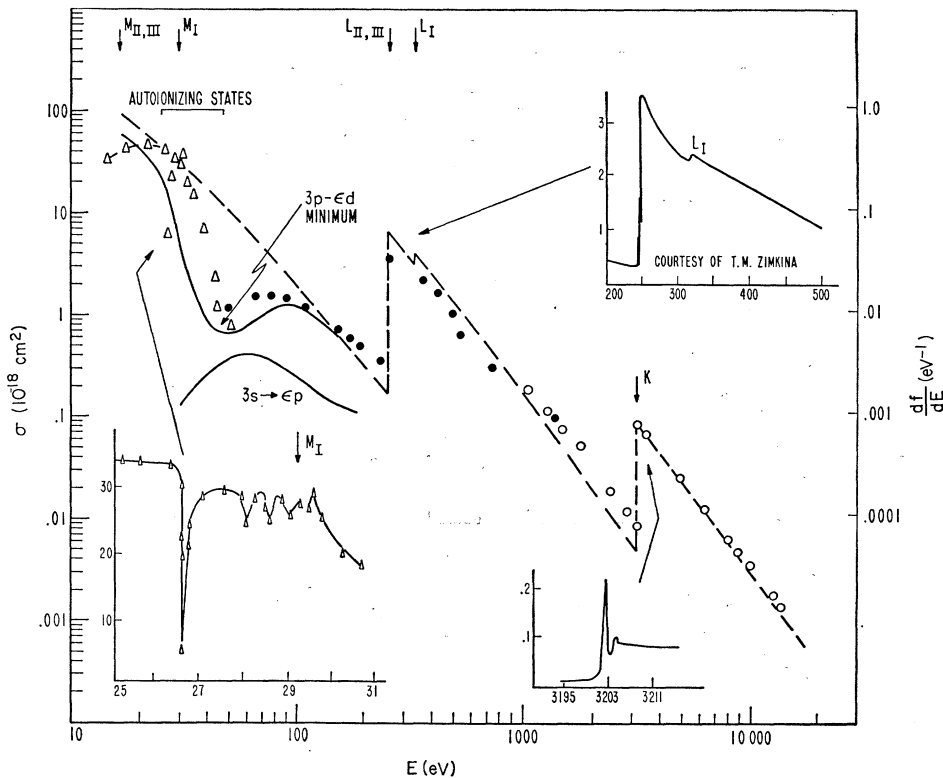


FIG. 5. Absorption spectrum of Ar. Experimental points:  $\Delta$  Sa66,  $\bullet$  LZ63,  $\circ$  Be58. — Hydrogenic approximation, — one-electron mode (MC68). Insets: Details of the  $M_I$  (Sa66),  $L$  (LZ63), and  $K$  (Sc63) thresholds.

genic approximation shown in Figs. 4–7 constitute one of the prominent features of these spectra (see Introduction). The single-electron model using realistic central potentials provides a reasonable first-order estimate of  $df/dE$  as will be more fully discussed in this section and the next. Data based on this approximation are shown for Ar, Kr, and Xe. Rather extensive calculations have recently been performed for Ne (HL67) (see Sec. 5.5) and He (BMcV65, BK67) and results based on this work are shown in Figs. 3 and 4. Data on  $\text{CH}_4$  are also shown in Fig. 4(a) for comparison with Ne (see Sec. 4.6). Discrete lines due to excitation of autoionizing states have been observed in all of the rare gases in the spectral ranges indicated in each figure; they will be discussed in Sec. 8.1. Finally, absorption has been studied in detail near the higher thresholds in Ar, Kr, and Xe. Profiles of the behavior near thresholds are shown in the insets of Figs. 5 and 7(a), and 6(b) and 7(c). The detailed structure near the first ionization threshold for these gases has been treated in detail elsewhere (Sa66) and is not indicated in these figures.

The absorption spectra of the alkalis, which are easily vaporized, have been observed since the twenties (FMC26) in the quartz ultraviolet range. Recent work (HC65, HC67) has extended earlier measurements on Li, Na, and K to photon energies of  $\sim 21$  eV and has increased the accuracy of measured cross sections to  $\sim 10\%$ . Absorption spectra for the alkalis in this range

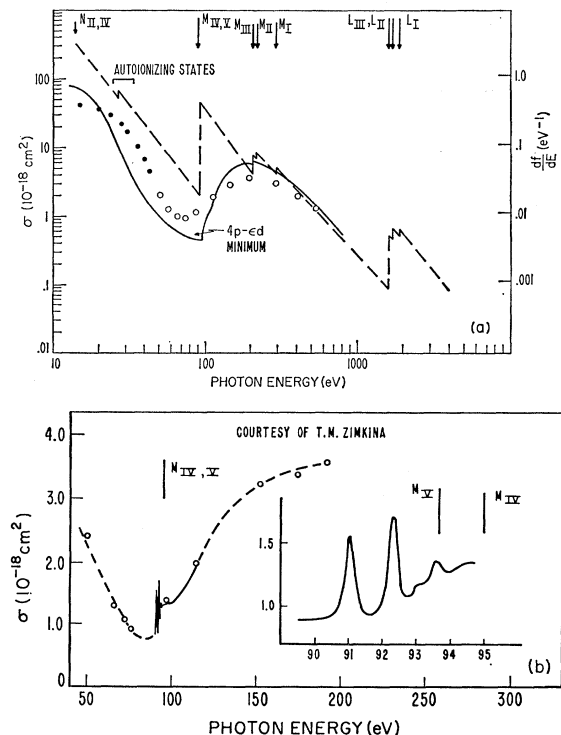


FIG. 6. Absorption spectrum of Kr. (a) Experimental points:  $\Delta$  Sa66,  $\circ$  LBZ64. — Hydrogenic approximation, — one-electron model (MC68). (b) Details near the  $M_{IV,V}$  threshold (LBZ64).

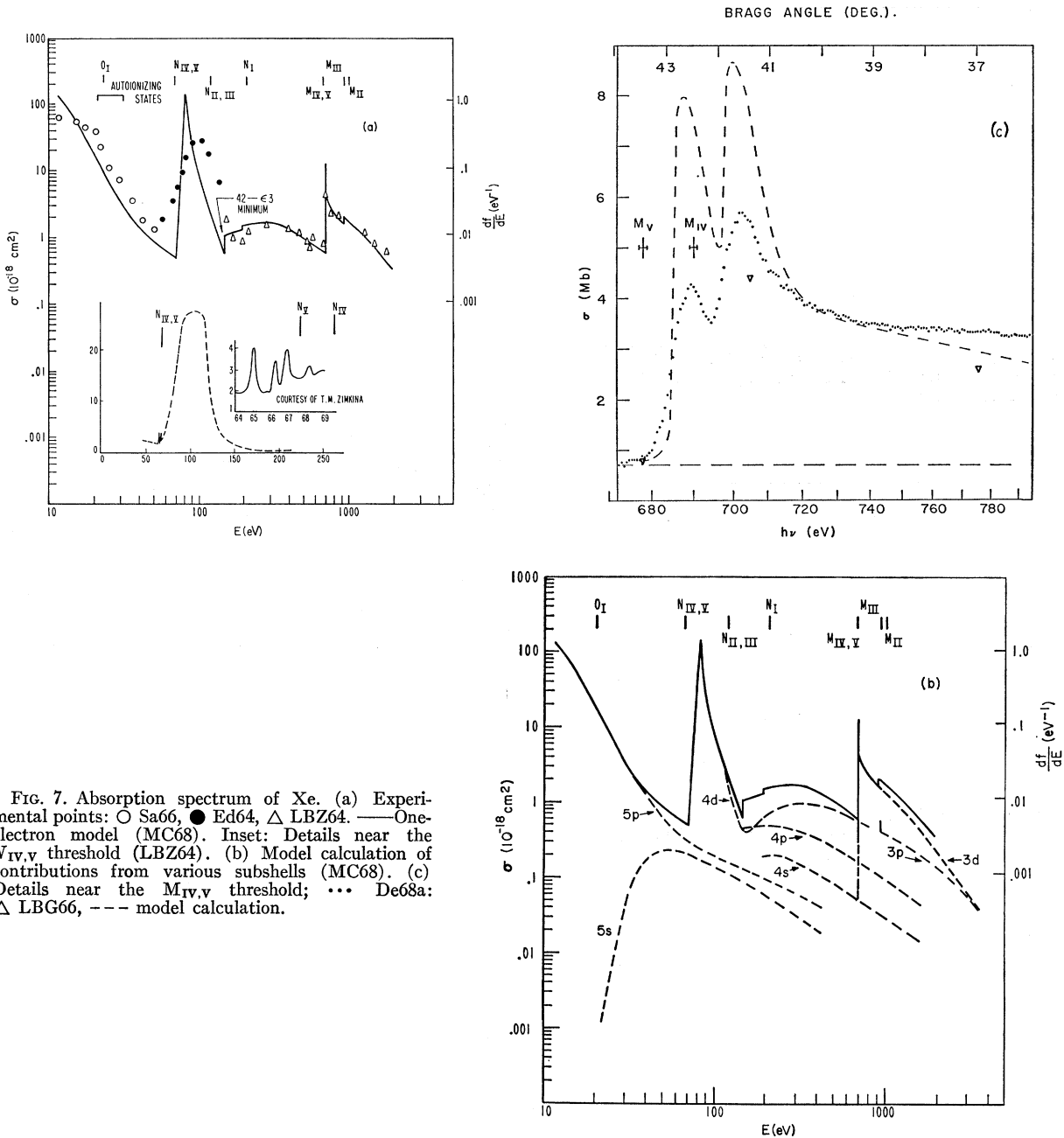


FIG. 7. Absorption spectrum of Xe. (a) Experimental points: ○ Sa66, ● Ed64, △ LBZ64. — One-electron model (MC68). Inset: Details near the  $N_{IV,V}$  threshold (LBZ64). (b) Model calculation of contributions from various subshells (MC68). (c) Details near the  $M_{IV,V}$  threshold; ⋯ De68a: △ LBG66, --- model calculation.

are shown in Figs. 8–11. Theoretical estimates for Li and Na are also shown in Figs. 8 and 9 and are discussed in Sec. 4.5. These curves are plotted on a linear energy scale beginning at the ionization threshold and, in contrast to the plots for the rare gases, represent an extremely small fraction of the total oscillator strength.

While extensive work has been done in the ultraviolet range for a number of other metals which can be vaporized (Ga66), interest has focused on the discrete structure of their spectra. Consequently, absorption cross sections have been measured for only a few elements of this type; i.e., Mg, Ca, Sr, Ba, Tl, and Cd.

Absorption spectra for Ca and Tl (on a wavelength scale) are shown in Fig. 12 and for Ba in Fig. 28. These plots are included to show the presence of large absorption peaks due to autoionizing states lying above the ionization threshold. Note that discrete structures are quite apparent in particular ranges of the continuous spectra of most elements, e.g., the ranges indicated in Figs. 4–7 for the rare gases and the region above 13 eV in the K spectrum shown in Fig. 10. Normally, discrete structures do not contribute a major share of the absorption averaged over 5–10 eV; the near ultraviolet spectra of certain metals appear exceptional in this

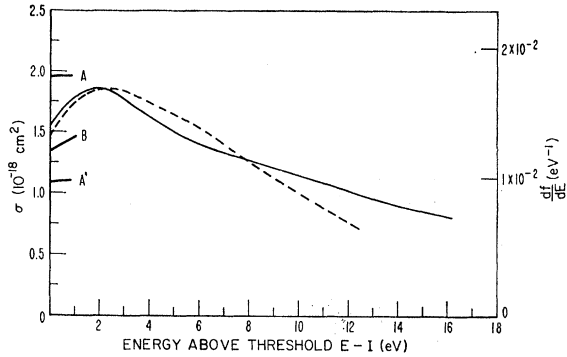


FIG. 8. Absorption spectrum of Li. — Experiment (HC67); - - - Hartree-Fock calculation (Se67); A and A': Best wavefunction calculations (length and velocity) (Ta64). B: Quantum defect method (BS60).

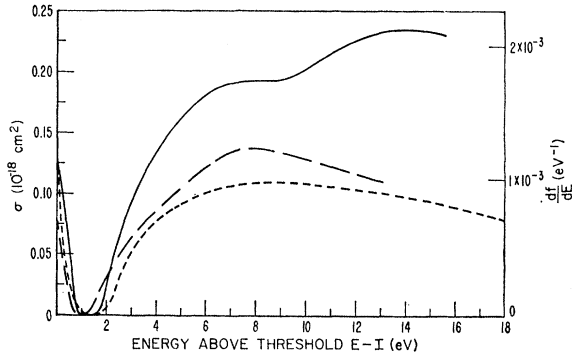


FIG. 9. Absorption spectrum of Na. — Experiment (HC67). - - - (MC68) and - - - (Bo64) model calculations.

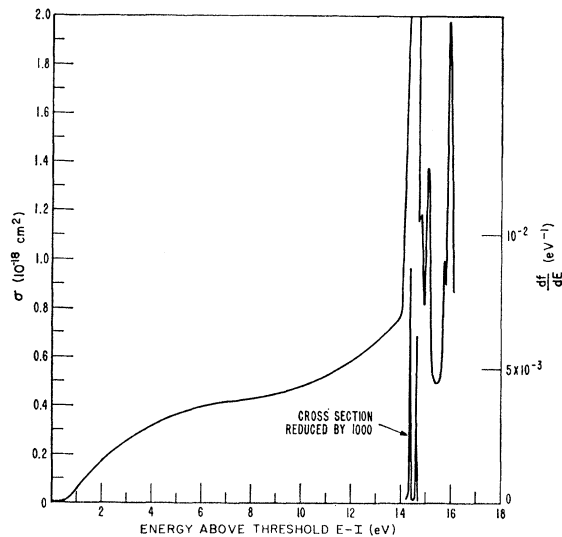


FIG. 10. Absorption spectrum of K showing discrete M-shell excitations above 14 eV (HC67).

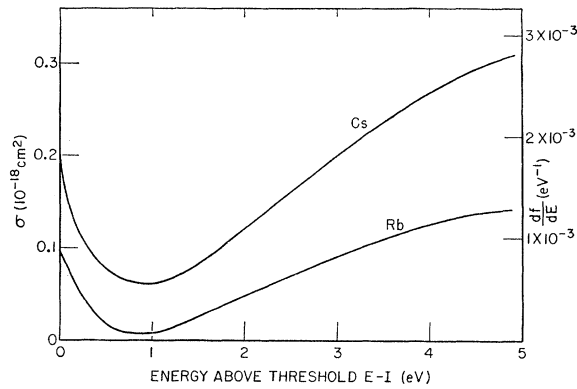


FIG. 11. Absorption spectra of Rb and Cs near threshold (Ma67b, pp. 115 and 116).

respect, for reasons discussed in Sec. 7.2. For a discussion of the profiles of discrete structures in the continuum, see Sec. 8.1.

Data have been obtained on the absorption cross sections for a number of materials in the form of thin metal films (WG55, JM66, JMD67, To57, Sa66a, ZFGZh67, HKSS68). While the emphasis in this research has been on solid-state properties of the metals, the cross sections at high energies represent to a large

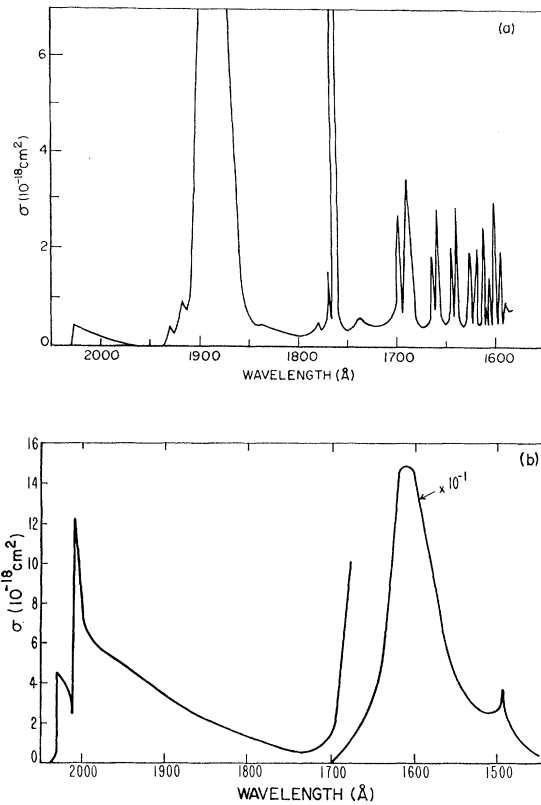


FIG. 12. (a) Absorption spectrum of Ca (DH60). (b) Absorption spectrum of Tl (Ma54).

extent the absorption by free atoms. Figure 13 shows a portion of the oscillator strength spectrum of metallic Cu obtained with a synchrotron light source (HKSS68). It also shows the corresponding integral spectrum (see Sec. 2.4) together with a theoretical estimate of this spectrum obtained by a single-electron-model calculation for the free Cu atom (MC68). Figure 14 shows a comparison of the absorption cross section for Au films in the 100–400-eV range with the analogous one-electron model calculation (MC68) for free atoms. Similar calculations (CFH67) for both Au and Bi indicate that solid-state effects have little influence on the spectral behavior of the cross sections for these elements in this spectral range.

The spectral behavior of absorption for a number of elements with atomic numbers between 50 and 71 has

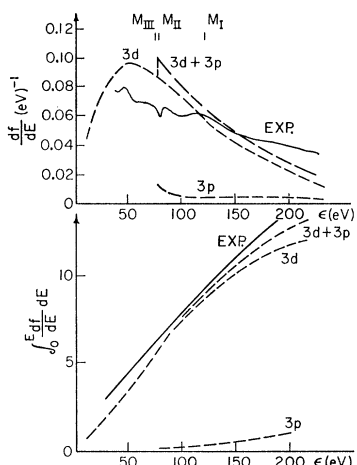


FIG. 13. Differential and integral spectra of oscillator strength for Cu. — Experimental (HKSS68) (The integral curve includes information on low energy data from other sources.) - - - Calculation by single-electron model (MC68) (The contribution of the 4s and 3s electrons is not included.)

been measured in the 50–500 eV-range (ZFGZh67) and is shown for  $Z=50, 57, 60, 62, 67$ , and  $71$  in Fig. 15. While these data consist of unnormalized cross sections, they represent a first attempt at studying the spectral behavior of absorption as a function of  $Z$ .

The transmission and reflection of light by thin metallic films has been studied extensively for certain materials (CHH64, HJH67, CMHA66) chiefly because of the practical importance of the optical properties of such films (HAT65). Data of this type can be reduced to absorption cross sections; however, little work has been done toward this end.

The absorption spectrum of silicon has been measured near the ionization limit (Ri67) by dissociating  $\text{SiHCl}_3$  in a shock tube. Data on the absorption of the atmospheric gases ( $\text{N}$  and  $\text{O}$ ) in their atomic states also has recently been obtained (SC65, CE67, CHLT66) by dissociating these gases by successive discharges. While

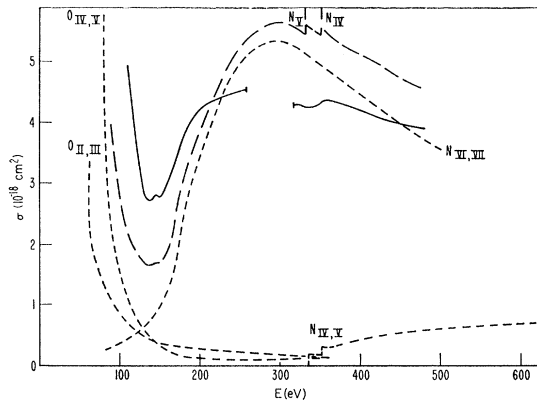


FIG. 14. Absorption spectrum of Au in the 100–500-eV region. — Experiment (JM66). - - - One-electron calculation, - · - individual subshell contributions (MC68).

these techniques provide useful data, the results obtained so far will not be considered here since they provide little information on the spectral shape of absorption cross sections. The relevance of the absorption spectra of molecular gases (e.g.,  $\text{N}_2$ ,  $\text{O}_2$ ) for atomic properties has not been established (CF66).

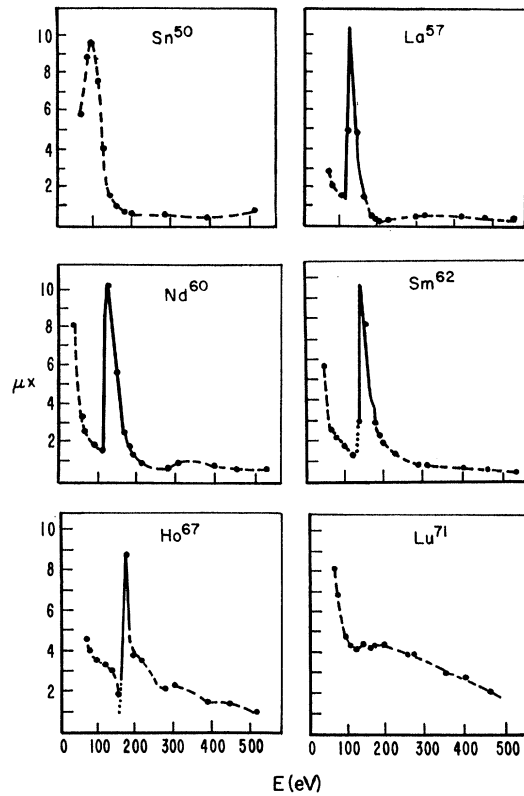


FIG. 15. Absorption spectra of Sn, La, Nd, Sm, Ho, and Lu in the 50–500-eV region. Ordinates represent  $\mu x$  (i.e., products of absorption coefficient and film thickness) but  $x$  has not been measured (ZFGZh67). Note added in proof: Absolute values of  $\mu$  have now been obtained by the same authors.

As noted in the introduction, the evidence on absorption coefficients in the x-ray range, above 10 keV, has been treated in detail in WG57. This treatment has been improved and extended partially toward lower energies in later works (McG59, HB66, SP67). Evidence on discrete absorption spectra of the light elements has been compiled by WSG66.

#### 4.2. Single-Electron Model

In this section we assume that the spectrum of oscillator strength of each atom results from the sum of contributions due to alternative independent transitions of any of its electrons from one stationary state to another one. Each of these one-electron states will be characterized by the usual set of quantum numbers  $nlms$ , applicable to particles moving in a central field without any appreciable spin-orbit coupling, that is, by a wave function

$$\psi_{nlms} = u_{nl}(r) Y_{lm}(\hat{r}) \chi_s. \quad (4.1)$$

Here  $\chi_s$  is a spin orientation symbol ( $s = \pm \frac{1}{2}$ ),  $Y_{lm}$  is a spherical harmonic, and

$$u_{nl}(r) = P_{nl}(r)/r \quad (4.2)$$

is a radial wave function. The index  $n$  takes all integral discrete values larger than  $l$  as well as values corresponding to the continuous spectrum, more properly designated by the residual kinetic energy  $\epsilon$  with which the electron leaves the atom. The wave function  $P_{nl}$  obeys a radial equation

$$d^2P_{nl}/dr^2 + (2m/\hbar^2)[E_{nl} - V(r) - l(l+1)\hbar^2/2mr^2] \\ \times P_{nl}(r) = 0, \quad (4.3)$$

where  $V(r)$  represents a potential chosen so as to achieve a desirable approximation, as discussed in the following sections.

In our model, all states with equal  $n$  and  $l$  are degenerate in energy and differ only in orientation. In accordance with Sec. 2.1 we consider only oscillator strengths for transitions  $nl \rightarrow n'l'$ , averaged over orientation. A standard calculation (BS57) reduces the expression (2.3) to

$$f(nl \rightarrow n'l') = \frac{2m(E_{n'l'} - E_{nl})}{3\hbar^2} \frac{l+l'+1}{2(l+1)} [R(nl, n'l')]^2, \quad (4.4)$$

where  $E_{nl}$  and  $E_{n'l'}$  are eigenvalues of (4.3) and

$$R(nl, n'l') = \int_0^\infty r P_{nl}(r) P_{n'l'}(r) dr. \quad (4.5)$$

The factor  $\frac{1}{3}$  in (4.4), being the average of  $(z/r)^2$  over the directions of  $\hat{r}$ , compensates for the replacement of  $z$  in (2.4) by  $r$  in (4.5). The factor  $(l+l'+1)/2(2l+1)$

arises from the averaging over  $m$  and  $m'$ . Selection rules restrict  $l'$  to the values  $l \pm 1$ .

The theoretical problem considered in this section consists of: (a) calculating  $P_{nl}$ ,  $P_{n'l'}$  and the radial integral (4.5), (b) assessing the influence of various physical circumstances upon the values of this integral, (c) comparing the results with the experimental evidence. Equation (4.4) provides theoretical information on the spectral distribution of the oscillator strength which pertains to the electrons of each subshell ( $nl$ ). The quantity to be compared with the absorption spectrum of an atom is, instead, the sum of the contributions of the electrons of all subshells. For an atom whose ground state has  $Z_{nl}$  electrons in its ( $nl$ ) subshell, we represent the total spectral distribution of oscillator strength by

$$\hbar^{-1} df/d\omega = \sum_{nl'n'l'} \sum_{l'=\pm 1} Z_{nl} f(nl \rightarrow n'l') \delta(E_{n'l'} - E_{nl} - \hbar\omega), \quad (4.6)$$

where  $f(nl \rightarrow n'l')$  is given by (4.4).

Notice that, even though the independent electron model considered in this section represents an approximation to be discussed further in Sec. 5, the analysis of the total spectrum into contributions from the different subshells is physically well defined. Subsidiary experiments that measure the energy of photoelectrons can determine the probability of photoabsorption by electrons of different subshells (or, more accurately, of absorption processes that leave a vacancy in different subshells). However, the contributions of different subshells cannot be clearly separated in the absence of extensive experimentation of this kind, so that theoretical data are at this time more detailed than their experimental counterparts (see Fig. 7). An experimental and theoretical study of the contribution of different  $M$  subshells of Kr to its photoabsorption between 300 and 1500 eV has been conducted quite recently (Kr68, CM68).

A few preliminary remarks can be made on the factors that influence the dependence of  $f(nl \rightarrow n'l')$  upon  $n'$ . The factor  $E_{n'l'} - E_{nl}$  is positive for photoabsorption processes and varies smoothly with  $n'$ . The profile of the spectral distribution of  $f(nl \rightarrow n'l')$  hinges then on the dependence of  $[R(nl, n'l')]^2$  on  $n'$ . Since the integrand of  $R$  includes the product of oscillating wave functions,  $R$  might conceivably be of either sign and its sign might change repeatedly as  $n'$  varies. Any point of zero of  $R$  is a zero of  $[R]^2$ , which is otherwise positive. It will be seen that in fact  $[R]^2$  appears to vanish only once or not at all, as a function of  $n'$ . It will be convenient, for the purposes of our study, to standardize the sign of  $R(nl, n'l')$  by requiring all radial wave functions  $P(r)$  to be positive for  $r \sim 0$ . This understanding attributes a definite sign to  $R$  and enables us to regard  $P_{n'l'}$  and  $R$  as continuous functions of  $n'$  and to conclude that whenever  $R$  turns out to have opposite signs in two separate ranges of  $n'$ , at constant  $n$ ,  $l$ ,

and  $l'$ , one zero (or, rather, an odd number of zeros) of  $R$  occurs between these ranges.

Mechanistically, one may think of resolving the process of photoabsorption into two stages, namely, the photoabsorption "proper" which takes place in the region of space occupied by the initial orbital ( $nl$ ) and the "subsequent escape" of the excited electron from this region. This escape through the outer layers of the atom may be regarded as a process of electron optics involving possible reflection of the electron or even its penetration of a potential barrier; accordingly the escape portion of the process can modify the probability of photoabsorption and the spectrum of  $f(nl \rightarrow n'l')$ . This mechanistic analysis corresponds, at least approximately, to a mathematical procedure which is carried out as a matter of routine convenience in calculations of (4.4). In the numerical solution of (4.3) to obtain the final state wave functions  $P_{n'l'}(r)$  one can, and often does, calculate initially a wave function  $\tilde{P}_{n'l'}$  with arbitrary normalization, specifically by choosing its series expansion  $r^{l'+1} + \dots$  to begin with a coefficient independent of  $n'$ . A (positive) normalization factor  $N_{n'l'}$  is evaluated in a second step. Thus one can set

$$\begin{aligned} P_{n'l'}(r) &= N_{n'l'} \tilde{P}_{n'l'}(r), \\ R(nl, n'l') &= N_{n'l'} \tilde{R}(nl, n'l'), \\ f(nl \rightarrow n'l') &= N_{n'l'}^2 \tilde{f}(nl \rightarrow n'l'). \end{aligned} \quad (4.7)$$

The factor  $\tilde{P}_{n'l'}(r)$  is still dependent on  $n'$  but it cannot vary much, in the region where it overlaps  $P_{nl}(r)$ , unless the energy  $E_{n'l'}$  varies by amounts comparable to the potential energy  $V(r)$  in this region, i.e., comparable to  $E_{nl}$ . Therefore  $\tilde{f}(nl \rightarrow n'l')$  can depend on  $E_{n'l'}$  only on a "coarse" scale determined by the binding of the electron in its *initial state* ( $nl$ ).

On the other hand,  $N_{n'l'}$  depends on the values of  $E_{n'l'} - V(r)$  in the outer portions of the atom where  $V(r)$  is small. If  $E_{n'l'}$  is itself small,  $N_{n'l'}$  can vary sensitively as a function of the "escape energy"  $E_{n'l'}$  on a "fine" scale comparable to the binding energy of the outer shell electrons. Therefore the factor  $N_{n'l'}^2$  of  $f(nl \rightarrow n'l')$  incorporates characteristics of the final state ( $n'l'$ ) that may shape the absorption spectrum near the threshold for photoabsorption where  $E_{n'l'}$  is small. For negative  $E_{n'l'}$ , i.e., below each threshold, one gathers from the quantum defect theory (Se58, Se66) that the factor  $N_{n'l'}^2$  determines the discrete structure of the spectrum as anticipated in the prescription for constructing the histogram in Fig. 1, while  $\tilde{f}(nl \rightarrow n'l')$  can be regarded as a continuous function of  $E_{n'l'}$ . For small positive values of  $E_{n'l'}$  one finds characteristic variations of  $N_{n'l'}$  to be discussed in the following sections.

A further distinction can be made between properties of  $N_{n'l'}^2$  that depend on the escaping electron's motion before it has reached beyond all other electrons and properties that depend on the motion still farther out,

where the field obeys the Coulomb law. The former have been studied only recently (Sects. 4.7 and 4.8), the latter include the energies and relative intensities of discrete lines and are treated accurately by the quantum defect procedures (see Sect. 4.3, Se58, BS60).

Notice that, since the spectra  $f(nl \rightarrow n'l')$  with the same ( $n'l'$ ) and different ( $nl$ ) contain the same factor  $N_{n'l'}^2$ , this factor will affect equally the spectra near the absorption edges corresponding to different subshells ( $nl$ ). In fact, the usefulness of the factorization (4.7) depends on its ability to suggest and interpret such similarities (see Sect. 4.7).

Notice finally that the normalization factor  $N_{n'l'}^2$  is related to the phase shift  $\delta_{n'l'}$  of continuum wave functions  $P_{n'l'}(r)$  in such a way that a maximum of  $N_{n'l'}$  as a function of  $E_{n'l'}$  coincides at least approximately with a maximum of  $d\delta_{n'l'}/dE_{n'l'}$ . This connection, whose formulation is called a dispersion relation (see, e.g., GW64, p. 281) and is complicated by the occurrence of the long-range Coulomb field, establishes a relation between the photoabsorption spectrum of a neutral atom and the scattering of free electrons by the corresponding positive ion. The coefficient  $N_{n'l'}^2$  has been called the "enhancement factor" because of its role in collision theory (GW64, p. 274). The approximate calculation of phase shifts and normalization constants in a Coulomb field is treated in (SP62).

### 4.3. Hydrogenic Calculations

The wave functions  $P$  and the integrals  $R$  have analytic expressions when the potential  $V(r)$  of (4.2.3) obeys the Coulomb law (Go29, Su29). These expressions lend themselves readily to extensive tabulation or graphical representation. Therefore, they have been widely relied upon in the past. However, the hydrogenic approximation fails to account for conspicuous characteristics of the absorption spectra as indicated in the introduction and demonstrated by comparison with experimental data throughout this section. Nowadays, computer application yields numerical values of the  $P$  and  $R$  readily, extensively, and at reasonable cost for potentials  $V(r)$  much more realistic than the Coulomb one. The results obtained in this manner are treated in the following sections.

At this time the hydrogenic approximation, with a suitable complement of semi-empirical adjustments, appears useful for the following purposes. (a) To provide an initial frame of reference in which experimental data may be fitted, as illustrated by dotted lines in the figures of this section. (b) To provide reasonably accurate data in the x-ray range, above approximately 10 keV, as developed in (WG57, McG59, HB66). (c) To provide extensive and reasonably accurate data for the discrete and for the near-threshold portion of continua, for atoms with one or very few valence electrons, which absorb under near-hydrogenic conditions utilizing a limited amount of experimental input

data. The procedures for purpose (c) have been developed by Bates and Damgaard (BS49) and extended by Seaton and Burgess (Se58, BS60) under the name of "quantum defect method".<sup>9</sup> Their applications have been summarized in Sec. 3.7 of (Gr64) and discussed in (BN67). We shall deal with the hydrogenic calculations only briefly because each of these applications is peripheral to our main subject.

Consider a photoabsorption process that takes place within a certain range of distances  $r$  from the nucleus,  $r_0 \leq r \leq r_1$ . Within this range one approximates the potential energy of an electron by the Coulomb-type law

$$V(r) = -(Z-s)e^2/r + V_0, \quad (4.8)$$

where  $(Z-s)e$  represents an effective value of the nuclear charge in the range of interest and  $V_0$  a constant discussed below. The solutions of the radial equation (4.3) with this potential, in the range  $r_0 \leq r \leq r_1$ , can be represented as superpositions of two independent wave functions  $F$  and  $G$  for a hydrogenic ion of atomic number  $Z-s$ ; we assume  $F$  to be regular and  $G$  irregular at  $r=0$  and that they oscillate with  $90^\circ$  phase difference in the range of interest and we set

$$P_{nl}(r) = \cos \sigma\pi F(r) + \sin \sigma\pi G(r). \quad (4.9)$$

The parameter  $\sigma$ , called "quantum defect," depends on the unspecified potential in the inner range  $r < r_0$ . If  $P_{nl}$  pertains to a bound state which is effectively confined within  $r \leq r_1$  the corresponding energy eigenvalue is

$$E_{nl} = -(Z-s)^2 I_H / (n-\sigma)^2 + V_0. \quad (4.10)$$

In practice this hydrogenic approximation has been applied either to inner electrons, with  $r_0=0$  and  $\sigma=0$ , or to outer shell electrons for which  $r_1=\infty$  and  $V_0=0$ . The significance of the parameters  $s$ ,  $V_0$  and  $\sigma$  is indicated in the following paragraphs.

(a) *Inner screening effect.* The attraction exerted by the nucleus on an electron is partially compensated by the repulsion exerted by the other electrons. Assuming these electrons to be distributed with spherical symmetry about the nucleus, the electric field generated by them at a point  $P$  is the same as though all electrons lying closer to the nucleus than  $P$  were actually located at the nucleus; electrons farther out than  $P$  yield no net field at  $P$ . Under this assumption, the net attractive field at a distance  $r$  is  $(Z-s)e^2/r^2$ , where  $s$  is the average number of electrons that lie closer to the nucleus than  $r$  and thus contribute to screen off the nuclear charge. The hydrogenic approximation (4.8) assumes a fixed value of the "inner screening constant"  $s$  for each shell (or subshell), thus disregarding the fact that the screening charge actually varies while an electron of that shell moves radially. Semi-empirical estimates of  $s$  are usually taken from an early work of Slater (Sl30).

<sup>9</sup> A more recent extension of this method (Se66), which takes channel interaction into account, will be discussed in Sec. 8.3.

(b) *Outer screening effect.* Electrons farther away from the nucleus than the electron under consideration exert no net repulsion upon it, as discussed under (a), and do not affect its ability to absorb radiation. To this extent, the contribution of an inner electron to the oscillator strength of an atom at a given frequency is *approximately independent of the presence of outer electrons*.

However, this presence makes itself felt after an absorption process. As an electron, having gained energy from radiation, moves outward through the region occupied by outer electrons, these electrons start exerting a net repulsion upon it and thus contribute to its final kinetic energy. This excess energy is indicated by  $V_0$  in (4.8), where  $V_0$  represents the potential energy possessed by the electron at its initial position owing to the presence of the surrounding layers of outer electrons. The "outer screening potential"  $V_0$  depends on the number and radial distribution of outer electrons and ranges up to  $\sim 20$  keV near the nucleus of heavy atoms. The assignment of a constant  $V_0$  to an electron constitutes, of course, an oversimplification. For data on  $V_0$  see (Le53a) and Fig. 20.

The definition of the outer screening potential implies that the threshold for photoionization of electrons of a given shell is *lowered* by the corresponding value of  $V_0$ . Similarly the excitation energy  $E_{n'l'} - E_{nl}$  for transitions to discrete levels is lowered by the difference of the values of  $V_0$  for the initial and final states. Thereby outer screening influences the spectrum of oscillator strengths, but only to the extent that it allows contributions to occur in spectral ranges where they would otherwise be suppressed.

(c) *Quantum defect.* The representation of the effect of inner screening by the parameter  $s$  influences the energy eigenvalue  $E_{nl}$  and the wavelength of the wave function  $P_{nl}$  (or  $P_{n'l'}$ ) in the range of  $r$  that contributes primarily to the radial integral  $R$ . However, it affords no control over the position of the nodes and maxima of  $P_{nl}$  and  $P_{n'l'}$  in this range, a factor that has great influence on the value of  $R$  as we shall see. The quantum defect parameter  $\sigma$  serves to make a wave function more realistic by adjusting its phase of oscillation in the range  $r_0 \leq r \leq r_1$ , more specifically, by fixing the value of its logarithmic derivative at the inner boundary,  $r_0$ , of this range. For electrons in the valence shell and in excited states, for which the outer screening  $V_0$  vanishes and the inner screening constant  $s$  equals  $Z-1$ , adjustment of  $\sigma$  serves also to yield realistic energy eigenvalues. In fact,  $\sigma$  is normally obtained for these electrons by requiring the eigenvalue  $E_{nl}$  (or  $E_{n'l'}$ ) to agree with the corresponding experimental value.

An attempt has been made (McG67) to extend the application of the quantum defect method, including also inner electrons, by adopting different Coulomb potentials in the inner and outer regions of an atom. Only the inner screening was considered in the outer

region with  $s=Z-1$ , both inner and outer screening in the inner region. The joining radius and the outer screening were adjusted to yield a continuous potential and to fit one relevant experimental quantum defect. The results are on the whole surprisingly good; in particular the absorption of  $4d$  electrons in Xe agree with experiment far better than those obtained from an apparently much more realistic potential.

For further details on the calculation of oscillator strengths utilizing the quantum defect adjustment, the reader is referred to the original papers (BD49, BS60) and to a recent review (BN67). The results of calculations without this adjustment are given by general formulas and graphs in (Le53a). Here we shall only indicate some qualitative features of the results which are presented in (Le53a) and, to a partial extent, in standard references such as (BS57).

In the first place the oscillator strength of excitations  $nl \rightarrow n'l'$  is nearly 10 times larger for  $l'=l+1$  than for  $l'=l-1$  at equal  $n'$ . This result is understandable on the basis of a classical model, since a particle in a circular orbit necessarily increases its angular momentum when it absorbs energy; the same remains partially true for elliptical orbits. The quantum calculation deals with angular and radial coordinates separately and proves less transparent.

Secondly the spectral density  $df(nl \rightarrow \epsilon' l')/d\epsilon'$  decreases smoothly as  $\epsilon'$  increases from the threshold, so that its log-log plot shows little curvature for all values of  $nl$  and  $l'$ , provided the same value of the quantum defect holds for the initial and final states,  $nl$  and  $l'$ . The strengths of discrete transitions  $nl \rightarrow n'l'$  yield a low frequency extrapolation of the same plot when displayed in accordance with Sec. 2.4. The asymptotic trend for high energy is

$$df(nl \rightarrow \epsilon' l')/d\epsilon' \propto \epsilon'^{-l-7/2}. \quad (4.11)$$

The smoothness of this spectrum finds again an easy plausible interpretation in terms of classical orbits, in that the velocity variations along Kepler orbits are smooth and hence their Fourier analysis should also yield a smooth spectrum. However, a search for a corresponding interpretation of the quantum expression proved fruitless.<sup>10</sup>

Each radial integral  $R(nl, \epsilon' l')$  is a smooth, positive, monotonically decreasing function of  $\epsilon'$ , again with the proviso that a single value of  $\sigma$  is used. Positive also are the  $R(nl, n'l')$  which contribute to the discrete spectrum of oscillator strength. However, for the transitions between degenerate states ( $n'=n$ ), which have zero frequency and zero oscillator strengths,  $R(nl, nl')$  is negative. This fact is apparent from the plot of wave functions in Fig. 16, which shows  $P_{nl}$

<sup>10</sup> The quantum-mechanical expression includes as a factor a polynomial  $\sum_r a_r (\epsilon' - E_{nl})^{-r}$ ; each coefficient  $a_r$  is the sum of terms of alternating sign, with no clue to indicate why all  $a_r$  should in fact be positive.

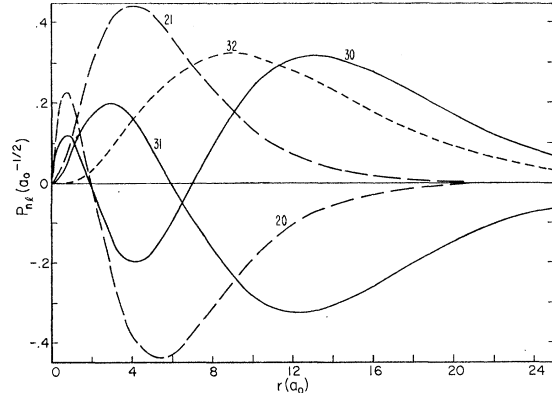


FIG. 16. Hydrogenic radial wave function  $P_{nl}$  for  $n=2$  and  $3$ .

and  $P_{n,l+1}$  to have opposite sign in the range of  $r$  where both of them are large; it has a key role in the interpretation of spectra in the nonhydrogenic approximation. On the other hand, applications with different quantum defects,  $\sigma$  and  $\sigma'$ , for the initial and final states lead to a different behavior of  $R$  and of  $df/d\epsilon'$ . In particular,  $R(nl, n'l')$  becomes negative also for  $n' \neq n$  when  $\sigma' - \sigma \sim 0.5$  (modulo 1). Seaton has interpreted the observed behavior of photoabsorption by alkaline atoms in the visible and near ultraviolet (Figs. 8-11) on the basis of the appropriateness of such values for  $\sigma' - \sigma$  (Se51, BS60).

#### 4.4. Average Electric Field and Centrifugal Repulsion

Realistic data on the average electrostatic potential energy  $V(r)$  of an electron in an atomic field, to be entered in (4.3), are now available from extensive self-consistent-field calculations of the electron distribution within each atom of the periodic system. A convenient complete tabulation has been provided by Herman and Skillman (HS63) using the Hartree-Fock-Slater approximation. Many other tabulations exist, which are less complete though often based on a higher approximation; earlier catalogs of them were provided by Hartree (Ha57, App. I) and Knox (Kn57).

Whereas self-consistent potentials have to be determined by separate calculations for each kind of atom, a less accurate representation applicable to all atoms is provided by the Thomas-Fermi formula  $V(r) = -Ze^2\varphi(r/\mu)/r$ . Here  $Z$  is the atomic number,  $\varphi(x)$  a universal tabulated function (Fe28), and  $\mu (=0.47Z^{1/3} \text{ \AA})$  is a suitable unit for radial distances. This formula does not reflect the shell structure of the atom but is reasonable for values of  $r/\mu$  of the order of unity. Systematic errors arise from the fact that it yields an excess density of electrons near the nucleus and again in the outermost layers of an atom.

The attractive electric force,  $dV/dr$ , amounts to approximately  $Ze^2/r^2$  for small  $r$  and to  $e^2/r^2$  for large

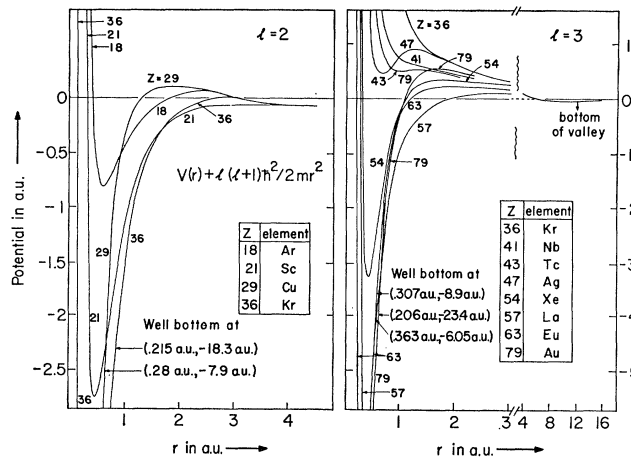


FIG. 17. Sum of electrostatic and centrifugal potentials for electrons with  $l=2, 3$  (RF68).

$r^{11}$  For intermediate  $r$  it hardly follows the Coulomb law assumed by the hydrogenic approximation but varies more steeply. It follows more nearly an  $r^{-3}$  law, in the range  $\mu < r < 4\mu$ ; more specifically, it approximates  $0.9Ze^2\mu/r^3$ , as implied by the fact that the Thomas-Fermi function  $x_\varphi(x)$  has a flat maximum with peak value 0.48. For still larger values of  $r$  the attraction decreases even more rapidly than  $r^{-3}$  before attaining its limiting form  $e^2/r^2$ .

These properties of the attractive force law prove very important when considered together with the repulsive centrifugal force which—for a fixed angular momentum—also follows a  $r^{-3}$  law, namely,  $l(l+1)\hbar^2/mr^3$ . The total force will then be attractive or repulsive in the broad range  $\mu < r < 4\mu$  depending on the sign of  $0.9Ze^2\mu - l(l+1)\hbar^2/m$ , that is, of  $0.8Z^{2/3} - l(l+1)$ . For each value of  $l$  it changes rapidly from strongly repulsive to strongly attractive as  $Z$  increases along the periodic system and overtakes the critical value  $[\ell(\ell+1)/0.8]^{3/2}$ . This critical balance between attractive and repulsive forces has long been known to underlie the chemical and spectroscopic properties of the transition and rare-earth elements (Fe28).

Even when this balance is favorable to attraction for  $r < 4\mu$ , it may still shift in favor of centrifugal repulsion for larger  $r$  near the edge of the atom where the attraction drops faster than  $r^{-3}$ . Indeed, as emphasized by Goeppert-Mayer (GM41), the combination of electric attraction and centrifugal repulsion may give rise to a two-valley profile for the combined potential of (4.3),

$$V(r) + l(l+1)\hbar^2/2mr^2. \quad (4.12)$$

Figure 17 illustrates this fact,<sup>12</sup> which also influences the spectrum of oscillator strengths.

<sup>11</sup> The Thomas-Fermi formula must be modified (Fe31) to ensure this behavior for large  $r$ .

<sup>12</sup> The data in the figure disagree with the statement of (GM41) that two separate valleys occur for  $l>2$  but not for  $l=2$ . The discrepancy stems from inaccuracy of the Thomas-Fermi method as applied in (GM41), see footnote 11.

It was pointed out in Sec. 4.3 that outer screening has no effect on the spectrum of oscillator strengths, within the hydrogenic approximation. Accordingly  $df/d\omega$  would depend on the photon energy  $\hbar\omega$  and on the forces in the portion of the atom where radiation absorption occurs, that is, in the range of  $r$  where  $P_{nl}(r) \neq 0$ . Except for the occurrence of the absorption edge,  $df(nl \rightarrow \ell'l')/d\omega$  would not be expected to vary much within any energy range  $\Delta(\hbar\omega) \ll E_{nl}$ . This assumption implies that the traversal of outer shells by an excited electron does not influence the probability of its excitation. Its validity hinges, in turn, on the applicability of the semi-classical WKB approximation to the wave function  $P_{n'l'}$  where it no longer overlaps  $P_{nl}$  (Ro36). Now, this application is indeed warranted under near-hydrogenic conditions but it is frustrated by the occurrence of the potential ridge in Fig. 17, for electrons escaping with  $l \geq 2$  and with a residual kinetic energy of the order of 10 or even 50 eV. The consequences of this breakdown are discussed in Sec. 4.7.

Whereas the Thomas-Fermi potential varies smoothly as a function of the atomic number  $Z$ , a more realistic potential  $V(r)$  does not vary uniformly, especially at radial distances of the order of 0.5–1 Å. At constant  $r$  and increasing  $Z$ ,  $V(r)$  experiences oscillations that follow the successive filling of valence subshells, i.e., the periodicity of chemical elements. It also experiences irregular variations associated with irregularities in the orderly filling of subshells. All these variations are affected by the chemical state of each atom, but we consider here isolated neutral atoms only. These variations of  $V(r)$  extend over a range of the order of 30% as shown in Fig. 18, that is, they are by no means small. Complete data on  $V(r)$ , calculated in the Hartree-Fock-Slater approximation, are contained in (HS63) and, at least implicitly, in other tabulations of Hartree-Fock data. However the oscillations of  $V(r)$  have been

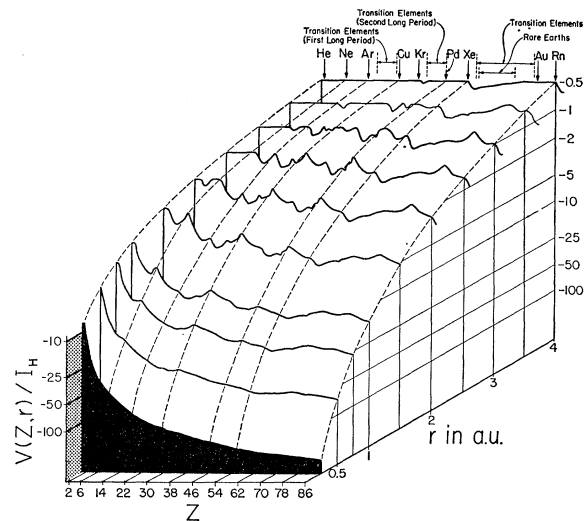


FIG. 18. Relief map of  $V(Z, r)$  (RF68).

emphasized (RF68) only after their influence on absorption was brought out by calculations (MC68) to be discussed in Sec. 4.8.

We have discussed the potential  $V(r)$  thus far as though it were well defined within the frame of the single-electron model and of self-consistent-field theory, but actually it is not. Firstly exchange effects are not represented correctly by any "local" potential. Secondly exchange effects differ for the initial and final states  $P_{nl}$  and  $P_{n'l'}$ , as they depend on the symmetry of the whole many-electron state and on the angular momentum of each electron. Finally, the change of state of the electron under consideration changes the average field affecting the other electrons and thereby disturbs the self-consistency of the whole system. These circumstances introduce considerable arbitrariness in the determination of the potential  $V(r)$  to be utilized in the radial equation (4.3).

The Hartree-Fock-Slater method utilized by (HS63) represents exchange effects by adding to the potential a term proportional to the  $\frac{1}{3}$  power of the electron density. The calculations of oscillator strengths by Cooper (Co62) utilized a potential  $V$  such that (4.3) would be obeyed by the same eigenfunction  $P_{nl}(r)$  of the electron under consideration and eigenvalue  $E_{nl}$  as are obtained by an accurate Hartree-Fock calculation. Thereby  $V(r)$  allows correctly for the effect of exchange on  $P_{nl}$ , but the use of the same  $V(r)$  for the calculation of  $P_{n'l'}$  leads to substantial error as discussed in 4.5 and in Sec. 6. The readjustment of other electrons following the transition  $nl \rightarrow n'l'$  was disregarded in these calculations, on the premise that its influence may be allowed for separately (see Sec. 7).

The use of different potentials  $V(r)$  for the calculation of  $P_{nl}$  and  $P_{n'l'}$  may well yield more realistic wave functions but it disturbs the calculation of the oscillator strength and indeed its very definition. Wave functions  $\psi_{nlms}$  and  $\psi_{n'l'm's'}$ , obtained from different potentials, are no longer solutions of the same Schrödinger equation. Therefore, the formulas of Sec. 2.1 no longer rest on a consistent, albeit approximate, theoretical construct. In particular the alternative expressions of  $f_s$  (2.3), (2.8), and (2.10) are no longer consistent. Actually, the degree of approximation achieved in the calculation of  $f_s$  has often been tested by comparing the values obtained from the alternative formulas. Discrepancies of 10–50% are not uncommonly found in such tests (see Sec. 5.5).

#### 4.5. Resonance near Threshold

The oscillator strength of the valence electron of the alkali atoms Na, K, Rb, and Cs has long been known to be strongly concentrated in the lowest line,  $ns \rightarrow np$ . The intensity of successive lines  $ns \rightarrow n'p$  decreases rapidly with increasing  $n'$ ; photoabsorption in the ultraviolet a little beyond the ionization threshold is very low (DJM53) (Figs. 9–11). Calculations with

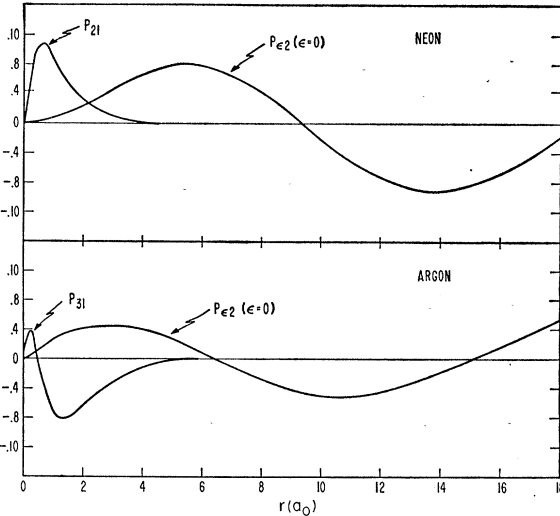


FIG. 19. Radial discrete ( $P_{21}$  and  $P_{31}$ ) and continuum wave functions  $P_{e2}$  with  $\epsilon=0$  for Ne and Ar. Abscissa in units of Bohr radius ( $a_0$ ) and ordinates in units of  $a_0^{-1/2}$  for discrete and of  $(a_0 l_H)^{-1/2}$  for  $P_{e2}$ .

$P_{n0}$  and  $P_{n'1}$  obtained by the Hartree-Fock method (Se51) and by the hydrogenic approximation with different quantum defect parameters  $\sigma(l=0)$  and  $\sigma'(l'=1)$  (BS60) reproduce this trend. They also show that photoabsorption actually goes through a near-zero minimum in the ultraviolet, owing to a sign reversal of the radial integral  $R(n0, \epsilon'1)$  as  $\epsilon'$  increases [That the minimum does not quite reach zero stems from the existence of slightly different fine structure wave functions  $P_{\epsilon'1/3/2}$  and  $P_{\epsilon'1/1/2}$  for which the  $R$  integrals vanish at slightly different energies.] The accuracy of this prediction (Se51) has been verified only recently (HC65).

Systematic calculations have shown this behavior of alkali spectra to be only one example of a general feature of absorption spectra due to the nonhydrogenic character of realistic potentials  $V(r)$  (Co61, Co62, Fa61). As noted in Sec. 4.3, hydrogenic matrix elements  $R(nl, n'l')$  are normally positive, but they are negative for the degenerate case  $n'=n$  which corresponds to zero-frequency transitions. In nonhydrogenic atoms one finds consistently that  $R(nl, n'l')$  is also negative for a range of values of  $n' \geq n$ , when states with  $n'=n$  exist and are not occupied in the ground state of the atom. Negative but small values of  $R$  may also persist in a few atoms following the complete occupation of the ground state subshell  $n'l'$ . The immediate cause of this behavior emerges from an examination of the wave functions in the integrand of  $R$ .

Consider the pair of wave functions  $P_{31}$  and  $P_{e2}$  of Ar, for  $\epsilon=0$ , in comparison with  $P_{31}$ ,  $P_{32}$ , and  $P_{42}$  of H (see Figs. 19 and 16). The product  $P_{31}P_{e2}$  for Ar resembles the product  $P_{31}P_{32}$  of H much more than it resembles  $P_{31}P_{42}$  despite the fact that  $\epsilon=0$  in Ar corresponds to a higher degree of excitation than  $n=4$

in H. The integral  $R(31, \epsilon 2)$  for Ar at  $\epsilon=0$  is easily seen to be negative from the figure. On the other hand Fig. 19 also shows that  $R(21, \epsilon 2)$  for Ne is positive at  $\epsilon=0$ .

The condition indicated above for the occurrence of  $R < 0$  implies more detailed guide rules restricting this occurrence. (Recall that we deal here only with transitions out of the ground state of the atom.) These rules are:

- (1)  $R < 0$  for  $l'=l+1$  only, since  $(n'=n, l'=l-1)$  is always occupied when  $(nl)$  is; this rule excludes only a minor fraction of the total oscillator strength as noted in 4.3.
- (2)  $R < 0$  for  $n > l+1$  only, since  $(n'=n=l+1, l'=l+1)$  does not exist; this rule excludes He and Ne for which  $n=l+1$  altogether as well as the 1s, 2p, 3d, and 4f subshells of all atoms.

The range of  $n'$  over which  $R$  is negative varies greatly, depending on the degree of departure from hydrogenic conditions and on the binding energy of the  $nl$  electrons. For example, in the Li atom which resembles H most closely,  $R$  is found to be negative for  $n'=n=2$  only, but already positive for  $n'=3$ . Thus the point of zero appears to occur in Li between  $n'=2$  and  $n'=3$  as it does in H, whereas it occurs beyond the ionization threshold in the other alkalis. The plot of  $df/d\omega$ , extended to include the discrete spectrum as indicated in Sec. 2.4, rises in Li from  $n'=3$  to a second maximum a little beyond the ionization threshold [Figs. 2(b), 8]. The same maximum has been detected for Na and K only recently in the far ultraviolet (HC67). In the absorption spectra of Ar, Kr, and Xe the minima corresponding to zeros of the  $R$  integrals occur well beyond the ionization thresholds at  $\hbar\omega \gtrsim 2|E_{nl}|$ . In  $\text{Ag}^+$  the zero is estimated to occur at  $\hbar\omega \sim 6|E_{42}|$  (Co62).

In general, the oscillator strength spectrum of an atom shows a point of minimum wherever a sign reversal occurs in the  $R$  integral that contributes most of the strength in the relevant spectral range. These points are marked by arrows in the figures representing the spectra (with indication of the quantum numbers  $n$ ,  $l$ , and  $l'$  of the relevant transition). The oscillator strength drops extremely rapidly toward the minimum from the low energy side, but on the high-energy side the rise is usually slow and the following second maximum of  $R^2(nl, \epsilon l')$  is rather low. This rise and second maximum are often obscured in the complete spectrum of oscillator strength by the rapidly rising contribution of another transition; even the minimum of  $df(51 \rightarrow \epsilon 2)/dE$  is obscured for Xe.

The characteristics of the spectral maxima associated with negative values of  $R$  stem in part from each of the factors that are separated in (4.7). The resonance character, inherent in the concentration of oscillator

strength within a limited spectral range, relates to the occurrence of a strong maximum of the enhancement factor  $N_{n'l'}^2$ . The steep drop of  $f(nl \rightarrow n'l')$  beyond the maximum to a point of zero stems from the factor  $\tilde{f}$  and more specifically from the sign reversal of  $\tilde{R}$ .

The resonance character and the peaking of  $N_{n'l'}^2$  should relate to the variations of the phase shift  $\delta_{n'l'}$  of the wave function  $P_{n'l'}$  as the excitation energy increases. (The relevance of phase-shift variations was noted at the end of Sec. 4.2.) Actually the overlap of ground-state and excited-state wave functions, which we discussed above, depends on the trend of  $P_{n'l'}$  not for  $r \rightarrow \infty$  but near the edge of the atom, more specifically on the logarithmic derivative  $d \log P_{n'l'}/dr$  at some suitable radius  $r=\rho$ . This derivative is indeed related to  $\delta_{n'l'}$  and to the corresponding quantum defect  $\sigma_{n'l'}$  for discrete levels but in a manner that depends on  $n'$  through properties of Coulomb field wave functions. [The quantum defect  $\sigma_{n'l'}$  is equivalent to a phase shift in accordance with the formula  $\delta_{n'l'} = \sigma_{n'l'}\pi$  (see, e.g., Se58); we refer to  $\delta$  or  $\sigma$  indifferently. The quantum defect is normally practically constant over the restricted energy interval,  $\sim 2$  eV, occupied by most of a Rydberg series but variations of  $\delta$  over a range of 5–10 eV are often substantial.]

The analytical relationship between  $\delta_{n'l'}$  and  $(d \log P_{n'l'}/dr)_\rho$ , described, e.g., in (Ga63), has not been evaluated or discussed. However, an extensive set of calculations of  $R(nl, n'l')$  with hydrogenic wave functions has been carried out and studied in detail (BS60). This reference presents the results by means of a formula that brings out an oscillatory dependence of  $R$  on  $\sigma_{n'l'}$ ,

$$R(nl, n'l') \propto \cos \pi [\sigma_{nl} - \sigma_{n'l'} - \chi(nl, n'l')]. \quad (4.13)$$

The empirical parameter  $\chi$  compensates implicitly for the fact that  $(d \log P_{n'l'}/dr)_\rho$  actually matters rather than  $\sigma_{n'l'}$  itself. The change of sign of  $R$  for the atoms of alkalis and alkaline earths near the ionization threshold is traced in (BS60) to variations of  $\sigma_{n0} - \sigma_{n'l'} - \chi$  across a half-integer value. The cosine itself in (4.13) remains small in absolute value near the ionization threshold for these atoms.

The guide rule for the occurrence of negative  $R$ , that the state  $(nl')$  be not occupied while  $(nl)$  is, implies that  $\sigma_{nl'} < \sigma_{nl}$ . A lag of  $\sigma_{n,l+1}$  with respect to  $\sigma_{nl}$  arises because the centrifugal repulsion hinders the penetration of electrons with  $l'=l+1$  into the inner region of strong attraction to a greater extent than it does for the  $(nl)$  electrons. An increase of  $n'$  through the discrete spectrum and into the continuum implies an increase of the electron's energy which will enable it to penetrate deeply into the atom so that  $\sigma_{n'l'} + \chi$  approaches  $\sigma_{nl}$ . If this increase of  $\sigma_{n'l'} + \chi$  is rapid, amounting to a substantial fraction of unity over a limited energy range, it constitutes the earmark of a resonance. It implies then

the existence of a semi-stationary discrete state of the electron with a half-life inversely proportional to the maximum slope of the plot of  $\sigma_{n'l'} + \chi$  versus  $E_{n'l'}$  and with a large value of  $P_{n'l'}$  in the region where it overlaps  $P_{nl}$  (Wi55, Sm60, GW64).

The wave-function plots in Fig. 19 show that at resonance  $P_{n'l'} = N_{n'l'} \tilde{P}_{n'l'}$  has a high amplitude antinode region which overlaps the corresponding region of the bound state wave function  $P_{nl}$  extensively. In this sense  $P_{n'l'}$  represents a virtual eigenstate of the nonhydrogenic potential which binds the  $(nl)$  electrons within the confines of the ground-state radius. This eigenstate is virtual in that its higher energy permits the electron to escape into the outer region where the field is hydrogenic or even beyond it, away to infinite distance. The formation of a series of discrete bound states in the outer (hydrogenic) region is incidental to the nature of the virtual state. That is, the virtual state is unrelated to the oscillator strength of individual discrete transitions but it determines the envelope of the histogram that represents the whole series.<sup>13</sup> A similar situation occurs in the spectrum of the "giant resonance" of nuclear photoabsorption.

In the example of absorption by the valence electrons of alkaline or alkaline earth atoms, the  $\sigma_{n'l'}$  of excited  $\phi$  states lags by no more than  $\sim 0.5$  with respect to  $\sigma_{n0}$ . Hence the resonance may be said to lie near, or even below, the lowest line of the absorption spectrum, particularly so for Li. For these atoms  $\sigma_{n'l'} + \chi$  varies near the ionization threshold by 0.1–0.2 over a few eV. For the noble gases Ar, Kr, and Xe the calculations have not been carried out by the method of (BS60) or fitted into its pattern. The resonance appears to be near its peak at their ionization thresholds and to extend well into the continuum. Since  $l'=l+1=2$  for these atoms, the value of  $(d \log P_{n'l'}/dr)_\rho$  and their dependence on  $n'$  are influenced greatly by the "two-valley" character of the combined potential (4.12) and depend critically on it (see Fig. 17). Inadequacies of the model potential  $V(r)$ —even though minor—have a large influence on (4.12) and are presumably responsible for the large departures of calculated spectra shown in Figs. 5, 6, and 7 from the experimental results. (Recall the inherent limitations of any model potential indicated in Sec. 4.4.) The two-valley character of the potential is even more developed for  $l'=3$ . Here the resonance lies altogether at higher energy than the absorption threshold, as will be discussed in Sec. 4.7. Here again the quantitative disagreement between calculation for the  $4d$  electrons of Xe (MC68) and the experimental data (Fig. 7) stems presumably from inadequacy of  $V(r)$ . This matter is developed in Sec. 6.

To illustrate further the resonance near threshold one may consider the oscillations of charge density as-

<sup>13</sup> An example of such histogram envelopes—due to a different mechanism—is shown in Fig. 28.

sociated with photoabsorption in the relevant band of the spectrum. As noted in Sec. 2.1, the action of an oscillating electric field changes the ground state wave function  $\psi_0$  of an atom into an oscillatory superposition of  $\psi_0$  and of various excited state wave functions  $\psi_s$ . The absorption of photons of energy  $\hbar\omega = E_s$  may be interpreted as resulting from work exerted by the field upon the oscillating charge density

$$|\psi_0 + \psi_s \exp(-iE_st/\hbar)|^2.$$

Here we consider the charge-density oscillations

$$|\psi_{nlm} + \sum_{n'} \psi_{n'l'+1m} \exp[-i(E_{n'l'+1} - E_{nl})t/\hbar]|^2, \quad (4.14)$$

where  $(nlm)$  and  $(n'l'+1m)$  are quantum numbers of the ground-state and excited-state wave functions, and where the  $\sum_{n'}$  extends over the states with excitation energies ranging up to the point of zero absorption. As a first step of analysis, let us set  $t=0$  in (4.14) and compare the result with the corresponding expression for the H atom, which is

$$|\psi_{nlm} + \psi_{n'l'+1m}|^2. \quad (4.15)$$

(Recall that the position of radial nodes in the nonhydrogenic wave functions  $\psi_{n'l'+1m}$  throughout the resonance range of the spectrum corresponds to that of the hydrogenic  $\psi_{n'l'+1m}$ .) Now, the superposition of wave functions in (4.15) represents a "hybrid orbital," of the type which is involved in chemical bond formation; its charge density stretches in the negative  $z$  direction.<sup>14</sup> This orbital represents a stationary state of the H atom for which  $E_{n'l'+1} = E_{nl}$ . In nonhydrogenic atoms, where hybrid orbitals are actually relevant to bond formation, an orbital that forms a bond in the  $-z$  direction is appropriately represented by the wave function in (4.14) with  $t=0$ . The state represented by this orbital for an isolated nonhydrogenic atom is not stationary because  $E_{n'l'+1} - E_{nl} \neq 0$  (though it can become stationary in a molecule owing to the stabilizing action of bond formation). In order to follow the evolution of the nonstationary charge distribution (4.14) we can rewrite it in terms of a mean excitation energy  $\langle E_{n'l'+1} \rangle$  as follows

$$|\psi_{nlm} + \exp[-i(\langle E_{n'l'+1} \rangle - E_{nl})t/\hbar] \sum_{n'} \psi_{n'l'+1m} \times \exp[-i(E_{n'l'+1} - \langle E_{n'l'+1} \rangle)t/\hbar]|^2. \quad (4.16)$$

Insofar as the resonance band is comparatively narrow we can assume

$$|E_{n'l'+1} - \langle E_{n'l'+1} \rangle| \ll \langle E_{n'l'+1} \rangle - E_{nl} \quad (4.17)$$

and thus regard the  $\sum_{n'}$  in (4.16) as comparatively constant for a sufficiently short interval of time during

<sup>14</sup> This direction results from assuming a sign normalization such that  $Y_{10}(0) = Y_{1+10}(0)$ ; the normalization  $Y_{10}(0) = -Y_{1+10}(0)$  would yield an orbital stretching toward positive  $z$ .

which the exponential factor in front of it oscillates. These oscillations cause the sign of the interference of  $\psi_{nlm}$  and  $\sum_{n'} \psi_{n'l'm'}$  to reverse alternately. Accordingly the charge density represented by (4.17) pertains at  $t=0$  to a hybrid orbital in the negative  $z$  direction but at later times alternately to orbitals in opposite directions.<sup>14</sup> This oscillation is then damped, usually rather rapidly, to the extent that (4.17) represents only a crude approximation and the various terms of the  $\sum_{n'} \psi_{n'l'm'}$  soon get out of phase with one another. Nevertheless we conclude from this qualitative analysis: (a) The occurrence of the absorption peak near threshold for photoionization of  $\psi_{nl}$  states is associated with the ability of the atom under consideration to form orbitals by hybridization of  $\psi_{nl}$  and  $\psi_{n'l+1}$ . [The rules (1) and (2) above agree with this interpretation.] (b) The absorption process is associated with oscillations of a charge distribution that coincides alternately with that of hybrid orbitals in opposite directions.

One further aspect of the resonances near threshold deserves attention because it appears foreign to the familiar similarity between the spectra of successive elements in a column of the periodic system. The resonance appears only in the absorption of electrons with  $n > l + 1$ , according to rule (2), but not for  $n = l + 1$  even though atoms with electrons ( $n = l + 1$ ,  $l$ ) and ( $n > l + 1$ ,  $l$ ) belong to the same column. Thus absorption by the  $(2p)^6$  electrons of Ne exhibits no resonance, but absorption by the  $(3p)^6$  of Ar does; similarly no resonance occurs for the  $(3d)^{10}$  of Kr but there is one for the  $(4d)^{10}$  of Xe. In fact, other physicochemical differences have been known in the past to set the first element of each column apart from all the successive ones. The similarity of the first element to the successive ones appears confined to the systematics of their energy levels. Indeed, one can relate the differences in absorption spectra discussed here to differences in the ground-state characteristics by means of sum rules, as will be shown in Sec. 4.9.

#### 4.6. Nonresonant Absorption

The absorption spectra of  $l \rightarrow l+1$  transitions depart substantially from the hydrogenic profile even outside the spectral range and the circumstances where one observes the resonance near the threshold. A hydrogenic profile is observed rather soon after threshold only for absorption by sufficiently deep inner shells, such as the  $L_{II,III}$  of Ar near 250 eV (Fig. 5). However, the spectra of the  $l \rightarrow l-1$  components of absorption appear to approach the hydrogenic profile rapidly above their thresholds, at least as a rule.

Consider first the transitions  $(nl) \rightarrow l+1$  with  $n = l+1$ , which contribute the main absorption by  $2p$ ,  $3d$ , and  $4f$  electrons and for which no resonance occurs near threshold. Here the absorption is depressed near threshold by centrifugal effects discussed in Sec. 4.7, which are increasingly important with increasing  $l$ .

After the photoelectron escape energy  $\epsilon$  has increased sufficiently to overcome centrifugal effects a maximum of photoabsorption is reached. However the spectrum still remains rather flat beyond this maximum over a range of a few times the threshold energy, as demonstrated by the  $2p \rightarrow d$  transitions in Ne (Fig. 4) and  $3d \rightarrow f$  in Kr (Fig. 6).

This flatness, followed eventually by the onset of a rapid hydrogen-like decrease, may be interpreted as an effect of screening gradient. As noted in Sec. 4.3, the representation of the effect of inner screening by a parameter  $s$  with a fixed value for each subshell constitutes a drastic schematization. In a very rough sense one might regard each subshell as an onionlike construct of layers with different screening constants. Its absorption spectrum would then be regarded as the sum of hydrogenic spectra contributed by the various layers with correspondingly different thresholds.

This interpretation seems reasonably adequate for the  $2p$  electrons of Ne, for which the appropriate values of  $Z-s$  range from 1 to 8 (note that the  $2p$  and  $2s$  subshells interpenetrate considerably). The dependence of the absorption spectrum on the range of appropriate ( $Z-s$ ) values is demonstrated by the comparison in Fig. 4 of the spectra of the Ne atom and of the  $\text{CH}_4$  molecule, which have the same number of valence electrons. The effective ( $Z-s$ ) values for the  $\text{CH}_4$  valence electrons do not exceed 4 and the corresponding absorption spectrum is very nearly hydrogenic. Centrifugal effects near threshold are also weaker for  $\text{CH}_4$  than for Ne owing to the larger radius of the  $\text{CH}_4$  molecule. For inner  $3d$  and  $4f$  subshells, the range of relevant effective  $s$  values throughout the periodic table is also substantial, namely,  $\sim 10$  to 27 for the  $3d$  and  $\sim 28$  to 60 for the  $4f$  subshells; this range might account for the profiles of the corresponding absorption spectra, even though it is not as large as for the  $2p$  subshell.

The variations of effective screening across the thickness of a subshell become progressively less important as the atomic number increases, since the relative variation of  $Z-s$  matters rather than that of  $s$ . Indeed the wave functions  $P_{nl}$  and  $P_{\epsilon, l+1}$  become approximately hydrogenic, and so does the absorption spectrum of the  $(nl)$  subshell, as the increasing nuclear charge draws the subshell into an inner region where the nuclear charge predominates and the net field becomes approximately Coulombic.

Let us consider now the absorption spectra of  $(nl) \rightarrow l+1$  transitions with  $n > l+1$ . The circumstances that produce the resonance near threshold influence these spectra even beyond the spectral range where the resonance occurs and even in spectra where the resonance does not occur at all. As described in Sec. 4.5, the resonance effect stems from the occurrence of large negative values of the radial integral (4.5), namely,  $R(nl; \epsilon, l+1)$ . The resonance terminates at the value of  $\epsilon$  for which  $R$  vanishes. Above this energy  $R$  becomes

positive and passes through a "second maximum" before decreasing again with a trend that eventually becomes hydrogenic. Therefore the hydrogenic trend does not set in until  $\epsilon$  has attained values considerably in excess of that for which  $R$  vanishes. Evidence of the comparative flatness and of the spectral width of this nonhydrogenic second maximum can be observed, e.g., in Figs. 5 and 7, and particularly in the more extensive calculated data of (CF67) and (MC68).

The occurrence and character of this second maximum appears thus straightforward in the spectra of transitions  $(nl) \rightarrow l+1$  that actually exhibit the resonance near threshold. Consider now how the spectrum of such a transition varies as one compares atoms with increasing  $Z$ . As the subshell of bound states  $(n, l+1)$  becomes progressively filled up in the ground state of this sequence of atoms, the threshold for  $(nl) \rightarrow l+1$  transitions moves up in the spectrum and through the resonance. The threshold appears to reach the point of zero of  $R(nl, \epsilon l+1)$  at approximately the  $Z$  value at which the  $(n, l+1)$  subshell is just completed; a calculation shows  $R(31, \epsilon 2)$  to vanish just above threshold for Cu, the first element with a full  $3d$  subshell (MC68, see also Sec. 4.8).

For atoms with still higher  $Z$  values, the resonance near threshold does not occur at all but the "second" maximum remains as the main nonhydrogenic characteristic of the  $(nl) \rightarrow l+1$  spectrum above threshold. Thus we interpret the existence of a low flat maximum in the relevant spectra in the context of the interpretation of the resonance near threshold and of the variation of spectra along the periodic system. In the language of Eq. (4.13) one may say that the values of  $\sigma_{n'l'} + \chi$  near and above threshold are still smaller than  $\sigma_{nl}$  though not sufficiently smaller to make  $R(nl; \epsilon, l+1)$  negative.

As the atomic number increases further, well beyond the point where  $(n, l+1)$  is filled in the ground state, the threshold for  $(nl) \rightarrow l+1$  transitions moves further up in the spectrum and overtakes the second maximum as well. Thereafter the values of  $\sigma_{n'l'} + \chi$  approach  $\sigma_{nl}$  and the spectrum of these transitions eventually approaches the hydrogenic profile.

The asymptotic behavior of the oscillator strengths for large photon energies is given by

$$df(nl \rightarrow \epsilon l') / d\epsilon = \text{const } \epsilon^{-l-7/2} \quad (4.18)$$

under nonrelativistic conditions but irrespective of the hydrogenic approximation (RF67). The constant in this equation should be somewhat larger than predicted by the hydrogenic approximation by a factor  $\sim(1+5s/Z)$  as pointed out by Bethe (see WG57, note 7) owing to the actual lack of inner screening in the region nearest the nucleus which contributes most of the photoabsorption in the high energy limit. Recent calculations, with model potentials that do not utilize the schematized screening of Sec. 4.3, yield improved

agreement with experimental data in the 10–20-keV region (Ro65, MC68).

#### 4.7. Depression and Apparent Shift of Absorption Edges

According to the hydrogenic approximation, absorption spectra in the vicinity of thresholds should have the aspect illustrated in Fig. 5 for the  $K$  edge of Ar. They should exhibit a few absorption lines of a Rydberg series converging to the threshold, which are broadened by Auger-effect decay of the corresponding discrete levels<sup>15</sup>; this broadening causes most lines of the series to merge smoothly into one another and into the adjoining continuum. The actual threshold position is, therefore, not detectable. Nevertheless the absorption coefficient rises very substantially from the low to the high-energy side of the discrete lines. It is this net rise of absorption, confined within a spectral range of 3–5 eV, which one calls an "absorption edge"; its magnitude is called "jump ratio." Absorption edges below about 1 keV depart substantially from the pattern described above for various reasons and in various manners.

One such departure consists of the absence of any detectable jump ratio at the threshold for ionization of the outermost  $s$  electrons of the noble gases Ne, Ar, etc., which lie generally just below the valence subshell  $p$ . A 2–3% rise in absorption would be detectable. Actually autoionizing lines of Rydberg series converging to the relevant threshold have been observed. The analysis of their profiles, discussed in Sec. 8.1, shows that the net rise would only be approximately 1% in Ne and that it would indeed be negative by an amount of the same order in Ar, Kr, and Xe. A very small decrease of absorption can in fact be accounted for by configuration interaction (see Sec. 8) provided direct photoabsorption by the  $s$  subshell amounts to no more than  $\sim 1\%$  of the valence shell absorption at the relevant energy. The smallness of this ratio is now understood (MC68) in terms of proximity to the point of zero of the integral  $R(n0, \epsilon 1)$  as discussed in Sec. 4.6. The somewhat larger  $s$  absorption in Ne may be related to its point of zero occurring at lower energy for Ne ( $n=2$ ) than for Ar, Kr, and Xe, much as it occurs at lower energy for Li than for Na, etc. (see Sec. 4.5).

Available information does not suffice to judge to what extent the jump ratios of other subshells or atoms are similarly suppressed. The  $3d$  ( $M_{IV,V}$ ) threshold appears wholly suppressed in Lu near 190 eV, following the complete filling of the  $4f$  subshell (ZFGZh67, Fig. 15). The inner shell  $2s$  ( $L_1$ ) threshold in Ar has a jump ratio of  $\sim 1.05$  (Fig. 5). The  $3s$  ( $M_1$ ) threshold in Cu fails to appear in Fig. 13.

For transitions to final states with  $l' \geq 2$  the jump ratios are depressed at the edge by the centrifugal potential acting on the electron after the absorption process. Insofar as the net potential (4.12)—which

<sup>15</sup> The line broadening and profiles are treated in Sec. 8.

represents the combined contributions of electric attraction and centrifugal repulsion upon the escaping electron—is positive and varies smoothly as a function of  $r$ , the radial integral  $R(nl, \epsilon l')$  will be depressed at  $\epsilon \sim 0$  and will rise smoothly with increasing  $\epsilon$ . This behavior appears to occur in the absorption by the  $2p$  valence electrons of Ne, as we have seen in Sec. 4.6 (Fig. 4). However, we have also seen in Sec. 4.4 that the balance between the attractive and centrifugal forces is rather critical and tends to shift in favor of attraction as one proceeds toward lower  $r$  values across the valence shell of the atom. As shown in Fig. 17 this shift occurs at the peak of a potential ridge whose height is low and often negative for  $l'=2$  but often rises to the order of 10 eV for  $l'=3$ . Owing to this circumstance, rapid rises of absorption are observed in the spectra when  $\epsilon$  increases to a critical value  $\epsilon_c$  that permits the escaping electron to pass over the potential ridge, if any. This rise at  $\epsilon \sim \epsilon_c$  might be called a “delayed edge”. Figure 6(b) shows a clear example of spectral distortion by centrifugal forces near the threshold for absorption by the  $3d$  ( $M_{IV,V}$ ) electrons of Kr. One notices between 90 and 95 eV a threshold behavior of rather hydrogenic appearance with a modest jump ratio  $\sim 1.6$ ; this threshold is followed by a second, smoother but much larger rise that sets in above 100 eV. The hydrogenic edge was identified by its discoverers (CM64, LZB64) as representing only the contribution of  $3d \rightarrow p$  transitions, owing to the absence of any detectable  $3d \rightarrow nf$  lines in the discrete. The delayed edge above 100 eV represents the onset of  $3d \rightarrow ef$  transitions whose intensity becomes appreciable only for  $\epsilon > \epsilon_c \sim 10$  eV. A corresponding behavior is observed near the  $4d$  ( $N_{IV,V}$ ) edge of Xe (Fig. 7); here the onset of  $4d \rightarrow ef$  transitions yields a far sharper rise than in Kr, because it is boosted by the occurrence of a “resonance near threshold” (Sec. 4.5). Notably, model calculations (Co64, MC68) predict this rise to be even sharper than it is, a discrepancy that will be discussed in Sec. 6.

Proceeding now to different values of  $l$ , the absorption by  $4f$  electrons in  $4f \rightarrow eg$  transitions in Au and Bi has been observed (JM66, JMD67) and calculated (CFH67, MC68) to rise rapidly far above threshold ( $\epsilon_c \sim 50$  eV), which is not surprising since  $l'=4$  in this case (Fig. 14). At threshold even the  $4f \rightarrow d$  transitions should be depressed by a centrifugal barrier; the threshold itself has not yet been observed. With regard to the absorption spectra due to  $p \rightarrow d$  transitions by valence electrons, we have seen that Ne shows a depression near the edge but no sharp rise at higher energy that would constitute a delayed edge. For Ar, Kr, and Xe the influence of the centrifugal barrier is not readily disentangled from that of the resonance near threshold.

Actually the influence of the centrifugal barrier stands out, isolated from other factors, in the profiles of absorption edges in the 200–1000-eV range corresponding to subshells well below the surface of an atom.

Under these circumstances the factor  $\tilde{f}(nl; n'l')$  of the oscillator strength expression (4.7) may be regarded as practically independent of  $n'$  over a substantial range of energies near the threshold and the centrifugal effect bears entirely on the normalization factor  $N_{n'l'}^2$ . The examples of the  $2p$  ( $L_{II,III}$ ) edge in Ar and  $3d$  ( $M_{IV,V}$ ) in Xe are shown in Figs. 5 and 7(c), respectively. The  $2p \rightarrow d$  transitions in Ar appear to depart from the familiar hydrogenic profile of  $K$  edges (see, e.g., the Ar  $K$  edge in Fig. 5), in that the peaks of discrete lines lie well below the absorption-coefficient values observed beyond the edge. We interpret the rise in absorption over a  $\sim 5$ -eV range, from the peak (or average) of the resolved lines to its maximum beyond the edge as a change of the coefficient  $N_{n'l'}$ . Data with improved resolution seem necessary to determine how much of this change stems from hydrogenic and how much from nonhydrogenic effects.<sup>16</sup> The  $3d \rightarrow ef$  transitions in Xe yield a sharp rise in absorption at  $\sim 10$  eV above each of the well separated thresholds  $M_{IV}$  and  $M_V$ . Each rise reaches a maximum followed by a fairly rapid decrease, leveling off at about one half the preceding rise; this profile could be described as the effect of a virtual resonance in the  $ef$  states. The  $3d \rightarrow p$  transitions should produce an edge with small jump ratio at the actual threshold; this edge is barely visible in Fig. 7(c) (De68a).

The experimental and theoretical evidence on these centrifugal effects is thus far rather fragmentary. Attempts to establish their systematic trend over the periodic system are presented in the next section. Effects depending on  $N_{n'l'}^2$  should persist in edges above 1 keV for heavy atoms. As noted in Sec. 4.2 the effects arising from the escape of photoelectrons over the centrifugal barrier should be closely associated with phenomena in electron-ion scattering at energies  $\sim \epsilon_c$  which have not yet been investigated.

#### 4.8. Variation of Spectra Along the Periodic System

According to the hydrogenic approximation, the absorption spectrum of each subshell varies smoothly as a function of the atomic number  $Z$ . Its profile would

<sup>16</sup> Earlier attempts at interpreting the structure of this edge (LZ63) have been hindered by lack of data on the  $L_{II,III}$  splitting, whose value ( $\sim 2.2$  eV) has only recently been determined (De68). An interpretation of the low intensity of discrete lines has been given by Barinskii (Ba59) on the basis of a hydrogenic formula. The coefficient  $N_{n'l'}^2$  calculated in the hydrogenic approximation includes a factor  $III'_{p=0} (1 - p^2/n'^2)$ , which is called  $A(n', l')$  by Seaton (Se66). This factor does not depart very much from unity for the states with  $l'=1$  excited near a K edge. Barinskii emphasizes that for  $l'=2$  ( $L$  edge) and  $n' \sim 2.85$  ( $3d$  level of Ar) this coefficient is sufficiently lower than 1 to account approximately for the profile reported originally by (LZ63). The nonhydrogenic portion of the combined potential (4.12) pertaining to the  $n'd$  functions of Ar may in fact be confined to sufficiently low values of  $r$  for the hydrogenic coefficient  $A(n', l')$  to have a controlling influence on  $N_{n'l'}$ . We thank Dr. Barinskii for calling these matters to our attention. A higher resolution spectrum of the  $L_{II,III}$  edge of Ar has been obtained recently with the Tokyo synchrotron light [Sagawa *et al.* (to be published)].

not change much on a log-log plot; the spectrum would shift progressively toward higher frequencies and its peak intensity would decrease progressively.

The main nonhydrogenic features of the spectra could be obtained by model calculations with the Thomas-Fermi potential (Sec. 4.4) which still varies smoothly with increasing  $Z$ . The spectra thus obtained should also vary smoothly with  $Z$  but many of their qualitative characteristics would evolve and disappear as each subshell is drawn into the inner region where hydrogenic conditions prevail. Specifically each resonance near threshold would progressively be overtaken by the threshold, as this threshold moves toward high frequencies with increasing  $Z$ , and the resonance would eventually disappear. So would the "second maximum" be overtaken and disappear as anticipated in Sec. 4.6. Similarly, the threshold features described in Sec. 4.7 would vary smoothly with increasing  $Z$ .

Nonmonotonic variations of the spectra with increasing  $Z$ , due to the nonmonotonic variations of more realistic potentials described in Sec. 4.4, have emerged from systematic calculations (CF67, MC68), even though these calculations pertain only to a limited set of elements rather widely spaced along the periodic system. These variations of spectra are confined primarily to an energy range of the order of 10–50 eV from each threshold, since they originate from variations of  $V(r)$  near the edge of atoms. The major nonmonotonic variations apparently occur in the centrifugal effects described in Sec. 4.7; they derive from large variations of the height of the ridge in the effective potential (4.12).

Notice in this connection that the nonmonotonic variations of  $V(r)$  relate to variations of the electron density distribution in outer shells and therefore also to variations of the outer screening potential  $V_0$  discussed in Sec. 4.3. Empirical values of  $V_0$  can be obtained from (4.10) by entering experimental thresholds  $E_{nl}$  on its left-hand side and on its right-hand side standard values of  $s$  (Sl30) and  $\sigma=0$ . The values of  $V_0$  thus obtained (Fig. 20, see also Le53a) show periodic oscillations related to those of  $V(r)$  and to the structure of the periodic table. These oscillations may be related to

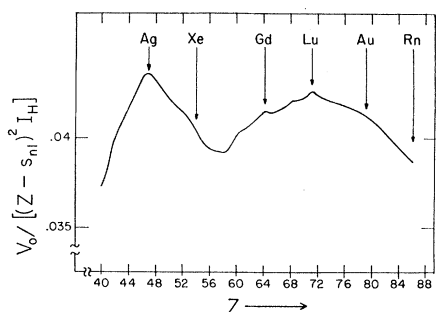


FIG. 20. Outer screening energy of 4s electrons (RF68).

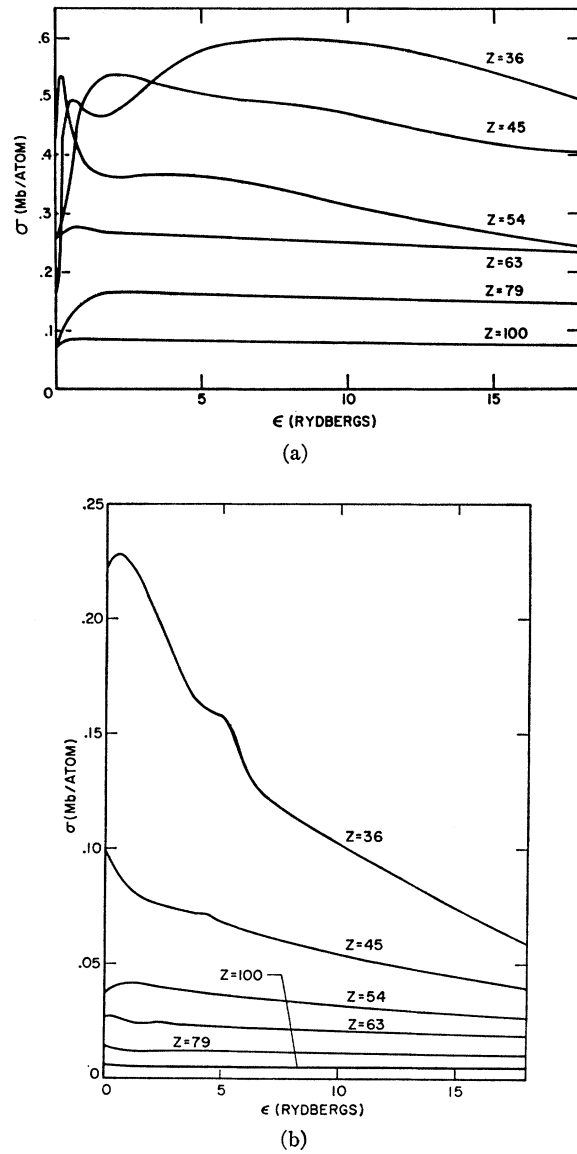


FIG. 21. Calculated cross sections for elements between  $Z=36$  and 100 (MC68). (a)  $3p\rightarrow ed$  transitions. (b)  $3p\rightarrow es$  transitions.

those of the critical values  $\epsilon_c$  of the electron escape energy at which a radial integral  $R(nl, \epsilon)$  rises sharply because  $\epsilon$  overtakes the ridge in the effective potential (Sec. 4.7). The variation of  $V(r)$  causes  $V_0$  and  $\epsilon_c$  to vary in opposite directions so that the critical photon energy  $h\nu_c = \epsilon_c - E_{nl}$ , at which a major rise of absorption appears in the spectrum, should vary more smoothly with increasing  $Z$  than the actual threshold energy.

The calculations of (MC68) also indicate the occurrence of minor maxima in the absorption spectra in the proximity of a threshold, which have not been discussed in preceding sections, but are indicated in Fig. 21.

Each of these nonresonant maxima in the spectrum of  $(nl \rightarrow nl')$  transitions appears to be overtaken by the threshold, as  $Z$  increases, approximately at the value of  $Z$  at which the filling of an  $(n'l')$  subshell is completed in the ground state. These maxima behave in this respect like the resonances near threshold. They might arise from systematic variations of the factors  $N_{el}^{-2}$  in (4.7) but this point remains to be investigated. The disappearance of each maximum upon completion of the  $(n'l')$  in the ground state is associated with a substantial reduction in the total oscillator strength of  $(nl \rightarrow nl')$  transitions. This reduction may be attributed to the "transfer" of oscillator strength from the  $(nl)$  to the  $(n'l')$  subshell, a subject to be discussed in Sec. 5.2.

A single experimental study appears to have been carried out to demonstrate the systematic variation of a major nonhydrogenic feature of the absorption spectrum (ZFGZh67, FZGZh67). This study concerns the height, width, and distance from the threshold of the resonance near the  $4d$  ( $M_{IV,V}$ ) threshold throughout the rare-earth group. The threshold position is not well defined, the more so as the experiment utilized absorbers in metallic state and as the standard data on threshold energies (BB67) are undependable in this spectral range. Discrete lines observed near the threshold are presumably characteristic of the metallic state. A sample of the results is shown in Fig. 15.

Any detailed study of the variations of absorption spectra of neutral atoms along the periodic system would be naturally complemented by a study of the variations along isoelectronic sequences of neutral atoms and ions. However, samples of ions adequate for absorption studies are not readily available.

#### 4.9. Sum rules for the Single-Electron Model

The sum rules discussed in Sec. 2.5 apply also to single-electron processes of the type considered in this section; they can even be extended to provide more detailed information. However, their interpretation is complicated here by the circumstance that the complete set of transitions out of a state  $(nl)$  includes transitions to lower energy states  $(n'l')$  with  $n' < n$  and/or  $l' < l$ . These transitions would correspond to radiation emission rather than absorption and have negative values of the oscillator strength (4.4). They do not actually occur in practice owing to the exclusion principle, as the lower states  $(n'l')$  are occupied in the ground state of an atom, but they have to be included in the computation of sum rules. Sec. 5.2 will show how to deal with negative- $f$  transitions in the frame of a many-electron model. Here we regard them as real.

Within this extended frame one may also consider the relationship between the oscillator strengths of reciprocal transitions  $(nl \rightarrow n'l')$  and  $(n'l' \rightarrow nl)$ . They have opposite sign but have not the same magnitude owing to averagings over orientation; as seen from (4.4) they

are related by

$$(2l+1)f(nl \rightarrow n'l') = -(2l'+1)f(n'l' \rightarrow nl). \quad (4.19)$$

The sum rules [(2.22), (2.23), and (2.24)]—relating to the moments  $S_{-1}$ ,  $S_0$ , and  $S_1$ —apply to single-electron oscillator strengths provided that:

(a) the set of eigenfunctions  $P_{n'l'}$ , for all  $n'$  including the continuum, forms a *complete* set of solutions of the radial equation (4.3) with  $l=l'$ ;

(b) the same potential  $V(r)$  applies in the equations that determine  $P_{n'l'}$  and  $P_{nl}$ . However, the calculation of  $S_{-1}$  does not depend on proviso (b). The application of the sum rule (2.25) for  $S_2$  will be discussed separately.

Separate sum rules can be formulated for transitions to  $l'=l+1$  and  $l'=l-1$  (BS57, Sec. 61 and 62). Defining

$$S_r(nl \rightarrow l') = \sum_{n'} (E_{n'l'} - E_{nl})^r f(nl \rightarrow n'l'), \quad (4.20)$$

one finds

$$\begin{aligned} S_{-1}(nl \rightarrow l') &= \frac{l+l'+1}{2(2l+1)} \frac{2m}{\hbar^2} \langle z^2 \rangle_{nl} \\ &= \frac{l+l'+1}{6(2l+1)} \frac{2m}{\hbar^2} \langle r^2 \rangle_{nl}, \end{aligned} \quad (4.21)$$

$$S_0(nl \rightarrow l') = \frac{(l'-l)(l+l'+1)(2l'+1)}{6(2l+1)}, \quad (4.22)$$

$$\begin{aligned} S_1(nl \rightarrow l') &= \frac{2(l+l'+1)}{2l+1} \left\langle \frac{p_z^2}{2m} \right\rangle_{nl} \\ &= \frac{2(l+l'+1)}{3(2l+1)} \left\langle \frac{p^2}{2m} \right\rangle_{nl}. \end{aligned} \quad (4.23)$$

The value of  $S_{-1}$  follows directly from (4.4), that of  $S_1$  almost immediately, but the calculation of  $S_0(nl \rightarrow l')$  requires some manipulation.

Notice that  $S_0(nl \rightarrow l-1)$  is negative, owing to the prevalence of transitions with negative  $f$ . For  $r=1$  and  $-1$ , all contributions to  $S_r$  are positive, even for negative  $f$ . The excess of  $S_{\pm 1}(nl \rightarrow l+1)$  over  $S_{\pm 1}(nl \rightarrow l-1)$  indicates the prevalence of transitions  $l \rightarrow l+1$  previously mentioned in Sec. 4.3, the more so because  $S_{\pm 1}(nl \rightarrow l-1)$  includes a larger contribution from transitions that are actually forbidden by the exclusion principle. Notice, finally, that in the single-electron model  $S_{-1}$  and  $S_1$  relate exactly to the properties  $\chi_m$  and  $\langle K \rangle_{nl}$  in accordance with (2.26) and (2.27).

The evaluation of  $S_2$  for the single-electron model differs from that for a whole atom. Since the non-Coulomb potential  $V(r)$  of (4.3) does not obey the equation  $\Delta V=0$  outside the nucleus, its derivatives in the expression of  $S_2$  cannot be expressed in terms of the electron density at the nucleus. Defining a "screened

charge"  $Z(\mathbf{r})$ , such that  $V(\mathbf{r}) = -Z(\mathbf{r})e^2/r$ , one finds

$$\begin{aligned} S_2(nl \rightarrow l') &= \frac{e^2 \hbar^2}{6(2l+1)m} \\ &\times \left\{ (l+l'+1) \left\langle 4\pi Z\delta(\mathbf{r}) - r^{-1} \frac{d^2 Z}{dr^2} \right\rangle_{nl} \right. \\ &\left. + 4(l'-l)l(l+1) \left\langle \frac{Z(r)}{r^3} - \frac{1}{r^2} \frac{dZ}{dr} \right\rangle_{nl} \right\}. \quad (4.24) \end{aligned}$$

The term with  $\delta(\mathbf{r})$ , akin to that in (2.25), contributes only for  $l=0$ , since otherwise the electron density at the nucleus vanishes owing to the centrifugal force. The next term is negative. The following group of terms vanishes for  $l=0$ ; it is positive or negative for  $l'=l\pm 1$ , as is  $S_0(nl \rightarrow l')$ . This group of terms gives no net contribution to

$$\begin{aligned} S_2(nl) &= \sum_{l'} S_2(nl \rightarrow l') \\ &= (e^2 \hbar^2 / 3m) \langle 4\pi Z\delta(\mathbf{r}) - r^{-1} d^2 Z / dr^2 \rangle_{nl}. \quad (4.25) \end{aligned}$$

The special role of electrons with  $l=0$  for  $S_2$  relates to the asymptotic law  $df(nl)/dE \sim E^{-7/2-l}$  for large  $E$  (RF67). In general  $S_{2+l}$  is large and finite,  $S_{3+l}$  is infinite.

As an application of sum rules, let us compare the values of  $S_{-1}$ ,  $S_0$ , and  $S_1$  for the valence electrons<sup>17</sup> of Ne and Ar which belong to the same chemical group but have quite different absorption spectra, as noted at the end of Sec. 4.5. More specifically, since the resonance in Ar belongs to the  $l \rightarrow l+1$  (i.e.,  $1 \rightarrow 2$ ) transition, we consider the  $S_r(nl \rightarrow 2)$  for the two atoms. Evaluation of (4.21), (4.22), and (4.23) with the Hartree-Fock wave functions of Ne ( $n=2$ ) and Ar ( $n=3$ ) yields (Co62) the ratios

	$S_0/S_{-1}$ eV	$S_1/S_0$ eV	$S_1 S_{-1}/S_0^2$
Ne	56	91	1.6
Ar	20	61	3.0.

The last column represents one of the shape parameters defined by (2.21), whose excess over unity indicates how much the spectrum departs from a single sharp peak. The large excess of 3.0 for Ar over the Ne value, 1.6, reflects the bi-modal versus unimodal character of

the two spectra. The large difference of the  $S_0/S_{-1}$  ratios for Ne (56 eV) and for Ar (20 eV) relates to the large difference between the linear dimensions of the two atoms, for which  $\langle r^2 \rangle_{n1}$  equals 1.2 and 3.4 atomic units respectively. This difference sets Ne apart from all the heavier noble gases whose mean square radii do not differ much and whose absorption spectra exhibit the resonance near threshold.

## 5. MANY-BODY FORMULATION

The results of calculations by the method of Sec. 4.2 are exact, within the limits of numerical accuracy, if interpreted on the basis of the single-electron model from which they are derived. They are, of course, intended as approximate representations of the actual properties of many-electron atoms. In this chapter we go over to a many-electron point of view in two steps. Firstly we consider a separable many-electron model which is a trivial extension of that of Sec. 4 and possesses essentially the same distribution of oscillator strength. However this model treats the exclusion principle explicitly as well as the influence of the resulting correlations upon the spectral moments  $S_r$ . Then we shall consider the wave functions of the many-electron model as initial approximations to the actual energy eigenfunctions of an atom. A procedure for the systematic improvement of these wave functions can be outlined (Sec. 5.3) but the corresponding consistent calculation of improved oscillator strengths meets an unresolved difficulty (Sec. 5.4). Independently of any such attempt to develop procedures for the treatment of the whole spectrum, numerous calculations have been carried out with many-electron wave functions for more limited purposes and with limited success. These calculations are reviewed in Sec. 5.5.

### 5.1. SLATER-DETERMINANT WAVE FUNCTIONS

Consider the  $N$ -electron separable model Hamiltonian

$$H_{\text{mod}} = \sum_{j=1}^N [p_j^2/2m + V(r_j)], \quad (5.1)$$

with a suitable potential function  $V(\mathbf{r})$ . Its eigenfunctions can be constructed from products of eigenfunctions (4.1),  $\psi_{nlms}$ , of the wave equation (4.3). An initial set of eigenfunctions of (5.1) which is complete, orthogonal and antisymmetric, consists of Slater determinants of order  $N$

$$\Psi_r = (N!)^{-1/2} \begin{vmatrix} \psi_{n_1 l_1 m_1 s_1}(1) & \psi_{n_1 l_1 m_1 s_1}(2) & \cdots & \psi_{n_1 l_1 m_1 s_1}(N) \\ \psi_{n_2 l_2 m_2 s_2}(1) & \psi_{n_2 l_2 m_2 s_2}(2) & \cdots & \psi_{n_2 l_2 m_2 s_2}(N) \\ \cdots & \cdots & \cdots & \cdots \\ \psi_{n_N l_N m_N s_N}(1) & \psi_{n_N l_N m_N s_N}(2) & \cdots & \psi_{n_N l_N m_N s_N}(N) \end{vmatrix}. \quad (5.2)$$

<sup>17</sup> This application of sum rules, to valence electrons only, differs from the applications to whole atoms in Table II and to intershell correlations in Table III.

Here the variables  $(1, 2 \dots N)$  of the  $\Psi$  indicate, respectively, the sets of position and spin coordinates of the  $N$  electrons and the subscript  $\nu$  of  $\Psi$  stands for a specific set of  $4N$  quantum numbers  $(n_1 l_1 m_1 s_1 \dots n_N l_N m_N s_N)$ . The eigenvalue of (5.1) corresponding to the eigenfunction  $\Psi_\nu$  is, of course, determined by the eigenvalues of (4.3) and by the set of quantum numbers represented by  $\nu$ ,

$$E_\nu = \sum_{j=1}^N E_{n_j l_j}. \quad (5.3)$$

The ground state of our model atom is represented approximately by the  $\Psi_\nu$  with lowest value of the  $n_l l_i$ ; if the number of electrons just suffices to occupy the outermost subshell completely. If the outermost shell contains a single electron or a single vacancy, the representation by a single  $\nu$  is still adequate. Otherwise there is further degeneracy corresponding to alternative mutual orientations of the electron orbits; construction of a linear combination of  $\Psi_\nu$ , by well known methods, is then required even to single out a ground-state wave function of specified net orbital angular momentum. An excited state is represented by a single  $\Psi_\nu$  only if it involves a core of electrons that occupy certain subshells completely plus a single excited electron, as in the case of alkaline atoms. We leave aside for the moment the matter of combining  $\Psi_\nu$  into eigenstates of angular momentum.

Once a set of radial functions  $u_{nl} = P_{nl}/r$  has been adopted and the corresponding set of determinants  $\Psi_\nu$ , constructed, dipole matrix elements between pairs of states

$$\langle \Psi_{\nu'} | \sum_j z_j | \Psi_\nu \rangle \quad (5.4)$$

can be calculated. Because each term of the operator  $\sum_j z_j$  depends on the coordinates of a *single electron*, its contribution to (5.4) vanishes unless  $\Psi_\nu$  and  $\Psi_{\nu'}$  differ only by the replacement of one single-electron wave function, say of  $\psi_{nlms}$  by a different  $\psi_{n'l'm's'}$ . In this event, the whole matrix element (5.4) reduces to the contribution of the relevant single-electron transition,

$$\langle \Psi_{\nu'} | \sum_j z_j | \Psi_\nu \rangle = \langle \psi_{n'l'm's'} | z | \psi_{nlms} \rangle. \quad (5.5)$$

The selection rules of the single-electron model further restrict nonzero values of this matrix element to  $l' = l \pm 1$ ,  $m' = m$ ,  $s' = s$ .

We can now calculate the oscillator strength of the transition  $\nu \rightarrow \nu'$  of the many-electron model atom. The energy difference  $E_{\nu'} - E_\nu$  coincides with  $E_{n'\nu'} - E_{n\nu}$ , owing to (5.3). The averaging over orientations proceeds as in the single-electron model and equalizes the strength of transitions from any degenerate  $\nu$  to any degenerate  $\nu'$ . The averaged  $f(\nu \rightarrow \nu')$  coincides with  $f(nl \rightarrow n'l')$  as given by (4.4). The spectrum of the combined oscillator strength of all possible transitions from the  $N$ -electron ground state also coincides with (4.6).

[In fact, the considerations of this section were implied, when we adopted (4.6) in the last section.]

The initial set of energy eigenfunctions  $\Psi_\nu$  can be replaced by a set of eigenfunctions of the energy and of the squared angular momentum  $|\mathbf{J}|^2$  by constructing linear combinations of  $\Psi_\nu$  with equal energy eigenvalues. The coefficients of the combinations are products of angular momentum coupling coefficients, called Wigner or Clebsch-Gordan coefficients (CS35). Unless otherwise stated, we shall imply that this operation has been performed according to the rules of *LS* (Russell Saunders) coupling. This operation has no effect on the energy eigenvalues as long as we deal with the model Hamiltonian (5.1). However it replaces the identical average oscillator strengths  $f(\nu \rightarrow \nu')$  of transitions between degenerate levels by an "array" of oscillator strengths of transitions between different eigenstates of  $|\mathbf{J}|^2$ , which generally differ from one another by a numerical coefficient. (For example the strength of transitions with  $|J - J'| > 1$  vanishes.) Details of the array structure and data on the relevant coefficients are given in spectroscopy texts such as (CS35).

Notice, finally, that no essential complication would have been introduced by adding a spin-orbit interaction term to each term of the model Hamiltonian (5.1). The quantum numbers  $m$  and  $s$  of  $\psi_{nlms}$  would have been replaced by different indices  $j$  and  $m$  and the energy levels  $E_{nl}$  would depend on  $j$ . The *LS* coupling mentioned above would be replaced by *jj* coupling. We shall disregard spin-orbit interactions for simplicity in the following, unless otherwise noted, with the understanding that it is often essential to consider it for specific applications. Further comments on this matter are found in Sec. 5.3.

## 5.2. Sum Rules in the Many-Body Formulation

Even though the many-electron dipole transition matrix elements (5.4) reduce to the one-electron matrix elements (5.5) in our formulation, characteristic differences occur in the structure of the sum rule expressions for the single-electron and many-electron problems. Consider, for example, the oscillator strengths of transitions from the ground state of the Kr atom, specifically the transitions involving one of its outer-shell ( $4p$ ) electrons. In the single-electron model this set of transitions would include those from  $4p$  to states of lower energy such as  $3d$  or  $2s$ . These transitions do not occur in the many-electron formulation because the states  $3d$  and  $2s$  are already occupied, that is, they are included in the determinant wave function  $\Psi_\nu$  of the initial ground state. The single-electron model also regards these transitions as unrealistic but has nevertheless to include them in the formulation of sum rules in Sec. 4.9. We shall consider here how the structure of sum rules for a whole atom is affected by the discounting of unrealistic single-electron transitions.

To this end, let us specify more closely the structure

of the moments  $S_r = \sum_s E_s f_s$  in accordance with the many-electron model of Sec. 5.1. Each excitation  $s$  of an atom in its ground state corresponds to the transition of an electron from an occupied subshell  $nl$  to an unoccupied subshell  $n'l'$ . (We assume here for simplicity that the ground state consists only of fully occupied subshells.) The corresponding excitation energy  $E_s$  equals  $E_{n'l'} - E_{nl}$ . Therefore we have

$$S_r = \sum_{nl}^{(occ)} 2(2l+1) \sum_{n'l'}^{(free)} (E_{n'l'} - E_{nl}) r f(nl \rightarrow n'l'). \quad (5.6)$$

The single-electron sum rules of Sec. 4.9 are not immediately relevant here because the sum over  $n'$  and  $l'$  is restricted to "free" states. However, this restriction has no net effect on  $S_0$  (and on all  $S_r$  with  $r$  even) because it excludes in fact only pairs of terms

$$(2l+1)f(nl \rightarrow n'l') + (2l'+1)f(n'l' \rightarrow nl), \quad (nl \text{ and } n'l' \text{ occ.}) \quad (5.7)$$

whose sum vanishes according to (4.19). We can thus remove this restriction, for  $r=0$ , in which case the  $\sum_{n'l'}$  yields 1, owing to (4.22) and the  $\sum_{n'l'}^{(occ)}$  yields

$$S_0 = N \quad (5.8)$$

in agreement with the general rule (2.23).

Any electron of the atom seems to contribute equally to  $S_0$  according to this calculation, irrespective of the shell  $nl$  to which it belonged initially. Actually the addition of each vanishing contribution (5.7) has spuriously reduced down to unity the contributions of the electrons with  $E_{nl} > E_{n'l'}$ , for which the term  $(2l+1)f(nl \rightarrow n'l')$  is negative, and increased to unity that of the electrons with lower energy  $E_{n'l'}$ . Considering that (5.6), which excludes these terms, consists only of positive contributions we conclude that in the absence of spurious contributions each outer electron—with higher  $E_{nl}$ —contributes to  $S_0$  more than an inner, lower energy electron. Thus the replacement of the one-electron model by a many-electron treatment with determinant wave functions may be said to effect a *transfer of oscillator strength* from inner to outer electrons. That this transfer attains large proportions is shown, for example, by the value of  $S_0(nl \rightarrow l+1)$  which is  $12/7$  for  $l=3$ , according to (4.22); that is, the 4f subshell of a tungsten atom contributes an oscillator strength of 24 to transitions 4f  $\rightarrow$  g, even though it contains only 14 electrons.

With regard to  $S_{-1}$  and  $S_1$  the limitation of  $\sum_{n'l'}$  in (5.6) to

$$\sum_{n'l'}^{(free)}$$

has more than formal significance, because the excluded contributions

$$\sum_{n'l'}^{(occ)}$$

are all positive, even when  $E_{n'l'} - E_{nl}$  is negative. Thus

TABLE III. Contributions of free and occupied orbitals to the moments  $S_{\pm 1}$  (Be65).

	$S^{-1}I_H$		$S_1/I_H$	
	(free)	(occ)	(free)	(occ)
Ne	2.02	1.1	303	39
Ar	5.50	3.2	$1.15 \times 10^3$	$0.3 \times 10^3$
Kr	7.86	5.3	$5.34 \times 10^3$	$2.0 \times 10^3$

we have

$$\begin{aligned} S_{\pm 1} &< \sum_{nl}^{(occ)} 2(2l+1) \sum_{n'l'} (E_{n'l'} - E_{nl})^{\pm 1} f(nl \rightarrow n'l') \\ &= \sum_{nl}^{(occ)} 2(2l+1) [S_{\pm 1}(nl \rightarrow l+1) + S_{\pm 1}(nl \rightarrow l'-1)]. \end{aligned} \quad (5.9)$$

The right-hand side of (5.9) can be regarded as an estimate of  $S_{\pm 1}$  based on the use of *unsymmetrized* product wave functions, which disregard the exclusion principle. Consideration of the exclusion principle, by discounting the forbidden transitions

$$\sum_{n'l'}^{(occ)}$$

is now seen to reduce systematically both  $S_{-1}$  and  $S_1$ .

The origin of this reduction emerges from an analysis of the calculation of  $S_{\pm 1}$  on the basis of (2.22) or (2.24) and of determinant wave functions (5.2). Determinant functions consist of *sums of products* of single-electron  $\psi_{nlms}$  rather than of simple products thereof. Accordingly they include correlations between the positions of different electrons, which are called "exchange correlations" because the various products of  $\psi_{nlms}$  differ by the interchange of electron coordinates. Calculation in accordance with the exclusion principle reduces  $S_{\pm 1}$  through the introduction of negative exchange correlation terms in (2.22) and (2.24). These terms account for most of the discrepancy between values of  $S_{\pm 1}$  calculated with unsymmetrized product wave functions and the "true" values estimated from the best experimental or theoretical evidence such as were shown in Table II. Table III shows examples of the corrections introduced by exchange correlations.

The reduction of both  $S_{-1}$  and  $S_1$ , while  $S_0$  remains unchanged, implies that exchange correlations increase the ratio  $S_0/S_{-1}$  and decrease  $S_1/S_0$ , thereby narrowing the gap

$$S_1/S_0 - S_0/S_{-1}. \quad (5.10)$$

According to Sec. 2.4, this narrowing indicates a reduction in the spread of oscillator strength distributions; it reflects the suppression by the Pauli principle of high frequency upward and downward transitions between occupied orbitals  $\psi_{nlms}$ .

Summarizing, we have seen that oscillator strengths calculated for a whole atom from a set of Slater determinant wave functions fulfill the Thomas-Reiche-Kuhn sum rule automatically. In this formulation the excitation of each shell does not contribute to the total strength in proportion to the number of its electrons; the contribution per electron is larger for outer than for inner shells. The electron-electron correlations implicit in the structure of determinant wave functions have a characteristic and very substantial influence on the parameters  $S_1$  and  $S_{-1}$ . They should modify similarly all  $S_r$  with odd  $r$ , but do not influence the even- $r$  moments at all, just as they do not influence  $S_0$ .

### 5.3. Successive Approximation Procedure

For an actual atom with atomic number  $Z$  and with  $N$  electrons the kinetic energy and electrostatic potential of the electrons are represented correctly by the Hamiltonian

$$H = \sum_j \left\{ p_j^2/2m - Ze^2/r_j + \sum_{i=j+1}^N e^2/|\mathbf{r}_i - \mathbf{r}_j| \right\}. \quad (5.11)$$

The spin interaction terms, omitted from this equation for simplicity, do not modify the substance of what follows.

Starting from the eigenfunctions  $\Psi_\nu$  of the model Hamiltonian (5.1) as initial approximations to the actual eigenfunctions of the atom we face the following situation. Consider the matrix of  $H$  which we indicate by<sup>18</sup>

$$(\nu' | H | \nu). \quad (5.12)$$

The diagonal elements  $(\nu | H | \nu)$  are approximate eigenvalues corresponding to the approximate  $\Psi_\nu$ . The magnitude of the off-diagonal elements, which would vanish if the  $\Psi_\nu$  were exact wave functions, indicates the degree of approximation reached at this point. More specifically the relevant approximation indices are the familiar ratios

$$(\nu' | H | \nu'') / [(\nu' | H | \nu') - (\nu'' | H | \nu'')] \quad (5.13)$$

for states  $\nu'$  and  $\nu''$  of discrete spectra. For states  $\nu'$  and  $\nu''$  of the continuum normalized per unit energy range, each matrix element  $(\nu' | H | \nu'')$  has the dimensions of a number and its value, compared to unity, serves directly as an approximation index.

Among the wave functions with the structure (5.2), the best approximation to an energy eigenstate is constructed with radial wave functions  $P_{nl}(r)$  that obey the Hartree-Fock system of equations instead of the model equation (4.3). We do not follow the Hartree-Fock approach here because it is not designed to provide a complete orthogonal set of  $\Psi_\nu$ . Thereby we sacrifice accuracy at the outset for the sake of maintaining manifest consistency over the entire spectrum. This require-

ment will prove important in the next section where we consider the calculation of improved oscillator strengths. Here we consider the preliminary steps involved in the calculation of improved wave functions. We are interested in optimizing the wave functions of the ground state and of the states reached from it by optical transitions of appreciable intensity. That is, we are interested in minimizing only certain submatrices of  $(\nu' | H | \nu)$ .

Improved wave functions  $\Psi_\mu$  can be constructed by linear combinations of the  $\Psi_\nu$ ,

$$\Psi_\mu = \sum_\nu \Psi_\nu U_{\nu\mu}. \quad (5.14)$$

In order that the  $\Psi_\mu$  be orthogonal, the matrix of coefficients  $U_{\nu\mu}$  has to be unitary. Improved dipole matrix elements are then also obtained as linear combinations of the initial ones,

$$(\mu' | \sum_j z_j | \mu) = \sum_{\nu'\nu} (U^{-1})_{\mu'\nu'} (\nu' | \sum_j z_j | \nu) U_{\nu\mu}. \quad (5.15)$$

The improvement is indicated by the reduction achieved in the magnitude of off-diagonal elements of the Hamiltonian,  $(\mu' | H | \mu)$ , which are given by a formula analogous to (5.15). The coefficients  $U_{\nu\mu}$  that would make  $(\mu' | H | \mu)$  exactly diagonal obey the infinite system of equations

$$\sum_{\nu'} (\nu | H | \nu') U_{\nu'\mu} = U_{\nu\mu} E_\mu. \quad (5.16)$$

In practice one deals with approximations to this system.

Note that the matrices  $U$  and  $U^{-1}$  consist of separate block submatrices, corresponding to different values of constants of the motion: parity, the total angular momentum quantum number  $J$ , and the corresponding  $M = \sum_j m_j$ . In fact, the matrix elements  $(U^{-1})_{\mu'\nu'}$  and  $U_{\nu\mu}$  in (5.15) belong to different independent blocks since the matrix elements  $(\nu' | \sum_j z_j | \nu)$  vanish unless  $\nu'$  and  $\nu$  have opposite parity. This independence might be emphasized, if desired, by utilizing for  $(U^{-1})_{\mu'\nu'}$ , a symbol  $V_{\mu'\nu'}$  unrelated to  $U_{\nu\mu}$ .

To provide a framework for the remainder of this article, we consider a program of progressive improvement of the wave functions of an atom and diagonalization of its Hamiltonian by successive approximations. The separation of the Hamiltonian matrix into blocks corresponding to different values of the "good" quantum numbers (parity,  $J$ , and  $M$ ) is assumed to have been accomplished in advance, as it presents no difficulty.<sup>19</sup> The desired progressive improvement of the wave functions will be sought by identifying the separate submatrices or terms of the Hamiltonian which correspond to various physical factors and diagonalizing them in succession. The successive steps of this process are achieved by a succession of diagonalizing matrices  $U^{(1)}, U^{(2)}, \dots$ , and the exact matrix  $U$  to be entered in

<sup>18</sup> We are replacing, here and in the following, the wave function symbol  $\Psi$ , by its index  $\nu$ .

<sup>19</sup> This operation removes some of the degeneracy of diagonal elements of the actual Hamiltonian, whereas it does not for the model Hamiltonian (5.1).

(5.14) and (5.15) is then understood to be the product

$$U = U^{(1)} U^{(2)} U^{(3)} \dots \quad (5.17)$$

The choice of the succession of steps to be followed should depend in any specific case on an assessment of the comparative magnitude of different matrix elements  $\langle \nu | H | \nu' \rangle$ , which can be determined by exploratory numerical calculations. More generally this choice may be guided by qualitative considerations of the kind presented in the following paragraphs.

For purposes of orientation and comparison we begin by reviewing the approach followed by the theory of discrete spectra (CS35, Ra55, Sl60) even though some departure from it will appear necessary at the outset. This theory takes up initially the diagonalization of submatrices of  $H$  pertaining to states  $\nu$  and  $\nu'$  of the same configuration, i.e., having identical sets of quantum numbers  $(n_i l_i)$ .<sup>20</sup> This diagonalization introduces correlations between the directions  $\hat{r}_i$  of different electrons and between their spin orientations, in addition to those introduced by the preliminary construction of eigenstates of  $J$ . As is well known, the submatrix diagonalization for a single configuration yields eigenvectors characterized by quantum numbers  $L$  and  $S$  when the effect of the electrostatic potentials in (5.11) predominates. However, the spin-orbit interactions, not shown in (5.11), are frequently of sufficient strength to complicate the diagonalization and the characterization of the resulting eigenvectors.

Initial diagonalization of the submatrix of each configuration is desirable insofar as the off-diagonal elements of such submatrices are more important than those that connect states of different configurations. This circumstance obtains in practice only in some simple cases, particularly for the lowest configurations which are better separated from one another energetically. However, the actual applications of the theory of discrete spectra are often successful even when this condition fails because they do implicitly part of what one has to do explicitly for continuous spectra, through the following device. Since diagonalization of submatrices calculated from the radial functions  $P_{nl}$  of (4.3) yields generally poor agreement with experimental energy levels, theory does not actually calculate the radial integrals included in each matrix element  $\langle \nu | H | \nu' \rangle$ ; instead it determines their values empirically, so as to achieve best fit to experimental levels. The empirical values include by implication a portion of the effect of configuration interaction, as noted below.

Treating each configuration separately from those with an electron excited to different levels of the same Rydberg series becomes increasingly unrealistic as the excitation level increases because levels of different configurations occur in the same spectral range and also because of complications of angular momentum cou-

pling. As the excitation energy increases, the orbit-orbit interaction between an excited electron and the rest of the atom decreases rapidly; soon it matters less than the spin-orbit interactions within the atomic residue. Therefore intermediate coupling or even extreme  $jj$  coupling actually prevail under most circumstances of interest to us in discrete spectra. The influence of the type of coupling upon the distribution of oscillator strength among the various levels of a configuration was noticed in early studies of line spectra and has been discussed occasionally in great detail (CS35). Efforts to account for such arrays of oscillator strengths by the theory of discrete spectra have increased recently (Me66, GVB65, Ga66a).

As one proceeds from the discrete into the continuous spectrum, it is no longer plausible at all to distinguish configurations with one electron at infinitesimally different energy levels. It becomes necessary to consider from the outset matrix elements  $\langle \nu' | H | \nu \rangle$  with  $\nu$  and  $\nu'$  corresponding to different excitation energies and thereby to depart from the sequence of approximation steps of the theory of discrete spectra. To this end we begin by replacing the concept of electron configuration with another one that is suited to continuous spectra and includes different levels of excitation.

Configurations whose sets of quantum numbers  $(n_i l_i)$  and  $(n'_i l'_i)$  differ only by the value of a single principal number  $n_j$ —that is, such that  $l'_i = l_i$  for all  $i$ ,  $n'_i = n_i$  for  $i \neq j$ , but  $n_j \neq n'_j$ —are said to constitute a series when  $n_j$  and  $n'_j$  belong to the discrete spectrum. When  $n_j$  and  $n'_j$  belong to the continuum they may be said to belong to the same “channel,” in accordance to the nomenclature of nuclear physics. Here we shall use the word “channel” to include series, because we are primarily interested in continuous spectra, and consider the diagonalization of Hamiltonian submatrices between all states of the same channel rather than only between states of the same configuration. Elements of these submatrices will be said to represent “intra-channel interactions”, while the name “interchannel interactions” will apply to Hamiltonian elements between states of different channels. From this point of view, the empirical fitting of the values of radial integrals practiced in the theory of discrete spectra can be looked upon as a substitute for a calculation that diagonalizes the interactions between all states of a channel rather than those of a single configuration.

Just as a configuration includes a set of states with alternative mutual orientations of individual electron orbits and spins, so does a channel—an aggregate of configurations with different  $n$  values—include a set of subchannels with alternative orbit and spin orientations. The possibility of diagonalizing the interactions between subchannels in an approximation step separate from the diagonalization within subchannels has not been examined. This question will be evaded within the limited range of examples considered in this article and in view of the present preliminary state of the problem. Only

<sup>20</sup> Under special circumstances the theory deals simultaneously with small sets of configurations, such as  $s^2 d^4$ ,  $s d^4 + 1$  and  $d^4 + 2$ , whose energies lie close to one another.

the intrachannel interaction within one subchannel identified by LS coupling will be discussed in Sec. 6.

With regard to the comparative importance of intra- and interchannel interactions, the former ones appear to deserve first consideration if one starts from the zero-order approximation of Sec. 5.1. Indeed intrachannel interactions will be shown to have a moderately large influence on the gross spectral distribution of oscillator strengths, being responsible for the major discrepancies between theory and experiment displayed in the illustrations of Sec. 4. These effects of intrachannel interaction are the subject of Sec. 6. For purposes of introductory clarification, we note here that the magnitude of intra-channel interactions depends on the choice of the initial model potential  $V(r)$  in (5.1) and on the resulting set of radial functions  $P_{nl}$ ; it can be minimized or even brought to zero for any single subchannel by utilizing  $P_{nl}$  that are solutions of a Hartree-Fock equation.

Interchannel interactions appear to have a lesser influence than intrachannel interactions upon the gross spectral distribution of oscillator strengths. They are nevertheless responsible for conspicuous features of photoabsorption, such as the occurrence of two-electron transitions and of broad lines in the continuum. A particular class of interactions can also be usefully singled out, which depends on the screening effect (Sec. 4.3) of one electron upon another and involves no exchange of angular momentum between these electrons. Effects of this class of interactions will be discussed in Sec. 7, other interchannel effects in Sec. 8.

In summary and loosely speaking, Secs. 6, 7, and 8 will deal, respectively, with the construction of three successive factors,  $U^{(1)}$ ,  $U^{(2)}$ , and  $U^{(3)}$  of (5.17). However the applications of theory are not so advanced that one actually performs this complete construction for any single atom.

#### 5.4. Consistency of Approximate Oscillator Strengths

Whereas procedures of successive approximation to the calculation of energy eigenfunctions and eigenvalues are straightforward in principle, as outlined above, the same does not hold for oscillator strengths. The formulas themselves, which provide the usual definition of oscillator strength in Sec. 2.1, are derived by methods that imply a knowledge of the exact eigenfunctions and eigenvalues. This is why the alternative formulas (2.3), (2.8), and (2.10) do not yield the same value of  $f_s$  when evaluated with approximate eigenfunctions and eigenvalues of the actual Hamiltonian (5.11). [This difficulty does not arise with regard to the model Hamiltonians (5.1) or (4.3) whose eigenfunctions and eigenvalues can be obtained in practice to any desired accuracy.] Therefore estimation of the accuracy of a calculation of  $f_s$  depends on knowledge not only of the errors in the eigenfunctions and eigenvalues that have been utilized but also of those in the formula one has applied. No established theory of the latter errors exists.

The expression (2.15) of the oscillator strengths in terms of a correlation function appears free from inherent error, because it can be derived from basic theory without reference to the eigenvalues and eigenfunctions of excited states. This expression does depend on the ground-state eigenfunction, but this eigenfunction is usually accessible to accurate determination and furthermore its errors can be estimated. Numerical evaluation of (2.15) requires in practice the use of a set of wave functions to provide a matrix representation of the operators, but the only essential requirement on this set is its completeness. (This is one reason for our emphasis on the use of complete sets.) Approximation of this set to the actual eigenfunctions of the Hamiltonian simplifies the numerical calculation greatly, but the formula takes into account the dependence of  $df/d\omega$  on the nonzero off-diagonal matrix elements of the Hamiltonian. Thereby it permits, in principle, an estimation of errors involved in performing any specific calculation. However, the approach suggested here has not been explored.

In the process of evaluating oscillator strengths by successive approximations, the successive variations of the moments  $S_r$  are of interest. We have seen in Sec. 5.2 how the progression from a single-electron model to a many-electron model which obeys the exclusion principle: (a) conserves the value of  $S_0$ , (b) transfers contributions to  $S_0$  from inner to outer shells, (c) introduces correlations among electrons which reduce the values of  $S_1$  and  $S_{-1}$ . Ideally, one may wish to display the influence of each step of approximation in a similar manner. Conservation of  $S_0$  constitutes an earmark of consistency of the approximation. This conservation imposes a restriction on the diagonalizing matrix  $U$  and on each of its factors in (5.17). It implies that in each successive step one obtains the exact eigenfunctions and eigenvalues of a new model Hamiltonian.

The concept of transfer of oscillator strength from inner to outer shells (Sec. 5.2) can be made more precise and general by considering the classification of excited and ionized states into "channels" on the basis of the intrinsic quantum numbers (angular momentum, etc.) of the residual core. Insofar as this classification is possible and  $S_0$  is conserved, the total oscillator strength can be allocated to different channels and one may consider its redistribution among channels as an indication of the physical effect of each step of approximation.

On the subject of the consistency of approximate formulas, one should recall that an atom interacts with radiation through its electron current, represented by the operator  $e\mathbf{v} = [\mathbf{H}\mathbf{r} - \mathbf{r}\mathbf{H}]i/\hbar$ . The velocity operator reduces to its familiar representation  $(\hbar/im)\mathbf{grad}$  provided  $\mathbf{H}$  includes only local potentials. Therefore the familiar gradient operator representation cannot be applied consistently together with wave functions that obey Hartree-Fock equations with nonlocal potentials.

The considerations presented in this section have the

intent of qualifying the significance of current methods of calculation and of indicating possible directions of further research. In practice, as described in the next section, approximate calculations have been carried out utilizing eigenfunctions and eigenvalues obtained by various approximation methods and one or another of the defining equations for  $f_s$  chosen on grounds of plausibility. One plausibility argument favors the use of the "velocity" formula (2.8) because it depends mostly on the values of wave functions at moderate values of the radial variable  $r$ , where large errors of the wave functions are less likely (Ch45). The following sections deal with approximate procedures designed to take into account the influence of various physical factors upon the oscillator strengths. Unless otherwise stated the definition (2.3) of the  $f_s$  will be implied without further consideration of consistency. This definition is also implied in each set of theoretical data presented in the figures except as indicated in the relevant caption.

### 5.5. Survey of Existing Calculations

Before proceeding with the program of the following sections, we interrupt our treatment and devote the concluding part of this section to a review of the results obtained by calculations with many-electron wave functions. Most of this work has differed in emphasis from the approach of the present article. Whereas we have been dealing with the distribution of oscillator strength over the whole spectrum, interest has centered in the past on the oscillator strength of specific transitions in the discrete spectrum or in the continuum near the photoionization threshold.

For the purpose of studying specific transitions, the straightforward approach consists of calculating wave functions for the ground and excited state,  $\Psi_0$  and  $\Psi_s$ , as accurately as possible directly from the Schrödinger equation. Therefrom the oscillator strength is obtained alternatively through (2.3), (2.8), or (2.10). These equations are called, respectively, the "length," "velocity," and "acceleration" formulas. The alternative formulas need not give the same result, as noted before, because the approximate wave functions  $\Psi_0$  and  $\Psi_s$  are not generally eigenfunctions of the same approximate Hamiltonian. The consistency of the results obtained from the alternative formulas serves as an index of their accuracy. We call this direct method of calculation the "best wave function" approach. Details on this subject are given by (Ba46, NS62, HL67, and BN67).

Naturally a wave function that is "improved" according to one test may actually have become "worse" according to another criterion. An example has occurred (We67) where an improvement in the approximation of energy eigenvalues was accompanied by worsening disagreement between the length and velocity of oscillator strength.

#### a. Discrete Transitions

For atomic states of all but the lightest atoms, best wave function calculations proceed usually by the Hartree-Fock method. The wave function  $\Psi_0$  or  $\Psi_s$  is expressed as a Slater determinant of the form (5.2)<sup>21</sup> and the single-electron radial functions  $P_{nl}(r)$  contained in the  $\psi_{nlm}$  are defined by seeking a minimum of

$$E_\nu = (\Psi_\nu | H | \Psi_\nu) / (\Psi_\nu | \Psi_\nu), \quad (5.18)$$

where  $H$  is the Hamiltonian (5.11). This definition leads to an equation for the  $P_{nl}(r)$  which differs from (4.3), namely,

$$\begin{aligned} d^2P_{nl}/dr^2 + (2m/\hbar^2)[E_{nl} - V_{nl}(r) - l(l+1)\hbar^2/2mr^2] \\ \times P_{nl}(r) = X_{nl}(r, P_{nl}(r)) + \sum_{n' < n} \lambda_{nn'} P_{n'l}(r). \end{aligned} \quad (5.19)$$

Three differences occur between (5.19) and (4.3). Firstly, the effective potential  $V_{nl}(r)$  differs for different subshells; therefore orthogonality of single-electron wave functions has to be ensured by the last term of (5.19) with the Lagrange multipliers  $\lambda_{nn'}$ . [The potential  $V_{nl}$  depends on the wave functions  $P_{n'l}(r)$  of other electrons.] Secondly, the term  $X_{nl}(r, P_{nl})$ , which is absent in (4.3) and arises from the antisymmetry of  $\Psi_\nu$ , is added here to represent the effect of electron exchange on the radial function  $P_{nl}$ . This term has the form of a linear integral operator on  $P_{nl}$  and thus has the character of a nonlocal potential. Finally (5.19) represents a system of equations in the  $P_{nl}(r)$ , one for each occupied subshell ( $nl$ ), which have to be solved simultaneously instead of remaining independent as in (4.3).

The Hartree-Fock method has been applied mostly to the calculation of ground-state wave functions but is also applicable to excited states. Most of the existing excited state calculations pertain to atoms with  $Z \leq 10$  (We63, Ke64, TSDJ57). These references represent only a sample of the extensive work done on the calculation of oscillator strengths of spectral lines. We are also restricting ourselves in this article to transitions from or to the ground state. The results of this work indicate that for a large class of discrete transitions the Hartree-Fock method provides an accuracy no better than approximately 25–50%. Moreover, the classes of transitions for which the Hartree-Fock method provides better accuracy are the very same to which the semi-empirical quantum defect method (BD49) applies and yields comparable accuracy.

Recently the Hartree-Fock method has been extended (We67, Za67) to the calculation of ground- and excited-state wave functions that are superpositions of several determinants, i.e., of the type (5.14) with the

<sup>21</sup> We disregard here for the sake of simplicity the desirability of starting with a linear combination of Slater determinants wherever any subshell is partially occupied, with more than a single electron or a single vacancy, or more than one subshell is partially occupied.

sum over  $\nu$  extended over a limited number of states. (The variational Hartree-Fock procedure also provides the values of the coefficients  $U_{\nu\mu}$ .) These calculations have yielded substantially more accurate values of the oscillator strengths. For example, accuracies of the order of 10% have been obtained for discrete transitions from the ground state of C (We67).

From the standpoint of Sec. 5.3, the basic Hartree-Fock procedure can be described as the inclusion of intrachannel interactions in the initial approximation. The superposition of determinants pertaining to different configurations corresponds to including also a certain amount of interchannel interaction. These improvements of the wave functions are, of course, applied separately to the ground state and to the excited states, as indicated in Sec. 5.3, and also independently for different excited states. The limitation of photoabsorbing transitions to single electron jumps, emphasized in Sec. 4.2, does not obtain in the Hartree-Fock method, owing to the independent determination of wave functions  $P_{nl}$  for the ground and the excited state. Thus the effects of core relaxation, treated in Sec. 7, are included in the Hartree-Fock method from the beginning, though effectively within the limitations of the "sudden" approximation (see Sec. 7.1).

### b. Photoionization

The wave function  $P_{n'l'}(r)$  of an excited electron becomes increasingly small—as  $n'$  increases—in the range of  $r$  where it overlaps the wave functions of other electrons. Therefore the role of this wave function in the process of self-consistent determination of all other  $P_{nl}$  becomes vanishingly small as  $n'$  increases and it vanishes altogether in the photoionization limit when  $n'$  belongs to the continuum. Accordingly, the calculation of Hartree-Fock continuum wave functions proceeds by two steps. One calculates first the wave functions of the bound electrons disregarding the continuum electron, i.e., as though the bound electrons belonged to a positive ion; then one solves (5.19) for the continuum electron utilizing the previously calculated wave functions of the other electrons for the determination of  $V_{nl}$  and  $X_{nl}$ .<sup>22</sup>

Calculations of photoionization employing this approach have been made for Li (St54), O (DHS64), N (He66), Ne (Se65, HL67), Si, and Ar (CLS67). (More refined calculations for He and Li are discussed separately below.) For O, Ne, Si, and Ar and with application of the length formula (2.3), the results of these calculations are in substantial (5–10%) agreement with experiment over a 10–25-eV range above threshold. However, application of the velocity formula

<sup>22</sup> Interchannel interaction often couples states with the continuum electron quantum numbers  $l'=l+1$  and  $l'=l-1$ . To take this interaction into account one starts with a sum of determinant wave functions and obtains coupled equations for the two  $P_{n'l'}$  functions (see, e.g., HL 67). This interaction effect is, usually, weak.

(2.8) yields results generally parallel to but lower than experiment by 10–30% for N, O, and Ne and by about 50% for Si and Ar. No tests with the acceleration formula (2.10) have been made for these atoms.

It has been argued (Ch45) that photoionization near threshold takes place near the outer edge of the atom so that the length formula, which gives greater weight to this region, should also be most dependable in this energy range. This argument would make the agreement of the length formula results with experiment appear more than coincidental and would discount the significance of disagreement with the velocity formula. Yet it seems doubtful, on the basis of the existing results, that the Hartree-Fock method can dependably approach 10% accuracy even in the region near threshold. In particular no calculation has yet reproduced the "knee" in the absorption spectrum of Ar near 30-eV photon energy.

Calculations of photoionization by the Hartree-Fock method have not been extended over a sufficient range of photon energies to permit tests of sum rules. However it follows from Sec. 5.4 that consistency should not even be expected for the Thomas-Reiche-Kuhn rule (2.23). More specifically, it has long been known (Fo34) that explicit inclusion of exchange forces produces a net increase of the total strength calculated by the length formula. A test of this effect has been made by deriving single-electron sum rule expressions corresponding to (4.21)–(4.23) from the Hartree-Fock equation (5.19) for the excited electron rather than from (4.3); a 10% increase of  $S_0$  was found for Ne.

The Hartree-Fock continuum wave functions considered above may be regarded as the first terms of an expansion of the exact wave functions into antisymmetrized products of ionic core and of free electron wave functions (Se53). Different terms of the expansion are coupled by interchannel interaction. A sample calculation along this approach has been made for Ar (LC67), which included the continuum channel  $(3s3p^6n'p)$  besides  $(3s^23p^5n's)$  and  $(3s^23p^5n'd)$ . This extension yielded no substantial improvement in the agreement with experiments.

### c. Improved Calculations for He and Li

Methods more powerful than that of Hartree-Fock or its simple extensions have been tested on the 2- and 3-electron atoms where their application is not excessively laborious. Wave functions have been calculated which include explicit electron correlations, many-channel interactions or distortion of the ionic core by the continuum electron ("polarized orbital method").

High accuracy Pekeris-type wave functions have been obtained and applied to the calculation of oscillator strengths for excitation from the He ground state to  $1s2p$  and  $1s3p$  (SP64). Here the length, velocity, and acceleration formulas yielded agreement within 2%, the

largest deviation occurring for the acceleration formula which depends critically on wave function accuracy near the nucleus. Comparable accuracy has been obtained by other authors (We67a, GJK66) for these and other He transitions. For the  $2s \rightarrow 2p$  transition in Li the results of the length and velocity formulas have also been brought to 2% agreement by a calculation with rather extensive configuration interaction (We63).

The photoionization of He and Li has been calculated extensively using ground-state wave functions with explicit electron correlations and various types of continuum wave functions (Hu48, SZ62, SW63, BMcV65, BK67). Among these calculations, that of Burke and McVicar seems best for He below the threshold of formation of  $\text{He}^+$  ( $n=2$ ) at 65.4 eV. This calculation utilizes an expansion of the He continuum wave functions into exact  $\text{He}^+$  eigenfunctions truncated at  $n=2$ . Its results agree with experiment (Sa64) within the experimental error and show a minimal deviation of  $\sim 1\%$  between length and velocity formulas. At higher energies the Bell-Kingston calculation, with continuum polarized-orbital (TL61) wave functions, appears best according to the same criteria; paradoxically its results are less accurate at lower energies. Hartree-Fock calculations for Li (St54, Se67) give results consistent with recent experiments (HC67). An interesting occurrence emerged from Tait's investigation (Ta64) of the influence of ground state correlations upon the oscillator strengths: the difference between the results of length and velocity formulas which was modest ( $\sim 10\%$ ) with an uncorrelated wave function rose to  $\sim 80\%$  upon introduction of a supposedly better ground-state wave function.

## 6. EFFECT OF INTRACHANNEL INTERACTION UPON THE RESONANCE NEAR THRESHOLD

The single-electron calculations reported in Sec. 4.5 yield resonance maxima that are generally sharper and occur at lower energy than observed experimentally. This discrepancy is particularly large for the absorption by the  $3p$  electrons of Ar and by the  $4d$  of Xe (Figs. 5 and 7), less so for the  $4p$  of Kr and  $5p$  of Xe. It is also noticeable for the nonresonant, flatter absorption spectrum of the  $2p$  electrons of Ne.

Large discrepancies of this type clearly concern the dominant transitions  $l \rightarrow l+1$ . They are not attributed to interaction with other channels in the same spectral range because experimental and computational evidence shows these interactions to be weak. Accordingly attempts have been made with some success to account for such discrepancies on the basis of intrachannel interaction.

These attempts, concerning particularly the photoionization of  $3p$  in Ar and  $4d$  in Xe, will be described in the present chapter. In one form or another, the intrachannel interaction takes into account correlations

among the electrons of the absorbing subshell, which are due to their Coulomb repulsion and tend to stiffen the atomic structure, i.e., to increase the frequencies of the absorption spectrum. It proves possible to present in a unified manner approaches that originate from quite different points of view, namely the approach of Sec. 5.3, a Hartree-Fock procedure and the theory of plasma-like collective excitations (BEL67, ACS67). The latter theory and a related RPA theory (AG64) also take into account interchannel interactions; the interchannel aspects will be described in Sec. 8.5.

As we shall see in Sec. 6.1, the intrachannel interaction calculated with the wave functions of Sec. 4.2 is sufficiently strong to modify substantially the theoretical results of Sec. 4 toward agreement with experimental absorption spectra. However, reasonably good agreement of theory with the observed spectrum has not been demonstrated for Ar, and for Xe only by a somewhat arbitrary choice of parameters.

### 6.1. The Influence of Excitation Transfer

The calculations whose improvement is being sought pertain to optical transitions of the spectroscopic types  $3p^6 1S \rightarrow 3p^5 n d^1 P^0$  and  $4d^{10} 1S \rightarrow 4d^9 n f^1 P^0$ . Actually we are concerned mostly with continuum states for which  $n$  should be properly replaced by an energy variable  $\epsilon$ . We consider the effects of the intrachannel interaction which causes the wave function of each excited (or ionized) state reached by these transitions to be replaced by a superposition of wave functions of the same channel with different first approximation energies.

Accordingly, we examine the structure and magnitude of the following types of off-diagonal matrix elements (5.12) of the Hamiltonian (5.11).

$$\begin{aligned} & \langle 3p^5 \epsilon d^1 P^0 | H | 3p^5 \epsilon' d^1 P^0 \rangle, \\ & \langle 4d^9 \epsilon f^1 P^0 | H | 4d^9 \epsilon' f^1 P^0 \rangle, \end{aligned} \quad (6.1)$$

where indication of complete shells has been omitted. The calculation of these matrix elements involves standard integrations over angular variables and then Slater integrals over products of radial wave functions  $P_{nl}(r)$  obtained by solving (4.3). The results of angular integrations are, of course, the same for the off-diagonal matrix elements (6.1) as for the diagonal elements with  $\epsilon' = \epsilon$ . Therefore, we begin by writing here expressions for the non-trivial portions of the diagonal elements (6.1) obtained from p. 299 of (CS35) and Chap. 6 of (Ha57); they are, respectively,

$$\begin{aligned} & -F^0 - \frac{1}{5} F^2 + \frac{14}{15} G^1 - \frac{9}{5} G^3, \\ & -F^0 - \frac{8}{35} F^2 - \frac{2}{21} F^4 + \frac{11}{7} G^1 - \frac{4}{21} G^3 - \frac{50}{231} G^5, \end{aligned} \quad (6.2)$$

where  $F^k$  and  $G^k$  indicate Slater integrals.<sup>23</sup> To obtain

<sup>23</sup> The tables in (CS35) are expressed in terms of renormalized integrals  $F_k$  and  $G_k$ , rather than of  $F^k$  and  $G^k$ .

TABLE IV. Sample values of  $G^1(31, \epsilon 2; \epsilon' 2, 31)$  for Ar.<sup>a</sup>

$\epsilon/I_H$	-0.135	-0.075	0	0.5	1.0	1.5	2.0
$\epsilon'/I_H$							
-0.135	0.719	0.745	0.735	0.518	0.322	0.209	0.143
-0.075		0.778	0.769	0.542	0.344	0.215	0.156
0			0.759 <sup>a</sup>	0.550	0.349	0.231	0.162
0.5				0.435 <sup>a</sup>	0.298	0.211	0.160
1.0					0.217	0.164	0.131
1.5						0.130	0.110
2.0							0.097

<sup>a</sup> An alternative calculation with wave functions derived from the more plausible potential of (HS63) yields 0.198 and 0.500 instead of 0.759 and 0.435 for the (0, 0) and (0.5, 0.5) elements.

the corresponding expressions for off-diagonal elements one simply replaces the diagonal Slater integrals  $F^k$  and  $G^k$  by the appropriate off-diagonal integrals which we shall indicate by script letters. [Matrix elements akin to (6.1) but pertaining to the other terms of the same configuration with equal  $j$  ( ${}^3P_1$  and  ${}^3D_1$ ) differ from (6.2) by the magnitude and sign of the numerical coefficients. These terms are relevant, owing to inaccuracy of the LS coupling, even though direct optical transitions to them are forbidden. We assume here that the breakdown of LS coupling only redistributes the oscillator strengths on a fine scale comparable to the energy of spin-orbit coupling; we disregard this redistribution in the present section.]

Among the terms of (6.2) those containing the exchange integral  $G^1$  loom most important because of the larger values of their coefficients. These terms represent the exchange interaction between the excited electron and all the electrons that remain in the ground-state shell  $3p^5$  or  $4d^9$ ; their coefficients reflect the large number of electrons remaining in these almost complete shells. For the off-diagonal elements  $G^1$  is replaced by

$$G^1 = \int_0^\infty dr_1 P_{nl}(r_1) P_{\epsilon' l'}(r_1) \int_0^\infty dr_2 P_{\epsilon' l'}(r_2) P_{nl}(r_2) e^2 r_</r_>^2, \quad (6.3)$$

where  $r_<$  and  $r_>$  indicate respectively the smaller and the larger one among  $r_1$  and  $r_2$  and where ( $n=3, l=1, l'=2$ ) or ( $n=4, l=2, l'=3$ ) for the two matrix elements (6.1). Strictly speaking,  $G^1$  does not represent an exchange energy (a name that pertains to the energy of a single configuration) but the contribution to electron correlation energy arising from the double transition process:

$$\begin{aligned} \text{electron 1} & \quad \epsilon' \rightarrow nl, \\ \text{electron 2} & \quad nl \rightarrow \epsilon' l', \end{aligned} \quad (6.4)$$

in which excitation is swapped between two electrons with transfer of one unit of angular momentum and

without energy conservation. Energy is conserved only for the diagonal element,  $\epsilon' = \epsilon$ , in which case  $G^1$  reduces to the usual  $G^1$ .

Evaluation of  $G^1$  with the wave functions utilized in (Co62) yields remarkably large results. Specifically, values corresponding to continuum states  $\epsilon$  and  $\epsilon'$  close to the ionization threshold approach unity, as shown in Table IV. The interaction corresponding to the interchanges (6.4) thus appears to have a large influence on excited states to which intense optical transitions occur. As we shall see in the next section, this interaction can be built into an initial approximation, if one replaces the equation (4.3) for excited electron wave functions  $P_{\epsilon' l'}$  by an equation that takes proper account of the exchange force between excited and ground-state electrons. This force is repulsive for electrons excited out of a complete subshell into a singlet state whereas it is attractive for electrons held in the ground state. Thus the alternative arises whether to start calculations with a universal potential as in (4.3), thus incurring a sizeable initial error to be corrected later, or to utilize from the beginning an improved equation for the specific radial wave functions  $P_{\epsilon' l'}$ .

In either event, theoretical methods suited to the handling of weak perturbations do not suffice to calculate the influence of the off-diagonal elements (6.1) or even of their main  $G^1$  components alone. Qualitatively, however, one may argue from perturbation theory that, since the diagonal elements ( $\epsilon' = \epsilon$ ) of the dominant interaction  $G^{(1)}$  are positive, the excited levels reached from the ground state by photoabsorption should be shifted toward higher energies. Moreover, as demonstrated by the second-order perturbation formula, any interaction causes energy levels to "repel each other"; accordingly the relevant excited levels should spread out in the spectrum. Notice that the position of individual levels actually has no meaning in the continuum but the distribution of transition probabilities over the energy spectrum is, of course,

well defined. In fact, the calculations in the following sections bear out the predictions from perturbation theory, in the sense that the interaction (6.1) flattens the absorption peaks predicted in Chap. 4 and shifts them toward higher energy. (Curiously, the position of levels of the discrete spectrum of Ar is not shifted appreciably, because it is controlled by spin-orbit coupling rather than by the LS coupling; this aspect will be discussed elsewhere.)

Let us consider now these modifications of calculated absorption spectra of atoms in the context of the spectral features of solids, plasmas, and nuclei that are called "plasma" or "collective" effects. A typical plasma effect consists of the occurrence of a strong absorption in an energy range where none was predicted by an independent particle model. All phenomena of this class are manifestations of particle correlations traceable to excitation transfers analogous to (6.4). Each of the terms "single-particle model," "plasma effect," "collective model" has not been used with a unique meaning and may have a different implication for different readers. In accordance with a recent trend, the following discussion attributes to each term implications that make different models most rather than least compatible.

Theoretical treatments of plasma excitations typically utilize collective coordinates which seem foreign to existing atomic theory. Therefore speculations arose concerning the possible occurrence in atomic spectra of plasma-type features which had remained unsuspected owing to weaknesses of ordinary theory and limited range of experimentation (LS53, Li54, Br58, BL63, Am65). However, it has become increasingly clear that theoretical spectroscopy and quantum mechanical many-body theories are in fact remarkably analogous. Differences in language and emphasis occur primarily between spectroscopy and semi-macroscopic plasma theories and even these tend to disappear in recent work (BL65, BEL67, ACS67, and Sec. 6.3 below). The extensive recent experimentation indicates that the major plasma-type effects actually occurring in atomic spectra are just those discussed in this chapter. They are not as striking as the occurrence of plasma excitations in metals. Yet the intrachannel interaction matrix elements (6.1) are larger than one might have expected from earlier experiences in spectroscopy.

These remarks may be illustrated by pointing out the correspondence between excited-state wave functions of atoms and of solids. Antisymmetrization of wave functions in accordance with Sec. 5.1 assigns an excitation to any one among the electrons of an atom or of a metal, rather than to a specific electron; similarly for a molecular crystal the degenerate excitations of its various cells are equivalent and have to be treated symmetrically. Symmetry considerations suggest that the excitations of physical interest are characterized by

"good" quantum numbers, namely, the orbital quantum number  $L$  for atoms and a wave vector  $\mathbf{K}$  for a metal or molecular crystal, and by the spin quantum number  $S$  in all cases; the corresponding states are superpositions of independent-particle excited states with non-invariant quantum numbers, namely,  $m$  and  $s$  for an atom, cell number for a molecular crystal and one-electron wave vector  $\mathbf{k}$  for a metal. In the language of excitation operators, the operator of collective excitation for a molecular crystal is a linear combination of operators, each representing excitation of a single cell; its atomic analog is, e.g., a  $^1P^0$  excitation operator which is a superposition of operators for excitations of individual ( $m, s$ ) states. Finally, to obtain the spectrum of stationary states excited by photon absorption or by particle collisions in each of these systems, one must take into account off-diagonal elements of the energy matrix between eigenstates of  $L$  or  $\mathbf{K}$  with different first approximation energies, such as (6.1). Thereby the excitation spectrum is modified, most drastically for metal excitation by the passage of charged particles, less so in the other examples.

These similarities between the representation of excitations in different systems have been somewhat obscured because plasma-type treatments of atoms have normally utilized a semimacroscopic statistical model. The model starts from an initial equilibrium distribution of electron density, and considers local elastic oscillations of the density and particularly the influence of electric forces between such inhomogeneities of density at different points. It is this influence which may alter the frequency spectrum of density oscillations drastically, to the point of introducing a characteristic frequency of the whole system in a spectral range different from that of independent local oscillations. This approach applies to atoms with difficulty as it ignores the dominant influence of shell structure. It also attributes a zero-approximation absorption spectrum to each volume element of an atom, whereas in the single-electron treatment of Sec. 4 each excited state is distributed over a whole atom. Yet early estimates of the influence of electron correlations upon the spectrum of local oscillations (LS53) appear comparable to those pertaining to the interaction matrix elements (6.1).

## 6.2. Direct Calculations

The diagonalization of an interaction matrix by solving Eq. (5.16) is complicated for continuous spectra by the occurrence of nearly degenerate states, i.e., of states with infinitesimally different energies. We outline here the nature of the difficulty and one procedure for overcoming it.

Let us rewrite the "improved" wave function formula (5.14) and the system of equations (5.16) obeyed by the diagonalizing transformation in a form appropriate to a continuous spectrum with intrachannel interaction

only. This form is<sup>24</sup>

$$\Psi_E = \int d\epsilon \psi_\epsilon(\epsilon | U | E), \quad (6.5)$$

$$\int d\epsilon' (\epsilon | H | \epsilon') (\epsilon' | U | E) - (\epsilon | U | E) E = 0, \quad (6.5')$$

where the integrals are understood to include a sum over an index  $n$  of the discrete spectrum. The general Hamiltonian matrix element  $(\epsilon | H | \epsilon')$  includes a diagonal part  $\epsilon\delta(\epsilon-\epsilon')$ , such that the coefficient of  $(\epsilon | U | E)$  in (6.5') vanishes at  $\epsilon=\epsilon=E$ . This circumstance implies that the diagonalizing matrix  $(\epsilon | U | E)$  is singular at  $\epsilon=E$  and that some appropriate analytical procedure must be utilized to solve (6.5') in a limited range of variables  $\epsilon'\sim\epsilon\sim E$ , prior to numerical solution in the residual range. Alternative equivalent procedures are available for this purpose.<sup>25</sup> In particular, one can

<sup>24</sup> As noted above, this section deals only with the calculation of one of the factors  $U^{(i)}$  of  $U$ ; the index  $i$  is dropped in (6.5) for simplicity.

<sup>25</sup> We indicate here the connections between our approach to the problem of constructing wave functions of the continuum states of an atom and the corresponding approach of collision theory. As noted at the end of Sec. 1, the interaction between photon and atom can be treated as a small perturbation but the interaction among different continuum states of an atom cannot be regarded as weak, at least in general.

Collision theory deals ordinarily with continuum states of a neutral atom by considering an electron incident on a positive ion and reemerging in various directions and in alternative channels. The wave functions of these states are *complex* because they represent a flow of electrons in specified directions. In this article, extending spectroscopy theory into the continuum, we regard the neutral atom (ion+electron) as a single system. We deal with angular momentum eigenstates of the whole system, rather than with specified directions of incidence and emergence of an electron. We also deal with standing rather than progressive waves, i.e., we construct *real* wave functions which represent incident and escaping electrons symmetrically. Real wave functions are adequate as long as we do not inquire about the relative probability of alternative directions or channels of escape of a photoelectron.

The most familiar form of collision theory, as it originates from Lippmann and Schwinger (see, e.g., GW64 or Sh67), replaces in effect (6.6) by an analogous expression with a small imaginary term added to the denominator  $E-\epsilon$  and with a non-Hermitian matrix instead of  $(\cdot | K | E)$ . An alternative to this familiar procedure, also mentioned in standard treatises, consists of calculating first the real hermitian reaction matrix  $K$  by solving (6.7) or its multichannel generalization and then constructing from the  $K$  matrix any desired set of real or complex wave functions relevant to a specific problem. We emphasize the latter alternative because it separates clearly the basic problem of calculating  $K$  and one complete set of wave functions by means of (6.7) and (6.6) from the subsidiary problem of fitting specific conditions. Also, the exclusion of imaginary elements from the basic problem is convenient for numerical applications.

Extension of the treatment given in the text to include multichannel interactions is formally straightforward. Each row or column of the matrices  $H$ ,  $K$ , and  $U$  is now labelled by a channel index  $\alpha, \beta, \dots$  in addition to an energy value  $E$ ,  $\epsilon$ , or  $\epsilon'$ . The actual solution of the generalized Eq. (6.7)

$$(\alpha\epsilon | K | \beta E) = (\alpha\epsilon | V | \beta E) + \sum_\gamma \int d\epsilon' (\alpha\epsilon | V | \gamma\epsilon') \times [\mathcal{P}/(E-\epsilon')] (\gamma\epsilon' | K | \beta E),$$

is complicated only by the multiplicity of channels. This multiplicity is infinite in principle, and must be dealt with by successive approximations as suggested in Sec. 5.3, an approach that remains largely undeveloped. The generalization of (6.5') yields now a

replace the singular dependent variable  $(\epsilon | U | E)$  by a nonsingular variable  $(\epsilon | K | E)$  through the substitution (Fa61a, FP64)

$$(\epsilon | U | E) = \{\delta(E-\epsilon) + [\mathcal{P}/(E-\epsilon)]\} (\epsilon | K | E) \times [1 + \pi^2(E | K | E)^2]^{-1/2}. \quad (6.6)$$

which makes the singularity of  $U$  explicit and defines it in a manner appropriate to our problem. The symbol  $\mathcal{P}$  in (6.6) means that the principal part is to be taken in any integration over the singularity; thereby the integral (6.5) is no longer singular. The last factor of (6.6) is a normalization constant. Notice that, apart from this normalization factor, (6.6) and the resulting form of (6.5) have the structure of a first-order perturbation formula, with the still unknown matrix  $K$  in place of the perturbation matrix.

The nonsingular matrix  $(\epsilon | K | E)$  is well known in collision theory<sup>25</sup> where it is called "reaction matrix." It is determined by numerical solution of the nonsingular equation which one obtains by substituting (6.6) into the equation (6.5') for  $U$ , namely,

$$(\epsilon | K | E) = (\epsilon | V | E) + \int d\epsilon' (\epsilon | V | \epsilon') \times [\mathcal{P}/(E-\epsilon')] (\epsilon' | K | E). \quad (6.7)$$

Here,  $(\epsilon | V | \epsilon')$  indicates in our problem an element of the matrix (6.1) shorn of its zero-order diagonal part, i.e.,

$$(\epsilon | V | \epsilon') = (\epsilon | H | \epsilon') - \epsilon\delta(\epsilon-\epsilon'), \quad (6.7')$$

and the integration is intended to take the principal part over the singularity and to include a sum over the discrete spectrum. An approximate representation of the integral in (6.7) by a finite sum over terms corresponding to adjacent intervals of  $\epsilon'$  can be obtained with any desired accuracy. Thereby (6.7) reduces to a *finite* system of linear *inhomogeneous* equations, which can be solved numerically to yield  $(\epsilon | K | E)$  and hence  $(\epsilon | U | E)$ . Some numerical calculations by this method, extended to include the effect of intrachannel interactions, have been carried out for atomic problems (AM66, Al68) as well as for nuclear problems.

We indicate now the alternative procedure of diagonalization by solving an integrodifferential equation. Instead of calculating the matrix  $(\epsilon | U | E)$  of (6.6)

set of degenerate wave functions

$$\Psi_{\alpha E} = \sum_\beta \int d\epsilon \psi_\beta (\beta\epsilon | U | \alpha E)$$

labeled by channel indices. The total photoabsorption yield of states of energy  $E$  is proportional to the sum of partial oscillator strengths  $\sum_\alpha f(0 \rightarrow \alpha E)$ . One may also consider a particular state

$$\sum_\alpha [f(0 \rightarrow \alpha E)]^{1/2} \Psi_{\alpha E} / [\sum_\alpha f(0 \rightarrow \alpha E)]^{1/2}$$

to which all photoabsorption of the relevant energy is directed; states of the same energy orthogonal to this one are not produced by photoabsorption.

one calculates a new improved radial wave function  $P_{El'}^{(1)}(\mathbf{r})$  for the excited electron represented as a superposition of initial wave functions  $P_{\epsilon'v}$ ,

$$P_{El'}^{(1)}(\mathbf{r}) = \int d\epsilon P_{\epsilon'v}(\mathbf{r}) (\epsilon | U | E). \quad (6.8)$$

Since the matrix element (6.1) is constructed with determinant wave functions that contain the radial wave function  $P_{\epsilon'v}$  and with others that contain  $P_{\epsilon'v}$ , it can be represented by integrals over these functions of the form

$$\begin{aligned} & \langle nl^{4l+1}\epsilon l' 1P^0 | H | nl^{4l+1}\epsilon' l' 1P^0 \rangle \\ &= \int_0^\infty dr_1 P_{\epsilon'v}(r_1) H_d(r_1) P_{\epsilon'v}(r_1) + \int_0^\infty dr_1 \int_0^\infty dr_2 P_{\epsilon'v}(r_1) \\ & \quad \times H_x(r_1, r_2) P_{\epsilon'v}(r_2). \end{aligned} \quad (6.9)$$

The two terms on the right of this equation originate, respectively, from terms in the expansion of determinant products in which  $P_{\epsilon'v}$  and  $P_{\epsilon'v}$  depend on the same and on different variables. This specification implies that  $H_d(r_1)$  and  $H_x(r_1, r_2)$  represent respectively direct and exchange parts of a Hamiltonian operator and that they include integrations over all electron variables that are not indicated explicitly in (6.9).

After these preliminaries we return to the equation (6.5') which determines the transformation  $U$ , in the form appropriate to the continuum, multiply it by  $P_{\epsilon'v}(\mathbf{r})$  and integrate it over  $\epsilon$ , to yield

$$\begin{aligned} & \int d\epsilon P_{\epsilon'v}(\mathbf{r}) \int d\epsilon' \langle nl^{4l+1}\epsilon l' | H | nl^{4l+1}\epsilon' l' \rangle (\epsilon' | U | E) \\ &= \int d\epsilon P_{\epsilon'v}(\mathbf{r}) (\epsilon | U | E) E. \end{aligned} \quad (6.10)$$

Substitution of (6.9) and (6.8) and consideration of the

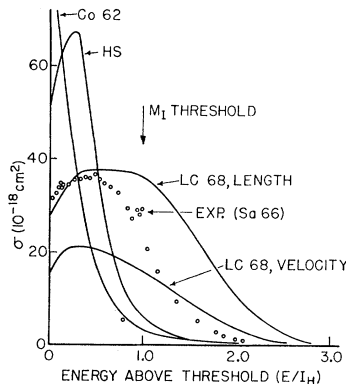


FIG. 22. Alternative calculations of Ar photoionization spectra. Co62: Model calculation of absorption by  $3p^6$  electrons, see Sec. 4.5. HS: Same, using Herman-Skillman potential (HS63). LC68: Wave function calculation by Eq. (6.13) augmented by weak interactions between 3 channels ( $3s^23p^6ed$ ,  $3s^23p^6es$  and  $3s3p^6ep$ ). Calculations via "length" (2.3) and "velocity" (2.8) formulas. Exp: Experimental data from Fig. 5.

completeness relation<sup>26</sup>

$$\int d\epsilon P_{\epsilon'v}(\mathbf{r}) P_{\epsilon'v}(r_1) = \delta(\mathbf{r} - \mathbf{r}_1) \quad (6.11)$$

reduces (6.10) to

$$\begin{aligned} H_d(\mathbf{r}) P_{El'}^{(1)}(\mathbf{r}) + \int_0^\infty dr_2 H_x(\mathbf{r}, \mathbf{r}_2) P_{El'}^{(1)}(r_2) \\ = P_{El'}^{(1)}(\mathbf{r}) E. \end{aligned} \quad (6.12)$$

Equation (6.12) is just the Hartree-Fock equation that one obtains by constructing a  ${}^1P$  combination of determinant wave functions  $\Psi_v$  for the excited state  $nl^{4l+1}El'$  in which only the excited electron function,  $P_{El'}^{(1)}$  is to be determined by a variational procedure.<sup>27</sup> A more explicit and standard form of (6.12) is

$$\begin{aligned} \{d^2/dr^2 + 2Z/r - (2/r) \sum_{ik} A_{ik} Y_k^{(i)}(P_i, P_i) - l'(l'+1)/r^2 \\ + E\} P_{El'}^{(1)}(\mathbf{r}) = (2/r) \sum_{ik} B_{ik} Y_k^{(i)}(P_i, P_{El'}^{(1)}) P_i(\mathbf{r}) \\ + \sum_i' \lambda_i P_i(\mathbf{r}), \end{aligned} \quad (6.13)$$

where atomic units and Hartree notations (Chap. 6 of Ha57) have been used. The symbol  $P_i$  and the  $\sum_i$  refer to all single-electron wave functions common to the ground state and to the excited state and the primed sum  $\sum_i'$  is limited to states with the orbital quantum number  $l'$ ; the role of the multipliers  $\lambda_i$  is explained in footnote 26. Equation (6.13) is formally the same as (5.19); however, the wave functions  $P_i$  are obtained here by a separate calculation pertaining to an atom in the ground state.

Notice how the single-particle wave equation (6.13) actually takes into account the electron correlation effects discussed in Sec. 6.1 through the numerical coefficients  $A_{ik}$  and  $B_{ik}$  and through the functional  $Y_k^{(i)}$ . This generalized Hartree-Fock equation can be

<sup>26</sup> Stated more accurately, the  $P_{\epsilon'v}(\mathbf{r})$  constitute a complete system of functions in the positive range of  $r$  that vanish at  $r=0$  as  $r^{l'+1}$ . Circumstances, not included in this example, may arise in which some discrete values of  $\epsilon$  correspond to single-electron states that are occupied in the many-electron ground state. These values are then excluded from the sums in (6.8) and (6.9) so that (6.11) is replaced by

$$\int^{\text{free}} d\epsilon P_{\epsilon'v}(\mathbf{r}) P_{\epsilon'v}(r_1) = \delta(\mathbf{r} - \mathbf{r}_1) - \sum_n^{\text{occ}} P_{n\epsilon'}(\mathbf{r}) P_{n\epsilon'}(r_1).$$

Consequently additional terms of the form

$$\sum_n^{\text{occ}} \lambda_n P_{n\epsilon'}(r)$$

appear in (6.12), where the  $\lambda_n$  depend on  $P_{n\epsilon'}^{(1)}$ ; however, the  $\lambda_n$  may be treated as Lagrange multipliers, to be fixed by requiring  $P_{n\epsilon'}^{(1)}$  to be orthogonal to the  $P_{n\epsilon'}$  for occupied  $n$ .

<sup>27</sup> For the treatment of interchannel interactions the generalization of (6.7) can be replaced by a system of integrodifferential equations akin to (6.12), in which  $H_d$  and  $H_x$  are matrices,  $(\alpha | H_d | \beta)$  and  $(\alpha r | H_x | \beta r_2)$ , and  $P_{El'}^{(1)} \rightarrow P_{\alpha El'}^{(1)}$ . These systems can be derived directly from the Schrödinger equation in its differential form and are called "close-coupling equations." Considerable effort has been directed to their approximate numerical solution [see, e.g., (Bu65) and Sec. 8.3.].

derived from the variation of a  $^1P$  superposition of determinant wave functions rather than of a single determinant.

The equation (6.13) has been solved numerically for Ar as a part of a more extensive set of calculations, see, e.g., (CLS67), which also consider effects of core relaxation (Sec. 7) and interchannel interactions. The solution of (6.13) yields greatly improved agreement with experiment when it is utilized, instead of the initial  $P_{\epsilon'l'}$ , in the calculation of the oscillator strength distribution by means of (6.8) and (4.5). As seen in Fig. 22, this agreement is as good as can be expected at this time from the threshold to the proximity of the  $M_I$  edge. Beyond this range, the procedure of this section appears to overcorrect the theoretical results shown in Fig. 5. Core relaxation (Sec. 7) and interaction with the channel of  $3s$  electron excitation do not appear to affect the residual disagreement appreciably.

The significance of these results is downgraded by the large discrepancy in Fig. 22 between the parallel results obtained utilizing the "length" and "velocity" formulas (2.3) and (2.8) for the oscillator strength. A discrepancy is not unexpected here according to Sec. 5.4 but its magnitude in this application is remarkable as was noted in Sec. 5.5.

### 6.3. Plasma-Type Treatment

This section treats an approximate form of the intrachannel matrix (6.1) for which the diagonalization problem of Sec. 6.2 is solved analytically. The approximation is suggested by the semimacroscopic models of plasma theories so that the resulting equation to be solved becomes equivalent in most respects to the main equation of plasma models. The analytical solution affords a basis for qualitative discussion of effects of intrachannel interaction.

In simple models of plasma-type theories one considers the electrostatic interaction between the oscillations of two particles, or groups of particles, clearly separated in space. For example, the interaction of oscillations confined within different unit cells of a crystal has been studied (Fa60). Under such conditions, the interaction energy is proportional to each of the dipole moments of two localized oscillations and to their mean reciprocal cube distance ( $V = \mathbf{u}_1 \cdot \mathbf{u}_2 / r_{12}^3$ ). Insofar as this mean distance is constant, i.e., independent of the oscillations, the interaction depends only on products of pairs of separate oscillation variables. Coupled motions of this class are solvable by a well known procedure.

In the coupling of particle motions within one atom, or nucleus, these motions cannot be regarded as localized in separate regions of space. However one can introduce an approximate form of the  $G^1$  integral in (6.3) which has the same properties as the interaction of two separate dipoles. The interaction energy in

(6.3) has the form  $e^2 r_</r_>^2$  which is equal to

$$e^2 r_<r_>/r_>^3 = (er_1)(er_2)/r_>^3. \quad (6.14)$$

Therefore, we can write

$$\begin{aligned} G^1 &= [e \int_0^\infty dr_1 P_{nl}(r_1) P_{\epsilon'l'}(r_1) r_1] \\ &\quad \times [e \int_0^\infty dr_2 P_{\epsilon'l'}(r_2) P_{nl}(r_2) r_2] \langle r_>^{-3} \rangle \\ &= e^2 R(nl, \epsilon'l') R(\epsilon'l', nl) \langle r_>^{-3} \rangle, \end{aligned} \quad (6.15)$$

where  $\langle r_>^{-3} \rangle$  is defined implicitly as a suitable average value and the  $R$  matrix elements are the same as in (4.5). To proceed as in the simple plasma theories one must assume that  $\langle r_>^{-3} \rangle$  is a constant, independent of  $\epsilon$  and  $\epsilon'$ , (ACS67) or at least that it is the product of two factors, one depending on  $\epsilon$  and one on  $\epsilon'$ . No general argument supporting the validity of this assumption seems to have been advanced. However a moderately good fit of the data of Table IV may be obtained by representing  $(\epsilon | H | \epsilon')$  as  $h(\epsilon)h(\epsilon')$ . Therefore, we accept this assumption for purposes of orientation and set

$$\kappa \neq G^1(\epsilon, \epsilon') = g(\epsilon)g(\epsilon'), \quad (6.16)$$

where  $\kappa$  is the coefficient of  $G^1$  in (6.2). We also disregard the other terms of (6.2). Having thus assumed that the off-diagonal part of (6.1) is factorable, its diagonalization proceeds readily utilizing the formulas of Sec. 6.2 which are appropriate to continuous spectra.

Setting the interaction matrix  $(\epsilon | V | \epsilon')$  of (6.7) equal to (6.16) yields

$$\begin{aligned} (\epsilon | K | E) &= g(\epsilon) \{ g(E) + \int d\epsilon' g(\epsilon') \\ &\quad \times [\mathcal{P}/(E - \epsilon')] (\epsilon' | K | E) \}. \end{aligned} \quad (6.17)$$

Notice that the expression in  $\{\dots\}$  depends on  $E$  but not on  $\epsilon$ . Therefore  $(\epsilon | K | E)$  itself can be factored in the form  $g(\epsilon)k(E)$ , where  $k(E)$  is still unknown. Substitution of this expression into (6.17) leads to the solution

$$(\epsilon | K | E) = g(\epsilon)g(E)/[1 - F(E)] \quad (6.18)$$

with

$$F(E) = \int d\epsilon [\mathcal{P}/(E - \epsilon)] g^2(\epsilon). \quad (6.18')$$

The transformation matrix (6.6) becomes then

$$(\epsilon | U | E)$$

$$= \frac{\delta(E - \epsilon)[1 - F(E)] + g(\epsilon)[\mathcal{P}/(E - \epsilon)]g(E)}{\{[1 - F(E)]^2 + \pi^2 g^4(E)\}^{1/2}}. \quad (6.19)$$

This result enables us to construct the "improved" wave function (6.5) and thereby to transform the radial dipole integral  $R(nl, \epsilon'l')$  of Sec. 4.2 into its im-

proved version

$$R^{(1)}(nl, El') = \int d\epsilon R(nl, \epsilon l') (\epsilon | U | E). \quad (6.20)$$

At this point one can utilize the proportionality of  $R$  and  $g$  implied by (6.15) and (6.16), namely,

$$R(nl, \epsilon l') = [\kappa e^2 \langle r_{>}^{-3} \rangle]^{-1/2} g(\epsilon), \quad (6.21)$$

which yields the remarkable simplification of (6.20)

$$R^{(1)}(nl, El') = \frac{R(nl, El')}{\{[1 - F(E)]^2 + \pi^2 g^2(E)\}^{1/2}}. \quad (6.22)$$

Notice that the improved dipole integral  $R^{(1)}$  is proportional to its initial approximation value at the same energy  $E$ . Moreover the proportionality factor depends on  $g^2(E) = \kappa G^1(E)$ , a diagonal element of the interaction matrix, and on  $F(E)$ , its Hilbert transform. A corollary of this proportionality is that the transformation (6.22) does not shift the points of zero in the spectra of oscillator strength which were discussed in Sec. 4.5. This result is not inconsistent with the comparison of experimental data and first approximation calculations in Figs. 5, 7(a), and 22. It hinges on the assumption, implicit in (6.16), that the first approximation state  $\psi_{E0}$  for which  $R(nl, E_0) = 0$  remains unperturbed by the interaction matrix (6.1).

Examination of the transformation (6.22) points up the following typical possible situations: (a) As expected,  $R^{(1)}$  remains close to  $R$  if the interaction  $\pi g^2(E) = \pi \kappa G^1$  and, consequently, its transform  $|F(E)|$  remain much smaller than unity throughout the spectrum. (b) If  $\pi g^2(E)$  is moderately smaller than or of the order of unity,  $R^{(1)}$  is reduced or boosted appreciably depending on the sign of  $F(E)$ . In particular, if  $R^2$  and (therefore)  $g^2$  have their large values concentrated in a single maximum,  $F(E)$  is negative on the low-energy side and positive on the high-energy side of this maximum. As illustrated in Fig. 23,  $R^{(1)2}$  has then a maximum flatter than that of  $R^2$  and shifted toward higher energy, as required to bring the initial theoretical results into better agreement with experimental evidence. (c) The characteristic phenomenon of plasma-type excitation occurs when  $g^2(E)$  is substantially larger than unity in a limited band of the spectrum and small, but nonzero, above this band. Then  $F(E)$  is large and positive in the region immediately above this band and decreases toward higher energy; where  $F(E) = 1$ ,  $R^{(1)2}$  experiences a sharp maximum ("plasma resonance"). Figures illustrating typical relationships between  $R^2$  and  $R^{(1)2}$  are also found in (BL65, BEL67, ACS67).

Further illustration of the effects of intrachannel interaction is provided by its influence on the phase shift of the wave function of the escaping photoelectron. As noted at the end of Sec. 4.2, photoabsorption is enhanced in a spectral range where the phase shift

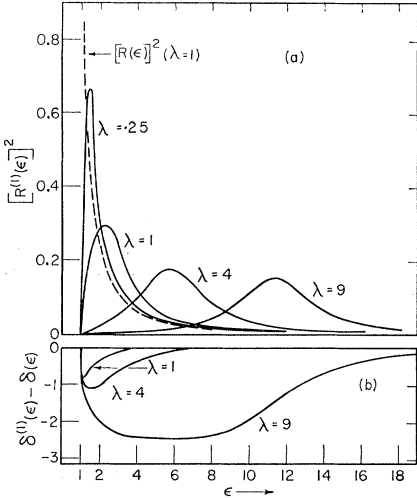


FIG. 23. Model calculations illustrating: (a) Eqs. (6.22) and (b) (6.23), with  $\lambda = \kappa e^2 \langle r_{>}^{-3} \rangle$ ,  $R(\epsilon) = 1/\epsilon$  for  $\epsilon > 1$ ,  $R(\epsilon) = 0$  for  $0 \leq \epsilon \leq 1$ . (Courtesy D. P. Chock and A.R.P. Rau.)

rises rapidly with increasing energy. From the asymptotic behavior of the "improved" wave functions (6.5), with the definition (6.6) of  $U$ , their phase shift can be shown to be

$$\delta_E^{(1)} = \delta_E - \arctan \pi (E | K | E), \quad (6.23)$$

where  $\delta_E$  is the initial approximation phase shift and the next term represents the effect of intrachannel interaction. As seen in the examples of Fig. 23, this effect depresses the phase shift by an amount that depends on the magnitude of  $g(E)$  but does not exceed  $\pi$ ; in the situation (c) described above the negative contribution returns to zero rapidly—i.e., with a steep slope—at the point of resonance.

As noted at the end of Sec. 6.1, the macroscopic plasma-type theory of atomic oscillator strengths started from the consideration of charge oscillations localized in different portions of an atom and emphasized the importance of interaction between oscillations at different points (LS53, Br58). More recent versions of this theory have taken as their point of departure the oscillations associated with single-particle excitations calculated in accordance with Sec. 4 and have emphasized and calculated the classical dipole-dipole interactions of alternative excitations of this type (e.g., BL65, BEL67, ACS67). These semi-macroscopic calculations differ from the derivation of (6.22) in the following minor aspect. The interaction of classical oscillators includes automatically the influence of virtual excitations of the ground state which are regarded in our treatment as effects of interchannel interaction. This influence brings about the replacement of  $E - \epsilon$  by  $E^2 - \epsilon^2$  in (6.18') and corresponding adjustments in the definition of  $g(\epsilon)$  and  $F(E)$  for reasons discussed in Sec. 8.5 in connection with the random

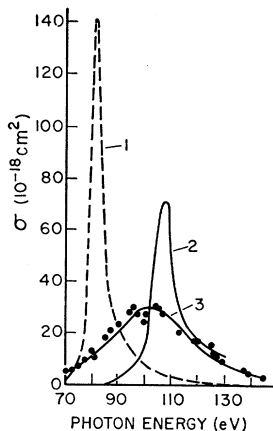


FIG. 24. Effect of plasma-model corrections upon single-electron model calculation of  $4d^{10}$  photoabsorption in Xe. (1) Calculated without correction (Co64) (see Sec. 4.5). (2) Calculated with correction (ACS67). (3) Calculated with correction (BEL67). ● Experimental data (Ed64). [The calculations of (2) and (3) differ in the adjustment of plasma-model parameters.]

phase approximation. That discussion will show why these virtual excitations have generally minor importance in atomic applications, in contrast to the more typical applications of plasma theory to solid and gaseous conductors. The plasma-type results are also more general than (6.22) in that they apply to interchannel as well as to intrachannel interactions and even to intershell interactions.

The macroscopic plasma-type theory has been applied to intrachannel effects only for the photoabsorption by the  $4d^{10}$  subshell of Xe (BEL67, ACS67) as shown in Fig. 24. In this application the spectral dependence of the function  $g(\epsilon)$  was obtained from the evaluation of  $R(nl, \epsilon l')$  in accordance with Sec. 4, but its absolute scale requires an estimate of the factor  $\langle r>^{-3} \rangle$  in (6.15). Dimensionally this factor is of the order of the reciprocal cube radius of the  $4d$  shell. This was the basis of the value chosen in (BEL67), even though the weighting factors multiplying  $r>^{-3}$  in the integrals of  $G^1$  weigh in favor of large values of  $r>$  and thereby depress the average  $\langle r>^{-3} \rangle$ ; this reference also utilized a linear expansion of  $1 - F(E)$  near its zero value. In (ACS67), on the other hand,  $\langle r>^{-3} \rangle$  was treated as an adjustable parameter. The results of Fig. 24 show that intrachannel interaction accounts at least qualitatively for the discrepancy between the results of Sec. 4 and the experiments.

## 7. CORE RELAXATION AND DOUBLE EXCITATIONS

An electron that has been ionized (or even only highly excited) by photoabsorption scarcely intermingles any longer with other electrons of the same atom. Therefore it no longer contributes to the screening of the nuclear attraction experienced by these "core" electrons. This change of screening, previously noted in Sec. 4.4, normally causes the core electrons to draw a little closer to the nucleus. Thereby it exerts a modest over-all influence on the oscillator strength distribution of atoms. However, it occasionally also induces one (or more) other electrons to become excited or ionized

as a by-product of the photoabsorption process. This phenomenon, called "electron shake off," is foreign to the single-electron model of Sec. 4 and to its many-electron version described in Sec. 5.1. However it is allowed for automatically by the "best wave function" approach of Sec. 5.5 and has also a place in the general procedure of Sec. 5.3.

We shall discuss the core relaxation initially through the "sudden" approximation which is rather familiar (Sc49) and of rather straightforward application. Then it will be shown how to derive the same results by a restricted treatment of interchannel interaction within the framework of Sec. 5.3. This point of view also indicates how one can evaluate the accuracy of the sudden approximation in particular examples and improve upon it, if and as required. Section 7.2 will then summarize existing information on double transitions. The summary will embrace all double transitions even though the core relaxation mechanism accounts only for a part of them, the rest arising presumably from more complex interactions with exchanges of angular momentum or from interaction effects upon the ground state.

In spite of our qualitative understanding of various mechanisms that contribute to double excitation, quantitative estimates of the probability of this process are most uncertain except in a few simple examples. Calculations appear to depend sensitively on details of the wave function; see in particular the successful but inadequately understood calculation of double ionization in He (BJ67) and the discussion in Sec. 8.4.

### 7.1. The "Sudden" Approximation

This approximation has been introduced in connection with radioactive processes which change the nuclear charge and hence the attraction experienced by atomic electrons within a time shorter than the electron orbital periods [see, e.g., Mi41, Wi52, Le53]. It is clearly relevant to the influence of photoionization of an inner shell electron upon the state of outer shell electrons, less clearly relevant when one deals with electrons of the same shell. It implies that the process of photoabsorption can be resolved into two successive stages. The first stage, namely, photoabsorption proper, proceeds in accordance with the models of Sec. 4 or Sec. 5.1. In the second stage one takes into account that the initial model potential  $V(r)$  is no longer appropriate for the calculation of the states of the previously undisturbed "core" electrons.

To this end one adopts a new model potential  $\bar{V}(r)$  which reflects a reduction of screening, one calculates a new complete set of radial wave functions  $\bar{P}_{nl}(r)$  for the core electrons and constructs with them a new set of determinant many particle wave functions  $\bar{\Psi}_\mu$ , which afford an improved representation of the alternative final states of the atom.

Calculation of the dipole matrix elements (5.4),

utilizing a wave function  $\tilde{\Psi}_{\mu'}$  instead of the original  $\Psi_{\nu'}$ , can now no longer rely on the orthonormality of single-electron wave functions for reducing (5.4) to its single-electron form (5.5). The overlap integrals  $(\bar{n}l | nl)$  no longer equal  $\delta_{\bar{n}n}$ . Nevertheless the off-diagonal overlap integrals, with  $\bar{n} \neq n$ , are generally small. Formulas will be written here only to *lowest non-vanishing order* in these small integrals.

Accordingly,  $\tilde{\Psi}_{\mu'}$  wave functions will yield nonzero matrix elements (5.4) if constructed by choosing  $N$  sets of single-electron quantum numbers  $(\bar{n}_i \bar{l}_i \bar{m}_i \bar{s}_i)$  as follows. One set  $(\bar{n}' l' m' s')$ , pertaining to the electron that absorbs the radiation, can be chosen as in (5.5). Each of the other sets must have  $\bar{l}_i$ ,  $\bar{m}_i$ , and  $\bar{s}_i$ , respectively, equal to  $l_i$ ,  $m_i$ , and  $s_i$  in a corresponding set of  $\Psi_\nu$ , otherwise the matrix element vanishes by orthogonality, but its  $\bar{n}_i$  need not be equal to  $n_i$ . To lowest nonvanishing order only 0, 1, 2... of the  $\bar{n}_i$  can differ from  $n_i$  for single, double, triple ... transitions. In this approximation one finds

$$(\tilde{\Psi}_{\mu'} | \sum_j z_j | \Psi_{\nu}) = \sum \left[ \prod_i^{\text{core}} \int_0^\infty \bar{P}_{\bar{n}_i l_i}(r) P_{n_i l_i}(r) dr \right] \times (\psi_{\bar{n}' l' m' s'} | z | \omega_{nlms}), \quad (7.1)$$

where the

$$\prod_i^{\text{core}}$$

extends over the  $N-1$  sets  $(\bar{n}_i l_i m_i s_i)$  other than  $(\bar{n}' l' m' s')$ , i.e., over electrons that do not participate in the photoabsorption directly and where the  $\sum$  extends over possible alternative permutations among the  $\bar{n}'$  and  $\bar{n}_i$  with  $l_i = l'$ . Equation (7.1) clearly would reduce to (5.5) if the wave function sets  $\bar{P}_{nl}$  and  $P_{nl}$  were identical so that the overlap integrals  $(\bar{n}l | nl)$  would equal  $\delta_{\bar{n}n}$ .

Any difference between a value of  $\bar{n}_i$  and that of  $n_i$  implies that one of the core electrons performs a transition as a result of the change of potential from  $V(r)$  to  $\bar{V}(r)$ , i.e., as a by-product of photoabsorption. According to (7.1) the total probability of double or multiple processes is

$$P^{(2)} = 1 - \prod_i^{\text{core}} \left[ \int_0^\infty \bar{P}_{n_i l_i}(r) P_{n_i l_i}(r) dr \right]^2, \quad (7.2)$$

namely, the complement of the probability that each core electron simply "relax" from its old wave function  $P_{n_i l_i}$  into the new one  $\bar{P}_{n_i l_i}$  with the same quantum numbers. When all  $\bar{n}_i = n_i$ , the matrix element (7.1) is of zeroth order; first-order corrective terms to this expression have been described by (Ba64) and (HL67).

We have introduced here the "sudden" approximation on the usual phenomenological basis, which relies on estimates of the time required by the absorbing electron to escape from the core. To derive it within the general formulation of Sec. 5.3, we should now identify

a property of the energy matrix  $(\nu'' | H | \nu')$  which obtains under the same circumstances as the "sudden" approximation and which allows a simplified approximate solution of the system of equations (5.16).

To this end we shall take into account only Hamiltonian matrix elements that represent a screening interaction between an escaping electron and one which can be "shaken off" into an excited state by core relaxation. The states of the escaping electron will be labeled  $e$  and those of the electron to be shaken off will be labeled  $c$ . Since nonzero matrix elements  $(\nu'' | H | \nu')$  occur only for pairs of states  $\nu''$  and  $\nu'$  that differ by no more than two sets of single-electron quantum numbers, the quantum number sets implied by  $\nu''$  and  $\nu'$  shall be restricted by  $(n_k'' l_k'' m_k'' s_k'') = (n_k' l_k' m_k' s_k')$  for all  $k$  other than  $e$  and  $c$ . Moreover, since screening interactions involve no transfer of angular momentum, we shall also have  $(l_k'' m_k'' s_k'') = (l_k' m_k' s_k')$  for  $k=e$  and  $k=c$ . The set of numbers  $(n_e' l_e' m_e' s_e')$  is to be identified, in alternative calculations, with each of the sets occupied in the ground state except that vacated by the escaping electron.

For the purpose of relating the actual screening interaction to that assumed in the model Hamiltonian (5.1), we represent the kinetic energy term of (5.11) as  $\sum_i p_i^2 / 2m = H_{\text{mod}} - \sum_j V(r_j)$ , so that

$$H = H_{\text{mod}} + \sum_j \{-Ze^2/r_j + \sum_{i>j} e^2/r_{ij} - V(r_j)\}. \quad (7.3)$$

Since  $\nu'$  and  $\nu''$  are eigenstates of the term  $H_{\text{mod}}$  of (7.3), this term does not contribute to off-diagonal matrix elements  $(\nu' \neq \nu'')$  which are relevant to us. For these elements we have then

$$(\nu'' | H | \nu') \rightarrow (n_e'' \epsilon_e'' | \sum_j \{-Ze^2/r_j + \sum_{i>j} e^2/r_{ij} - V(r_j)\} | n_e' \epsilon_e'), \quad (7.4)$$

where only the quantum numbers that differ in  $\nu'$  and  $\nu''$  have been indicated and where the quantum numbers  $n_e$  of the escaping electron have been indicated by the continuum variables  $\epsilon_e$  for proper emphasis.

Let us now take into account that the model potential  $V(r_j)$  is designed so as to minimize the mean value of  $\sum_j \{\}$  for the ground state. To begin with  $V(r_j)$  is understood to include a nuclear field contribution which cancels  $-Ze^2/r_j$ . We shall also assume that the contribution of  $V(r_j)$  to (7.4) cancels the contribution of all terms of  $\sum_{i>j} e^2/r_{ij}$  that correspond to interactions: (a) between all core electrons that occupy the same state in  $\nu'$  and  $\nu''$  and (b) between any of these electrons and either of the two electrons that perform transitions. Owing to the symmetry among all electrons, we may call these two electrons 1 and 2. Thereby (7.4) reduces to the form

$$(n_e'' \epsilon_e'' | e^2/r_{12} - V_e(r_1) - V_c(r_2) | n_e' \epsilon_e'), \quad (7.5)$$

where  $V_e$  indicates the portion of the model potential  $V(r_1)$  attributable to the repulsion of electron 1 by the escaping electron, and  $V_c$  indicates a corresponding potential for electron 2. More specifically,  $V_e(r_1)$  is defined implicitly by (7.5) as  $-Ze^2/r_1 + \langle \sum_{i>2} e^2/r_{i1} \rangle - V(r_1)$ , where the average is taken over the position of all electrons other than 1 and 2 in their ground state orbitals. This average can be calculated in any specific example. However, for our purposes an approximate but qualitatively meaningful estimate of  $V_e$  and  $V_c$  will be utilized below.

The matrix element of  $e^2/r_{12}$  consists, like (6.2), of a sum of terms corresponding to alternative transfers of angular momentum. Of these, we retain only the term for zero transfer because it represents the screening interaction. (In the special case of  $l_e' = l_e$ , another term corresponding to interchange of  $n_e''$  and  $\epsilon_e''$  would also occur.) The screening term is, with the notation of (6.3),

$$(n_e''\epsilon_e'' | e^2/r_{12} | n_e'\epsilon_e')^{(0)} = \int_0^\infty dr_1 P_{n_e''l_e'}(r_1) P_{n_e'l_e'}(r_1) \times \int_0^\infty dr_2 P_{\epsilon_e''l_e'}(r_2) P_{\epsilon_e'l_e'}(r_2) e^2/r. \quad (7.6)$$

We introduce now a notation suited to represent screening effects, namely,

$$q(n''n', r) = \int_0^r dr' P_{n''n'}(r') P_{n'n'}(r'). \quad (7.7)$$

Thereby (7.6) takes the form of separate screening effects of each electron upon the other,

$$(n_e''\epsilon_e'' | e^2/r_{12} | n_e'\epsilon_e')^{(0)} = \int_0^\infty dr P_{n_e''l_e'}(r) P_{n_e'l_e'}(r) q(\epsilon_e''\epsilon_e', r) e^2/r + \int_0^\infty dr P_{\epsilon_e''l_e'}(r) P_{\epsilon_e'l_e'}(r) q(n_e''n_e', r) e^2/r. \quad (7.8)$$

This notation enables us to formulate an estimate of the effect of mutual screening of electrons 1 and 2 which is implicitly included in the model potential  $V(r_1) + V(r_2)$  and is represented in (7.5) by  $V_e(r_1) + V_c(r_2)$ . Insofar as  $V(r)$  was chosen so as to be reasonably self-consistent for the atom in its *ground state*,  $V_e(r_1)$  represents the screening action of the escaping electron *as though* it were still in a bound ground state orbital  $n_e$ , that is,

$$V_e(r_1) \sim e^2 q(n_e n_e, r_1) / r_1. \quad (7.9)$$

For  $V_c(r_2)$  we make a corresponding estimate. Consider also that all matrix elements of  $V$  are diagonal in all quantum numbers except the  $n$  of a single electron. In conclusion we obtain for the screening contribution to

our matrix element the estimated value

$$(v'' | H | v') \rightarrow (n_e''\epsilon_e'' | e^2/r_{12} - V_e(r_1) - V_c(r_2) | n_e'\epsilon_e')^{(0)} = \int_0^\infty dr P_{n_e''l_e'}(r) P_{n_e'l_e'}(r) [q(\epsilon_e''\epsilon_e', r) - q(n_e n_e, r) \delta(\epsilon_e'' - \epsilon_e')] e^2/r + \int_0^\infty dr P_{\epsilon_e''l_e'}(r) P_{\epsilon_e'l_e'}(r) [q(n_e''n_e', r) - q(n_e'n_e', r) \delta_{n_e''n_e'}] e^2/r. \quad (7.10)$$

The goal of this evaluation of matrix elements for the screening interaction is to compare them with the assumption made in the "sudden" approximation approach, namely that the escaping electron does not contribute *any* screening effect to the core electrons. This assumption amounts to setting

$$q(\epsilon_e''\epsilon_e', r) \sim 0 \quad (7.11)$$

in (7.10). The sudden approximation also disregards by implication any effect of a core transition on the escaping electron, i.e., it disregards the second term on the right-hand side of (7.10) altogether.

An assessment of the validity of the "sudden" approximation can, therefore, be obtained by evaluating the left-hand side of (7.11) utilizing its definition (7.7) and the radial wave functions obtained by the model potential, in accordance with our general approach. The WKB approximation provides an initial estimate of this parameter which displays the relevant dimensional elements of the problem, namely,

$$q(\epsilon_e''\epsilon_e', r) \sim (\pi\hbar)^{-1} \int_0^r \frac{dr'}{v(r')} = \frac{\tau(r)}{\hbar}, \quad \text{for } \epsilon_e'' \sim \epsilon_e' \sim \epsilon. \quad (7.12)$$

Here

$$v(r) = \{2[\epsilon - V(r) - \hbar^2 l(l+1)/2mr^2]/m\}^{1/2} \quad (7.13)$$

is the classical velocity of the escaping electron at  $r$  and  $\tau(r)$  is the classical time of escape up to  $r$ . This estimate of  $q$  is nearly independent of the difference  $\epsilon_e'' - \epsilon_e'$  over a band width  $|\epsilon_e'' - \epsilon_e'| \lesssim q^{-1}$  and decreases outside this band. Upon substitution into (7.10) this estimate provides a contribution of the order of the ratio of the time of escape to the orbital period of the  $i$ th state, which is just the expansion parameter of the "sudden" approximation.

Accordingly, one might calculate the effect of core relaxation within the frame of Sec. 5.3 as follows. Evaluate  $q(\epsilon_e''\epsilon_e', r)$  and its contribution to (7.10) numerically. To the extent that the contribution is much smaller than unity—and therefore can be disregarded at the present level of approximation—one concludes that the "sudden" approximation is justified in the sense that the general method of Sec. 5.3 reduces to it. In this event one may apply to the wave functions

$\Psi$ , the transformation implied by the "sudden" approximation with

$$\bar{V}(r) = V(r) - q(n_e n_e, r) e^2/r, \quad (7.14)$$

namely,

$$(U^{-1})_{\mu\nu} = \prod_i^{\text{core}} \int_0^\infty \bar{P}_{\tilde{n}_i' l_i'}(r) P_{n_i' l_i'}(r) dr, \quad (7.15)$$

whose introduction in (5.15) yields just (7.1). This transformation diagonalizes the portion of a Hamiltonian submatrix (7.10) contributed by the term with the factor  $-q(n_e n_e, r) \delta(\epsilon_e'' - \epsilon_e')$ . However, if the other terms of (7.10) yield a nonnegligible contribution, the sudden approximation proves inadequate and a more elaborate procedure that diagonalizes the complete submatrix (7.10) is required.

## 7.2. Summary of Experimental Evidence on Double Transitions

Double transitions have been observed primarily in the photoabsorption spectra of noble gases and of the divalent and trivalent metals. Most of the observations concern excitation of two valence electrons, but some of them also involve inner electrons. In some instances double transitions clearly result from interactions with exchange of angular momentum. In a few cases core relaxation appears to be the main factor involved; in others the role of simple core relaxation cannot be disentangled from that of more complex interactions until the integrals (7.7) or equivalent parameters will have been evaluated. Some of the more detailed evidence emerges from experiments on particle collisions rather than on photoabsorption.

Absorption lines due to double transition processes have been known for a long time in the ultraviolet spectra of alkaline earth atoms, because some of them occur at comparatively low photon energies ( $\sim 5-8$  eV) and with rather striking intensity [see Fig. 12(a)]. Several circumstances contribute to this property of alkaline earths. Firstly, single transitions of valence electrons to highly excited discrete states or to the adjoining continuum have low intensity in the alkaline earths much as in the alkalis (Sec. 4.1 and 4.5), so that absorption by two-electron transitions stands out by contrast. Secondly the outer shell of group-II atoms contains only two electrons, with configuration  $n^2$  and with rather low binding energy. This configuration mixes strongly with the configuration  $np^2$ , because  $ns$  to  $np$  excitations (within the same shell) require a low energy; therefore, a transition from the ground state to a state  $npms$  or  $npmd$  may be regarded as a single-electron transition out of the  $np^2$  component of the ground state. Mixing with  $(n-1)d^2$  may also be important. This description attributes double transitions in the alkaline earths to a ground-state interaction with exchange of angular momentum between electrons, rather than to core relaxation. These considerations

TABLE V. Oscillator strengths of double excitation states in the rare gases, Ca and Sr.<sup>a</sup>

Atom	State	Wavelength (Å)	$10^4 f$	Ref.
He	$2s2p \ ^1P^0$	206.2	52	MC65
Ne	$2p^4 3s3p \ ^1P^0$	275.6	8	CME67
Ar	$2p^4 3d4p \ ^1P^0$	401.9	13	CME68
Ar	$2p^4 4s4p \ ^1P^0$	424.2	0.3	CME68
Kr	Not identified	501.2	0.04	Ed67
Kr	Not identified	492.3	0.2	Ed67
Kr	Not identified	461.8	0.3	Ed67
Xe	Not identified	560.0	0.01	Ed67
Xe	Not identified	595.9	0.11	Ed67
Xe	Not identified	579.2	0.086	Ed67
Xe	Not identified	570.8	0.12	Ed67
Ca	$3d5p \ ^1P^0$	1887.	240.	DH60
Ca	$3d6p \ ^1P^0$	1765.	40.	DH60
Ca	$3d7p \ ^1P^0$	1687.	20.	DH60
Ca	$3d5p \ ^3P^0$	1915.	2.	DH60
Ca	$3d6p \ ^3P^0$	1769.	1.	DH60
Ca	$3d7p \ ^3P^0$	1694.	1.	DH60
Sr	$4d6p \ ^3D^0$	2024.	0.8	HY63
Sr	$4d6p \ ^1P^0$	1970.	88.	HY63
Sr	$4d7p \ ^1P^0$	1811.	10.	HY63
Sr	$4d8p \ ^1P^0$	1756.	6.	HY63
Sr	$4d6p \ ^3P^0$	2018.	2.	HY63

<sup>a</sup> For the rare gases  $f$  was calculated via Eq. (8.6) from measured values of the profile parameters and thus is proportional to  $q^2$ . The values for Ca and Sr were obtained by integration over the line profiles and are thus proportional to  $q^2 - 1$  (see Sec. 8.1).

apply also to the Zn, Cd, Hg group and, to some extent, to metals of higher valence. Some data on the oscillator strength of double transitions in these elements are shown in Table V.

Transitions involving two valence electrons of atoms of other chemical groups occur in the far ultraviolet. Therefore their extensive observation dates only from the recent technical developments described in Sec. 3, particularly from the application of synchrotron light. Actually these observations are still confined mostly to the noble gas atoms. Four Rydberg series of absorption lines due to two-electron transitions have been observed and classified in helium between 60 and 75 eV (MC65) and a larger number in neon (CME67). Still higher numbers of lines have been detected in the spectra of Ar, Kr, and Xe (MC63, MC64) but their classification has only started. Indeed the line density in certain portions of the Ar, Kr, and Xe double excitation spectra is so high as to make analysis and detailed measurements very difficult.

Simple estimates by the "sudden" approximation indicate that core relaxation does not suffice to account for the observed intensity of He double excitations. Other evidence (Sec. 8.3) also indicates that a more complex interchannel interaction has a dominant influence on the doubly excited states of He. On the other hand, a calculation that treats the final state by the "sudden" approximation but whose ground state in-

volves extensive configuration mixing has accounted very well for the observed double photoionization of He between 100 and 500 eV (BJ67). The comparative simplicity of He may permit a thorough analysis of the role of different mechanisms in its double excitation.

Absorption spectra of the noble gases in the soft x-ray range have also given evidence of double transitions involving one electron from an inner shell and one from the valence shell. The energy required for this process may be of the order of 100 eV if the inner shell involved in it lies next below the outer one; in this energy range Codling and Madden (CM65a) have observed 7 such transitions in Kr and 21 in Xe, without fully classifying and interpreting them or estimating their oscillator strengths. In the x-ray energy range, the  $K$  absorption edge of Ar has been observed to be followed in energy by a small hump in the spectrum which presumably corresponds to double transitions, from the  $K$  shell and from the outermost ( $M$ ) shell (Sc63, BW63).

As shown in Table V the oscillator strengths of absorption lines due to double transitions in the rare gases are quite small, typically of the order of  $10^{-3}$  for the most intense of these lines. The lines stand out sharply because they are superposed on a continuum whose oscillator strength spreads over a wide spectral region and also because of their profile characteristics discussed below. To estimate the total oscillator strength of double transitions, one might take the measured value of the first line of each intense series, when available, and estimate by extrapolation the contributions of the subsequent lines and of the adjoining continuum. (This continuum is due to photoionization of one electron and simultaneous excitation of another one.) A basis for such an extrapolation has been outlined in (FC65)<sup>28</sup> but it has hardly been applied yet (CF67a). To these contributions there must be added that of double photoionizations, which cannot be singled out directly from the measurement of radiation absorption but can be obtained by the separate experiments outlined in Sec. 3.5. Gathering all evidence, from photoabsorption and from other processes, double transitions appear to contribute a few percent of the total oscillator strength of helium and a somewhat larger fraction of the strength attributable to the outer shell electrons of the other noble gases.

It may be noted, although of little relevance to oscillator strengths, that discrete energy levels with two excited electrons normally lie in the energy range of the continuous single ionization spectrum. Therefore doubly excited states are unstable and decay by autoionization into ionized states. This decay is rather rapid and hence broadens double excitation lines in the absorption spectra very appreciably; nevertheless successive lines of each series of double excitation often remain well separated, their widths amounting to only 1/10 or even 1/100 of their separations unless at least

one of the excited electrons has been lifted out of an inner shell. Moreover, interference between direct photoabsorption to ionized states and indirect ionization via double excitation causes a characteristic asymmetry in most profiles of double excitation lines (see Fig. 27); this asymmetry provides important information on configuration interaction, to be discussed in Sec. 8.1.

Finally it should be stressed that detailed experimental information on double transitions requires the observation of secondary processes, i.e., a determination of the final state of the atomic system, in addition to the study of photoabsorption spectra. Such evidence has been obtained by studying the charge distribution of ions following photoabsorption (CHK66) and ionization by electron impact<sup>29</sup> (Sc65), by observing fluorescence of ions which remain excited following electron impact ionization (StJL64, HW63, LL65, MdH67) and by observing the spectrum of photoelectrons following photoionization (CK65, Ca67). An analysis of double processes in He via the methods outlined in Sec. 2.6 indicates that the observed double ionization and ion fluorescence do not stem primarily from the effects represented by (2.38) but either from higher order or from nondipole interactions between the incident particle and the atomic electrons (WHW67).

Evidence on the charge distribution of ions following photoionization or electron impact is further complicated for heavier atoms by rearrangement processes (Auger effect and rearrangement with the emission of radiation) which occur following removal of an inner subshell electron. Detailed analysis of these processes (CHK66, KC67) indicate that the "sudden" approximation predicts the correct order of magnitude of double transitions when inner shell electrons are ionized but underestimates it for outer shell electrons (see Table VI). Direct evidence of multiple ionization from electron spectrometry (Fig. 25) is consistent with this finding.

On the whole, double transitions contribute only a minor fraction of atomic oscillator strengths, as we have

TABLE VI. Ratio of double to single ionization obtained from charge distribution data for average excitation energies large compared to the threshold value; sudden approximation values for electron shakeoff computed via Eq. (7.2) using Hartree-Fock wave functions (NTC66).

Element, shell	Exp	Sudden approximation
He	0.036	0.01
Ne, $K$	0.20	0.18
Ne, $L$	0.14	0.04
Ar, $M$	0.17	0.04

<sup>29</sup> Collision by sufficiently fast electrons or protons is certainly relevant to photoabsorption (see Sec. 2.6). However, the intense fluorescence of residual ions produced by low energy  $\text{He}^+$  bombardment of atoms (LNT65, DNST67) is not relevant to double photoprocesses, because the  $\text{He}^+$  carries an electron and acts primarily through the formation of a new molecular complex.

<sup>28</sup> The procedure of (FC65) is faulty as detailed in footnote 3.

seen. The interest of the rapidly accumulating evidence on the qualitative and quantitative properties of double transitions relates rather to the insight they provide into aspects of atomic mechanics that escape detection as long as only one electron is pried loose from the ground state. This subject lies beyond the scope of the present article, but will emerge again in the following chapter on interchannel interactions.

## 8. EFFECTS OF INTERCHANNEL INTERACTIONS

This chapter surveys effects of electron-electron interaction upon absorption spectra that have been identified up to this time and do not belong to the classes discussed previously. These effects are often very conspicuous when the spectra are examined with fair or better resolution. If, however, one considers the spectra on a coarse energy scale, i.e., only the absorption averaged over several eV, the influence of interchannel interactions has not been shown to amount to more than 5–10%. Most effects of interchannel interactions have not been analyzed thus far in detail, theoretically or experimentally. Hence our treatment will confine itself to preliminary outlines.

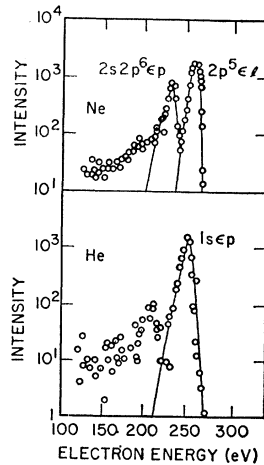
Yet these effects may well provide new substantial information on atomic dynamics, especially when complemented by observation and analysis of the by-products of photoabsorption, e.g., by measurements of the energy spectra of photoelectrons. In the language of Sec. 2.3 one may say that photoabsorption measurements yield the spectrum of the two-variable correlation function  $\langle z_j z_k(t) \rangle$  but that more detailed observations will provide data on dynamical properties represented by multi-variable correlation functions.

### 8.1. Profile of Lines Broadened by Autoionization

The absorption spectrum of a neutral atom contains numerous Rydberg series of lines whose convergence limits correspond to the various excited states of the residual positive ion.<sup>30</sup> Nearly all the lines of these series lie above the lowest ionization limit. Therefore they correspond to transitions of the atom from its ground state to discrete excited states which are stationary only in an independent-electron approximation. Corrections to this approximation, which have been classed in Sec. 5.3 as effects of "interchannel interaction," cause these discrete states to autoionize, that is, to decay into ionized (continuum) states of equal total energy. Autoionization is appropriately considered in the context of various transitions due to

<sup>30</sup> Some of these excited states differ from the ground state of the ion by having a vacancy in an inner shell or subshell rather than in the outermost subshell; they represent the thresholds for photoionization of an inner electron. Others belong to excited terms of the ground-state configuration. The remaining series limits correspond to processes in which a change of the ion's configuration occurs in addition to photoionization; these are double transition processes of the kind discussed in Sec. 7.2.

FIG. 25. Experimental spectra of photoelectrons extracted by 276-eV photons (Ca67). Solid curves represent electrons due to single transitions. Lower energy electrons are direct evidence of double transitions.



interchannel interactions as illustrated in Fig. 26. The limited lifetime of autoionizing states causes the corresponding absorption lines to be broadened, in accordance with the uncertainty principle. The extent of the broadening and other characteristics of the profile of these lines provide information on interchannel interactions, as detailed below.<sup>31</sup>

The formula which represents these line profiles, (8.5), was derived in (Fa61a, FC65) by solving a many channel generalization of (6.7). One considers for this purpose, besides the continuum states of one or more channels, one or more discrete states of other channels whose ionization thresholds lie above the energy  $E$  under consideration; these "closed" channels have only discrete zero-approximation energy levels  $\epsilon_n$  in the proximity of  $E$ . When a single  $\epsilon_n$  lies close to  $E$ , the important part of the generalized (6.7) can be solved analytically. An equivalent result is obtained (Sh67) by application of the general collision theory in which photoabsorption is regarded as a photon-atom collision process (see end of Sec. 1). From this point of view the absorption lines due to autoionizing states appear as resonances in the collision cross section, analogous to those observed, e.g., for collisions of slow neutrons with nuclei.<sup>32</sup> Here we aim only at describing the line profiles and interpreting them qualitatively.

The continuum states reached by decay of an auto-

<sup>31</sup> Discrete states are also known whose autoionization is energetically possible but is slowed down by many orders of magnitude owing to the conservation of spin multiplicity or to other selection rules (FN67). Excitation of these states by photoabsorption from the ground state is made altogether negligible by the very same selection rules.

<sup>32</sup> This analogy is also pertinent if one applies collision theory to the atomic states only, excluding the photon as in footnote 25, i.e., if one considers first an electron incident on a positive ion. When the total energy in the incident channel nearly equals that of a closed-channel discrete state, the channel interaction may cause the incident electron to be captured in this state. This process is indicated by the wavy downward arrows in Fig. 26. The discrete state of the neutral atom thus formed, which quickly autoionizes, is regarded from the point of view of collision theory as an unstable compound state resulting from the temporary association of an electron and a positive ion.

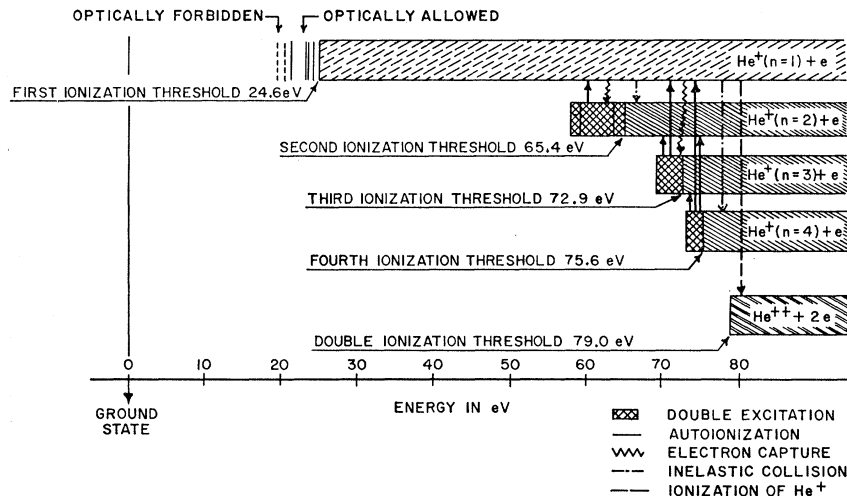


FIG. 26. Diagram showing several channels in the spectrum of helium and their interconnection by autoionization processes. Also shown are other interchannel transition processes which are implicitly related to autoionization.

ionizing state can also be reached from the ground state by direct photoabsorption, at least in principle. In this event no observable distinction exists between the direct transition and the indirect transition through absorption into a discrete state followed by autoionization. The distinction serves nevertheless as a tool of analysis for the purpose of describing the observed absorption spectra in terms of a small number of parameters and of interpreting the physical significance of these parameters. Under the circumstances, theory calculates separate probability *amplitudes* for the two transition processes and determines the absorption probability for each photon energy as the square of the sum of separate amplitudes rather than as the sum of separate probabilities. The departure of the square of the sum of amplitudes from the sum of their squares is an effect of interference between the direct and indirect transitions. In the absence of interference the contribution of a discrete state to the absorption spectrum would consist of a symmetric absorption line superposed on a smooth continuum. Interference destroys the simple separation of contributions and indeed causes striking asymmetries in most autoionization lines.

The origin of this asymmetry can be visualized as follows. The excitation of a discrete autoionizing state constitutes a “virtual” energy non-conserving process except for exact resonance, i.e., unless the energy of the absorbed photon coincides with the energy of the discrete state exactly. Therefore the sign of the probability amplitude of the discrete excitation depends on the sign of the difference between these two energies and has opposite values for photon energies above and below the resonance. The interference between the direct and indirect photoionizations becomes then constructive on one side of the line center (resonance point) and destructive on the other.

In each wing of a line the contribution of the interference term to the total absorption exceeds in magni-

tude that of the term representing the intrinsic absorption to the discrete level; in the wing where interference is destructive the total absorption will then fall *below* the level of the surrounding continuum. Thereby *reduced absorption* is observed in at least a portion of the line profile, even though one might naively expect the occurrence of a discrete level to yield only an increase of absorption.

This effect of reduced absorption is further magnified greatly by another effect of channel interaction, namely *spectral repulsion*. Repulsion is familiar in discrete spectra, when a level of one configuration happens to lie in the midst of a series of levels of other configurations; configuration interaction causes the levels of the second series to be shifted away from the perturbing level. [A second-order perturbation formula (La30) displays this effect clearly.] In our situation, where a discrete level of one series lies in the continuum of another channel, the levels of this continuum are also repelled, but in the sense that their oscillator strength is thinned out in the proximity of the perturbing level. This reduction of absorption is particularly conspicuous when it is not compensated adequately by the intrinsic absorption of the discrete perturbing level.

The following quantitative parameters determine the profile of lines broadened by autoionization and can, conversely, be evaluated by the observation of line profiles: (1) The spectral width  $\Gamma$  of a line depends on the interaction matrix element between the discrete autoionizing state  $\Psi_n$  and the continuum state  $\Psi_a$  that results from it by autoionization; it is reciprocal to the mean life of  $\Psi_n$

$$\Gamma = 2\pi(\Psi_a | H | \Psi_n)^2 = \hbar/\tau. \quad (8.1)$$

[The omission of the “absolute value” sign in (8.1) rests on a convention according to which  $\Psi_n$  and  $\Psi_a$  are real.] (2) The maximum fractional depth of the depression of the continuous absorption spectrum produced by spectral repulsion and interference is indicated by a

parameter  $\rho^2$ . This depth depends on the overlap integral

$$\rho = (\Psi_d | \Psi_a), \quad (8.2)$$

(also taken as real) of two continuum states, namely,  $\Psi_a$  which is generated by autoionization, and  $\Psi_d$  which is generated by direct absorption from the ground state  $\Psi_0$  (FC65). (In general, several alternative continuum channels can be reached by each of these processes. Details of the interaction determine which superposition of channels results from either of them. Clearly the spectrum of direct photoabsorption remains unaffected by interference if the two superpositions are orthogonal, i.e., if  $\rho=0$ .) (3) The maximum fractional rise of absorption within the line profile, above the absorption that would be observed in absence of the line, is indicated by  $\rho^2 q^2$ . The "profile index"<sup>33</sup>

$$q = (\bar{\Psi}_n | \sum_j z_j | \Psi_0) / [\pi (\Psi_n | H | \Psi_a) (\Psi_a | \sum_j z_j | \Psi_0)] \quad (8.3)$$

has a squared magnitude proportional to the relative oscillator strength of the autoionizing state compared to that of a suitable band of continuum states. Its sign depends on the relative signs of the matrix elements in (8.3) and determines whether the maximum or minimum absorption occurs on the low-energy side of the line.

The line profile extends over a range of the continuous spectrum proportional to the line width  $\Gamma$  and centered on a theoretically defined resonance energy  $E_r$ . Accordingly the profile is conveniently represented by a formula that gives the cross section for absorption of photons of energy  $E$  as a function of the reduced energy variable

$$\epsilon = (E - E_r) / \frac{1}{2} \Gamma. \quad (8.4)$$

The formula is (Fa61a, FC65)

$$\begin{aligned} \sigma(E) &= \sigma_c(E) \{ \rho^2 [(q+\epsilon)^2 / (1+\epsilon^2)] + 1 - \rho^2 \} \\ &= \sigma_c(E) [1 + \rho^2 (q^2 - 1 + 2qe) / (1 + \epsilon^2)], \end{aligned} \quad (8.5)$$

where  $\sigma_c(E)$  is the cross section that would be observed in the absence of the autoionizing state.

Figure 27 represents typical line profiles which have been observed and which differ very much from one another even though represented by the same formula. Since  $\Gamma$  is embodied in the energy scale, the profiles depend only on  $q$  and  $\rho$ . The factors that determine the dipole matrix elements in the expression of  $q$  have been discussed in preceding chapters, except for the effect mentioned in footnote 33 which has not been studied. The other factors affecting  $q$  also have hardly been studied (FC65). With regard to the overlap parameter  $\rho$ , Fig. 27 displays quite different examples: (a) The autoionization of the  $2s2p\ 1P^0$  level of He at

<sup>33</sup> The symbol  $\Psi_n$  indicates here a modification of the discrete wave function  $\Psi_n$ , which includes an appropriate admixture of continuum wave functions, as defined by Eq. (17) of (Fa61a).

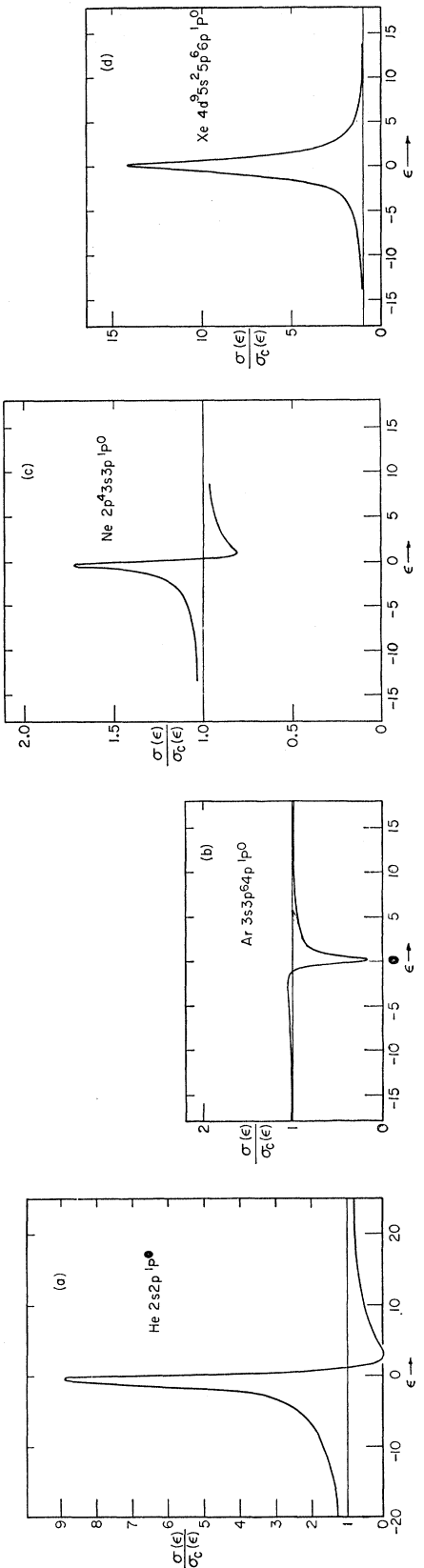


Fig. 27. Profiles of autoionization lines in the rare gases obtained from experimental data (MC65, CME67, CME68, Ed67). (a)  $2s2p\ 1P^0$  in He ( $q=-2.8, \rho^2=1$ ); (b) Inner shell excitation in Ar,  $3s3p64p\ 1P^0$  ( $q=-0.22, \rho^2=0.17$ ); (c) Two-electron excitation in Ne,  $2p\ 4s3s3p\ 1P^0$  ( $q=-2.0, \rho^2=0.17$ ). (d) Inner shell excitation in Xe,  $4d\ 4s\ 2s\ 66p\ 1P^0$  ( $q \sim 200, \rho^2 \sim 0.0003$ ).

60.1 eV and the direct absorption lead into a single continuum channel, so that a complete overlap ( $\rho=1$ ) and a zero value of minimum absorption result (CM65). (b) The autoionization of  $2s2p^63p^1P^0$  in Ne and  $3s3p^64p^1P^0$  in Ar and the corresponding direct absorption can lead into five alternative channels; nevertheless their final states overlap by 83% and 93%, respectively. (c) Double excitation leads to only  $\sim 40\%$  overlap in the  $2p^43s3p^1P^0$  line of Ne. This is typical of other double excitations which have been studied to date. (d) At higher photon energies autoionization normally yields doubly excited ions and direct absorption singly excited ones. Hence the overlap is quite small (and  $q$  is quite large) and no minimum of absorption has been detected in line profiles. Indeed, the profile of the  $4d^95s^25p^66p^1P^0$  resonance in Xe is Lorentzian within the experimental uncertainty.

In the second form of (8.5) the term proportional to  $q^2$  represents the intrinsic, Lorentz shaped, profile of an autoionization line, unaffected by interference. The next term, with coefficient  $-1$ , represents the effect of spectral repulsion and the last term the effect of interference. The interference term decays in the line wings in proportion to  $1/\epsilon$  only; therefore its effect is appreciable over a surprisingly broad spectral range. The contribution of the interference term averages out upon integration over energy across the line whereas the two preceding terms yield, respectively,

$$\sigma_c \rho^2 q^{21} \frac{1}{2} \Gamma \pi = 1.098 \times 10^{16} \bar{f}_n \text{ cm}^2 \text{ eV}, \quad (8.6)$$

$$\sigma_c \rho^{21} \frac{1}{2} \Gamma \pi = 1.098 \times 10^{16} \frac{1}{2} \pi \rho^2 \Gamma (df/dE)_{E=E}, \text{ cm}^2 \text{ eV}, \quad (8.7)$$

where  $\bar{f}_n$  is the discrete oscillator strength corresponding to the discrete wave function  $\bar{\Psi}_n$ .<sup>33</sup>

Equation (8.5), with constant values of  $\Gamma$ ,  $q$ , and  $\rho$ , is approximate only in the sense that it applies to the limit of a narrow isolated line, i.e., for  $\Gamma$  much smaller than the distance of another line or than the spectral range over which the continuum characteristics vary appreciably. Its derivation in (Fa61a) focussed on the influence of interchannel interaction between a discrete level and a continuum; accordingly it regarded all other steps of the wave function improvement program of Sec. 5.3 as having been completed previously. However, the same result can be obtained by representing suitably the formal solution of the Eq. (5.16) for the transformation matrix  $U$  (see also Sh67).

The treatment of the effect of spectral repulsion in (8.5) is incomplete, in that the continuum oscillator strength strength  $(df_c/dE)_{E,E} \frac{1}{2} \pi \rho^2 \Gamma$  pushed away from the proximity of the autoionizing state should reappear elsewhere in the spectrum, owing to the sum rules. Presumably this corrective effect occurs outside the range of applicability of (8.5) with fixed parameters. An alternative approach has been developed (CS66) which is internally more consistent at the price of

disregarding the energy matrix elements between the autoionizing state and continuum states removed from it by more than a limited energy amount.

The profiles of successive lines of a Rydberg series are similar provided the series is sufficiently regular (FC65). The criterion of regularity is that the distance of each resonance from the series limit fits the formula  $E_{\text{lim}} - E_s = I_H/(s-\sigma)^2$ , where  $I_H = 13.6$  eV,  $s$  equals successive integers and  $\sigma$  is a constant quantum defect. Within this approximation the profile index  $q$  should be fixed for the whole series and the product  $\rho^2 \Gamma$  should be proportional to the width of successive blocks in the histogram of Fig. 1, i.e., to  $dE_s/ds = 2I_H/(s-\sigma)^3 \sim \Delta E$ , where  $\Delta E$  indicates the interval between successive lines. Moreover  $\rho^2$  should also have the same value for a whole series when the excited electron participates in the autoionization, which occurs normally for series in the lower part of the spectrum below  $\sim 50$  eV. Available evidence agrees with these rules (CM65, CME67).

The patterns of intensity distribution in the spectra, discussed above in connection with autoionization, occur also below the first ionization threshold in the absence of autoionization or indeed across the threshold (Fig. 28). This observation need not cause surprise because the intensity distribution results from channel interaction, rather than from autoionization *per se*, and remains unchanged on a sufficiently coarse scale of photon energies upon replacement of the continuous spectrum by a dense series of discrete lines. In this example the  $6snp$  series becomes strongly perturbed by interaction with each state of the other channel ( $5dn_p$ , also  $5dn_f$ ) throughout the energy interval  $\Gamma$  that would apply if the series were a continuum. Each of the perturbed discrete states is shifted in energy and is replaced by a superposition of discrete states of its own channel and of the single relevant discrete state of the other channel. The latter state is similarly perturbed and its energy level is sandwiched-in between those of the series. The resulting intensity distribution in the spectrum averaged over line intervals is the same as one would observe for an autoionization line, as noted above (see, e.g., Fa61a).

## 8.2. Gross Effects of Spectral Repulsion

The depression of continuum absorption caused by the presence of a discrete autoionizing state, which was discussed in Sec. 8.1, is but an obvious example of a widespread phenomenon to which little attention has been directed and whose import remains to be investigated.

Consider any pair of channels whose states can be reached by photoabsorption and whose ionization thresholds lie at different energies in the spectrum. (The lowest level of the discrete spectrum of any channel should actually be considered as the onset of absorp-

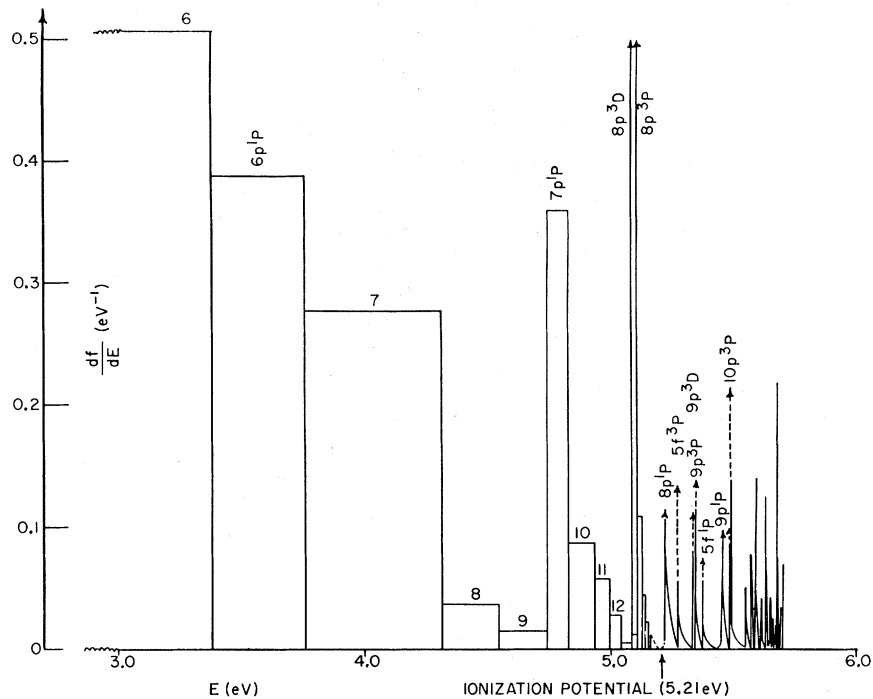


FIG. 28. Oscillator strengths of Ba in the discrete and continuum near threshold. Histogram for the discrete spectrum constructed in accordance with quantum defect theory (see Fig. 1). Numbered discrete lines are  $6snp^3P^0$ . Lines labeled  $nL^1,^3L$  correspond to  $5dnL^1,^3L^0$ . Note shape similarity of histogram distorted by  $5dnp$  lines and of continuum distorted by autoionization lines of same series. The histogram, based on a preliminary analysis of partial data, does not display all the desirable internal consistency. (Courtesy K. T. Lu; data from PS62, HC67a, GC60, To67.)

tion, instead of its ionization threshold.) Insofar as spectral repulsion is a general phenomenon, channel interaction tends to push the spectra of the two channels apart. More specifically, it should tend to increase the absorption pertaining to the channel with lower threshold in the spectral range below the onset of the other channel; it should tend to depress the absorption of both channels near the onset of the higher threshold channel; finally it should enhance the absorption of the higher threshold channel at high energies where the lower threshold channel presumably absorbs less than the upper channel. In other words, the channel interaction should tend to compensate the absorption jump which marks the onset of the upper channel.

In addition to spectral repulsion, channel interaction also produces transfers of oscillator strength among channels and prominent interference effects on line profiles and possibly on continuum distributions. Therefore the effects of spectral repulsion are not easily disentangled from the others without a detailed analysis. In the spectra below  $\sim 100$  eV reviewed in Sec. 4, successive absorption edges quite generally fail to stand out or at least stand out less than one might expect. Factors contributing to this phenomenon have been discussed in Sec. 4.7 and effects of interchannel interaction presumably also contribute to it. Yet the depre-

sion of edges, particularly as observed at the thresholds of the outer  $s$  subshells of Ar, Kr, and Xe, appears to constitute distinctive evidence of interchannel repulsion.

Here we shall only outline what can be learned about the depression of absorption edges by the analysis of line profiles. In any spectral range where discrete lines occur, the density of oscillator strength averaged over the line intervals extrapolates smoothly into the continuum beyond the convergence limit of Rydberg series. This result, which is a main feature of the quantum defect theory (Se58) has been proven with great generality by various authors (Ba59, FN59, Ga63). It enables one to determine the net change of absorption across the edge ("jump ratio") and the contribution of each new channel thereto from the analysis of line profiles which are more easily accessible to observation.

Specifically the depression of the jump ratio due to spectral repulsion is obtained by averaging over a line interval  $\Delta E$  the integrated effect of spectral repulsion upon one line, (8.7), in analogy to the construction of the histogram in Fig. 1. The resulting quantity, namely  $\sigma_{c2}^{-1}\pi\rho^2\Gamma/\Delta E$ , is uniform over a series insofar as  $\rho^2\Gamma/\Delta E$  is a constant. Accordingly it extrapolates beyond the series limit and may be regarded as the depression of the absorption jump. This depression is to be compared to

the positive contribution of the oscillator strength of the new channel, which is  $\sigma_c \frac{1}{2} \pi (\rho^2 \Gamma / \Delta E) q^2$  according to (8.6). Thereby the jump ratio is represented (FC65) by

$$1 + \frac{1}{2} \pi (\rho^2 \Gamma / \Delta E) (q^2 - 1), \quad (8.7)$$

in which the  $-1$  term corresponds to spectral repulsion. This term looms important for moderate or small values of  $q^2$ , especially of course for  $q^2 < 1$ , in which case the jump ratio becomes smaller than unity, that is, one obtained a downward jump.

As anticipated in Sec. 4.7 downward jumps actually occur in the spectra of the noble gases Ar, Kr, and Xe at the threshold for ejection of the  $s$  electrons just inside of the valence subshell. The existence of these downward jumps follows from the "window" appearance of the lines converging to the thresholds. For Ne the corresponding value of the jump ratio is 1.008, since  $q^2 = 2.6$  and  $\frac{1}{2} \pi (\rho^2 \Gamma / \Delta E) = 0.005$  (CME67).

### 8.3. Strong Coupling

Degeneracies between the spectra of different channels may boost the effects of interchannel interaction. A conspicuous example of this boosting occurs in the doubly excited states of He, in which different channels have identical ionization thresholds; specifically, the thresholds corresponding to the  $2s$  and  $2p$  levels of  $\text{He}^+$  coincide since  $\text{He}^+$  is hydrogenic, and the same occurs for  $3s$ ,  $3p$ ,  $3d$ , etc. This phenomenon came to attention when a single series of lines converging to the  $2s$  or  $2p$  limit of  $\text{He}^+$  was observed (MC63) instead of the three series corresponding to states  $2snp\ 1P^0$ ,  $2pns\ 1P^0$ , and  $2pnd\ 1P^0$  which would have been predicted by ordinary considerations of spectroscopy. Since the number of series converging to each limit is not changed by interchannel interactions, the initial observation of a single series meant that one series is much more intense than the other two. On the other hand, simple calculations show that transitions from the ground state to  $2snp$  and  $2pns$  should yield quite comparable absorption. Therefore, in view also of the fact that levels  $2snp$  and  $2pns$  should be almost degenerate, it was concluded that interchannel interaction changes the character of the channels completely (CFP63). A second but much weaker and narrower series converging to the same limit was observed subsequently (CM65).

The problem raised by strong interaction among a few channels can be handled theoretically by extension of the procedures which were described in Sec. 6.2 for the treatment of intrachannel interactions. The procedure of direct diagonalization of a Hamiltonian submatrix, by solution of (6.7), involves in this case a larger submatrix  $(\alpha \epsilon | V | \alpha' \epsilon')$ , where  $\alpha$  and  $\alpha'$  are discrete indices corresponding to the alternative channels.<sup>25</sup> The procedure by solution of an equivalent integrodifferential equation (6.13) involves instead the solution of a system of coupled equations, one for each value of  $\alpha$ .<sup>27</sup>

Both procedures have been utilized rather extensively in numerical calculations pertaining to the doubly excited states of He, either for these states alone or including also the continuum states which amounts to taking autoionization into account from the start; see, e.g., (LR66, AM65, OMG65, BTP67) and (BMcV65, Bu65, AM66) for the two procedures, respectively. These calculations have yielded a satisfactory agreement with experimental data as well as with one another. They have also revealed that analogous situations occur in many series of doubly excited states which cannot be reached by photoabsorption (see particularly Bu65). In particular the calculated intensity indices  $(\Gamma / \Delta E) q^2$  of the three  $^1P^0$  ( $\rho = 1$ ) series converging to the  $\text{He}^+(2s, 2p)$  limit bear the ratios 700:6:0.2 to one another,<sup>24</sup> which explains the failure to observe the weakest of them. Yet only a partial understanding of the characterization of these series has been obtained thus far despite persistent efforts (CFP63, Bu65, Ma66, Ma67), because the calculations provide no clear clue to the physical interpretation of their results. Two-electron excited states appear to have a collective character which expresses itself most obviously through differences in lifetime, but more intrinsically in the magnitude of the wave functions for small values of the radial coordinates of *both* electrons.

An indication also exists of this collective character of double excitations in atoms other than He which do not possess the same full degeneracy of ionization thresholds. The lowest state of doubly excited Ne has the spectral character  $2p^4(^3P) 3s 3p\ 1P^0$  and is common to the two series: (a)  $2p^4(^3P) 3s (^2P) np\ 1P^0$  and (b)  $2p^4(^3P) 3p (^2P) ns\ 1P^0$  whose limits are separated by nearly 4 eV. According to data of (CME67) the intensities and profiles of series (b) relate well to that of the lowest line whereas the  $n=4$  line of (a) is missing altogether and lines with  $n>4$  have a different profile and are probably observable only because of another interaction discussed below. Thus it appears that here as in He the oscillator strength of a series is suppressed by some selection rule of unknown origin. However, no similar suppression has been detected in other double excitation series of Ne. The appearance of lines of series (a) with  $n>4$  is attributed (CME67) to interchannel interaction with the single state  $2p^4(^1D) 3s 3p\ 1P^0$ . This interaction shifts the position of series (a) lines away from the energy of this state and transfers to them a portion of its oscillator strength, a phenomenon that is well known in ordinary spectra of single excitation.

In the examples just considered, the degeneracy or quasidegeneracy of series limits concerns states of the ion with one electron excited to an outer shell. Similar quasidegeneracies are quite common for lower states of the ion, when its ground state configuration has

<sup>24</sup> Actually, these ratios depend primarily on  $\Gamma / \Delta E$  since the values of  $q^2$  are comparable for the three series.

different terms (e.g.,  $O^+$  has  $^4S^0$ ,  $^2D^0$ , and  $^2P^0$ ) or when there are nearly degenerate configurations (e.g.,  $6s$  and  $5d$  in  $Ba^+$  or  $4s$  and  $4p$  in  $Ca^+$ ). Low-lying double excitations, surveyed in Sec. 7.2, occur in these circumstances and the alternative channels of single and double excitation may, but need not, interact strongly. In fact not many of the known double excitations in Table V exhibit evidence of strong interaction. A somewhat different effect of strong coupling occurs in the near ultraviolet spectra of trivalent atoms, whose ionic ground states  $ns^2$  interact strongly with  $np^2$  as the ground states of neutral alkaline earth atoms do (see Sec. 7.2). Owing to this interaction the main channels of excited states  $ns^2md\ ^2D$  and  $ns^2ms\ ^2S$  reached by photoabsorption from the ground state  $ns^2np$  are coupled strongly to the excited states  $nsnp^2\ ^2D$  and  $^2S$  (see Ma67b, p. 152ff, also KS67).

Calculations of strong interactions can be carried out in these situations by the same methods as for doubly excited  $He^+$  and have been in fact performed in a few instances. The inaccuracy of the underlying approximations increases, of course, with the structural complexity of the outer electron shell. The following calculations of photoabsorption in limited spectral ranges by strong coupling methods exist besides those for doubly excited  $He$ :  $H^-$  (Ma67a),  $Be$  (Al68),  $Ne$  and  $Ar$  (LC67),  $Mg$  (We67b, Za67),  $Al$  (We68). The  $H^-$  and  $Be$  results exhibit unusual features that have not yet been detected experimentally. Related calculations of channel interaction in  $Be$  (Mo67) and in  $C^-$ ,  $N^-$ , and  $O^-$  (SHB67) aimed at the cross sections for electron-ion or electron-atom collisions and did not yield photoabsorption data.

The analysis and calculation of strong interchannel coupling is helped by application of Seaton's multiple-channel quantum defect method (Se66). It was noted at the end of Sec. 4.2, with regard to single-electron calculations, that a normalization factor  $N_{n'n'}$  can be usefully factored out of wave functions, radial integrals or oscillator strengths, the residual factor being a smooth continuous function of the excitation energy even in the discrete spectrum. A subfactor of  $N_{n'n'}$  depends only on the Coulomb field which prevails in the outermost portions of an atom and can be calculated analytically. In the framework of this article, Seaton's method may be described roughly as a factorization of the energy diagonalizing matrix  $U_{\nu\mu}$  of (5.16),

$$U_{\nu\mu} \rightarrow N_\nu \bar{U}_{\nu\mu} N_\mu. \quad (8.8)$$

The coefficients  $N_\nu$  and  $N_\mu$  are provided by hydrogenic theory and the matrix  $\bar{U}_{\nu\mu}$  has in effect only one element per pair of channels, rather than per pair of states, and varies smoothly and continuously with energy in the discrete as well as in the continuum. [Actually one factors the reaction matrix  $K$  introduced in (6.6) rather than  $U$  itself.]

This factorization can be utilized in several ways (Be66, Mo66, Mo67, Lu68). Starting from experimental data on discrete level positions and on oscillator strength spectra, the method yields a compact representation in terms of a smaller number of matrix elements. From a purely theoretical point of view the method reduces the magnitude of calculations of interchannel interactions. Combined utilization of theoretical and experimental data is also possible. The treatment in Sec. 8.1 of lines broadened by autoionization, especially with regard to Rydberg series of lines, may be regarded as an application of multichannel quantum defect theory.

#### 8.4. Radial Correlations in the Ground State

The preceding sections have dealt mainly with the influence of channel interactions on the final states of photoabsorbing transitions and with relevant improvements of their wave functions. Improved wave functions for the ground state have been utilized in numerous calculations. The improvement was achieved either by calculating strong configuration interactions or by utilizing altogether different types of wave functions, e.g., Hylleraas functions for  $He$ . The results of such calculations have been reviewed, in the main, in Sec. 5.5. The inclusion of strong interaction effects in the ground state was also essential in the photoionization calculations for  $Be$  (Al68) and for  $Ca$  (Mo66) and in the calculation of double photoionization in  $He$  (BJ67). However, hardly any systematic information on the qualitative and quantitative influence of ground state improvements upon photoabsorption has emerged beyond the realization of the importance of admixing  $np^2$  or  $(n-1)d^2$  configurations into the  $ns^2$  ground states of divalent metals or of the ions of trivalent atoms.

Here we present a few considerations on the radial correlations among outer shell electrons in the ground state, which influence particularly the probability of double excitations.

Since the electron interaction is repulsive, it should cause correlations such that when one electron lies unusually far from the nucleus the others lie unusually close to it, and vice versa. We also know from Sec. 4 that outlying portions of an electron's radial distribution contribute more to the absorption of lower energy photons and vice versa. Therefore, radial correlations tend to associate the absorption of a lower energy photon by one electron with a more condensed distribution of the other electrons; in the language of Sec. 7, they tend to leave the core in a more relaxed state least likely to result in a second excitation by the shake-off mechanism. Conversely, absorption of a higher energy photon tends to leave the other electrons further away from the nucleus, in an unrelaxed state more prone to a second excitation.

Double transitions cannot result from absorption of

low energy photons because their energy threshold is rather high. Above this threshold the scarce evidence available at this time shows a little increase of the relative probability of double ionization with increasing photon energy but this probability appears to level off rapidly (Ca67, BJ67). It cannot be really judged whether the influence of correlations suggested by the arguments above is in agreement with fact.

To illustrate the analytical treatment of radial correlations without attempting any assessment of the various factors in the calculation of (BJ67), we consider here the correlated wave function of the He ground state

$$\Psi_0(r_1, r_2) = N_0 \{ \exp(-\alpha r_1 - \beta r_2) + \exp(-\beta r_1 - \alpha r_2) \} \quad (8.9)$$

$$N_0 = 2[(\alpha + \beta)/2]^3 \{ \frac{1}{2}[1 + (\alpha + \beta)^6/(4\alpha^3)] \}^{-1/2}. \quad (8.10)$$

The parameters  $\alpha$  and  $\beta$  can be chosen in various alternative ways. The choice

$$\alpha = 2/a, \quad \beta = 1.34/a, \quad (8.11)$$

(with  $a$  = Bohr radius) does not yield minimum energy but provides a correct asymptotic behavior for  $r_1 \gg r_2$  and  $r_2 \gg r_1$ , since  $(1.34)^2$  is the binding energy of He in units of 13.6 eV; for  $r_1 \sim r_2$  this choice approximates well the usual product of two exponentials with  $\alpha = \beta = 27/16$ . This wave function represents the He atom as consisting of an  $\text{He}^+$  core with an electron attached onto it with binding energy  $\hbar^2 \beta^2 / 2m$ .

For the final state of a photoabsorption process with single excitation one may adopt a wave function analogous to (8.9), namely,

$$\begin{aligned} \Psi_f(r_1, r_2) = N_f \{ & \exp(-\alpha r_1) u_f(r_2) \cos \vartheta_2 \\ & + \exp(-\alpha r_2) u_f(r_1) \cos \vartheta_1 \} / 4\pi. \end{aligned} \quad (8.12)$$

The dipole matrix element of the transition has then the form

$$\begin{aligned} \langle \Psi_f | z_1 + z_2 | \Psi_0 \rangle &= \frac{4}{3} N_f N_0 \left\{ (2\alpha)^{-3} \int_0^\infty u_f(r) \exp(-\beta r) r^3 dr \right. \\ &\quad \left. + (\alpha + \beta)^{-3} \int_0^\infty u_f(r) \exp(-\alpha r) r^3 dr \right\}. \end{aligned} \quad (8.13)$$

The two integrals in this formula correspond to excitations out of the two unequal 1s orbitals  $\exp(-\beta r)$  and  $\exp(-\alpha r)$ ; the first of them will predominate for a lower energy transition and the second for a high-energy one.

An important property of the correlated wave func-

tion (8.9) is that it permits direct transitions to doubly excited states. If the ground state wave function of the  $\text{He}^+$  ion,  $\exp(-\alpha r)$ , is replaced in (8.12) by an excited state wave function,  $\exp(-\alpha r/n) L_n(2\alpha r/n)$ , the first term of (8.13) vanishes owing to orthogonality of this function and  $\exp(-\alpha r)$ , but the second one does not.

From the point of view of core relaxation and double excitation one may describe the correlated wave function (8.9) as follows. Let us utilize from the start a set of one-electron wave functions  $\psi_{nlms}$  (5.1) appropriate to the positive ion core of the atom, rather than to its neutral ground state, namely, in our case the set of hydrogenic wave functions of  $\text{He}^+$ . The initial ground-state wave function is then described inadequately by a single determinant  $\Psi$ , constructed with this set. However, it might be fairly represented by a superposition of  $\Psi$ , which have a single outer shell electron excited to any orbital with a higher discrete (or continuum) quantum number  $n$ . This representation is obtained by expanding the factors  $\exp(-\beta r)$  of (8.9) into a series of  $\text{He}^+$  radial wave functions  $\exp(-\alpha r/n) L_n(2\alpha r/n)$ . From this point of view, the problem of core relaxation no longer arises, because our base wave functions are already suited to describe the final state. On the other hand, double excitation can result from photoabsorption as a matter of course, since the initial ground state is represented as already containing a certain amount of virtual excitation.

The probability of double excitation of He estimated by this method appears to be much higher than the unrealistically low value of 0.02 obtained from the uncorrelated ground state function with  $\alpha = \beta = 27/16a$  and application of the sudden approximation formula (7.3).

The point of view outlined above can be applied, of course, to the treatment of photoabsorption by any atom. However its internal consistency and its quantitative implications require further analysis.

### 8.5. The Random Phase Approximation (RPA)<sup>35</sup>

As mentioned before, particularly in Sec. 6.1, considerable discussion has taken place concerning the applicability to atomic oscillator strengths of methods developed for the study of electron excitations in plasmas and solids. Apart from the semimacroscopic studies mentioned in Sec. 6.3, Altick and Glassgold (AG64) have made a detailed calculation of atomic oscillator strengths making use of approximations suggested by the theory developed for extended systems.

From the point of view of Sec. 5.3, the approximation implies a particular selection of a submatrix of the Hamiltonian to be diagonalized which includes the intrachannel interaction considered in Sec. 6 together with additional portions of the matrix. The selection

<sup>35</sup> Dr. P. L. Altick's help in clarifying the subject of this section is gratefully acknowledged.

originally designed for large systems does not appear realistic for application to atoms but the (AG64) procedure was improved in this respect. Here it seems desirable to formulate first the basic "RPA" approach in the context of this article because its main lines do not emerge readily from (AG64) and because its initial steps may be of interest irrespective of further approximations.

A feature of this approach is that one does not attempt to calculate the ground state wave function (5.14),  $\Psi_\mu = \sum_\nu \Psi_\nu U_{\nu\mu}$ , and the  $\Psi_{\mu'}$  for the excited state in full detail but calculates only the differences between them that are relevant to the oscillator strength  $f(\mu \rightarrow \mu')$ . For example, since the exact  $\Psi_\mu$  contains first approximation  $\Psi_\nu$ , with pairs of excited electrons and the same virtual excitations may also be present in the exact excited  $\Psi_{\mu'}$ , one wants to exploit any approximate independence of the oscillator strength on the occurrence of such virtual excitations. In general, the approach may permit the use of approximations that are unsuited for the separate calculations of  $\Psi_\mu$  and  $\Psi_{\mu'}$  but quite appropriate for the calculation of  $f(\mu \rightarrow \mu')$ .

Notice that a program of simultaneous improvement of the ground state and excited state wave functions is probably essential to solve the problem of inconsistencies in the calculation of oscillator strength, which was stressed in Sec. 5.4. It is conceivable, though not clear at this time, that the RPA equation (8.23) derived below will serve this purpose.

We start from the expression of the dipole matrix element

$$(\mu' | \sum_j z_j | \mu) = \sum_{\nu' \nu} (U^{-1})_{\mu' \nu'} (\nu' | \sum_j z_j | \nu) U_{\nu \mu} \quad (5.15)$$

which is exact to the extent that the still unknown matrix  $U$  is exact. The dipole element  $(\nu | \sum_j z_j | \nu')$  on the right of (5.15) reduces to a single-particle element according to (5.5) and further to the radial integral (4.5),  $R(nl, n'l')$ , multiplied by a factor  $t$  (essentially a Clebsch-Gordan coefficient) that depends on orientation quantum numbers and is not relevant here. Being a function of a single particle transition, the same  $R(nl, n'l')$  may appear in numerous terms  $(\nu, \nu')$  of the sum in (5.15).

Accordingly, we introduce a notation that enables us to separate  $R$  from the rest of the calculation. Call  $q$  the transition from the set of quantum numbers  $(nlms)$  to  $(n'l'm's')$  and introduce a new matrix element defined by the following properties. When  $\nu$  contains the single electron orbital  $(nlms)$  and  $\nu'$  contains  $(n'l'm's')$  but  $\nu$  and  $\nu'$  coincide in all other respects,  $(\nu' | a_q | \nu)$  equals the factor  $t(q) = (\nu' | \sum_j z_j | \nu) / R(q)$ ; otherwise  $(\nu' | a_q | \nu)$  vanishes. For future convenience we restrict the symbol  $q$  to transitions with zero approximation energies  $E_{n'l'} > E_{nl}$  and call the inverse transitions  $-q$ . Thus we also introduce  $(\nu' | a_{-q} | \nu)$  which equals  $t(q)$  when  $\nu'$  and  $\nu$  include respectively

$(nlms)$  and  $(n'l'm's')$  and vanishes otherwise. With these definitions we write

$$(\nu' | \sum_j z_j | \nu) = \sum_q R(q) (\nu' | a_q + a_{-q} | \nu) \quad (8.14)$$

since  $R(-q) = R(q)$ . Thereby (5.15) takes the form

$$(\mu' | \sum_j z_j | \mu) = \sum_q R(q) \sum_{\nu \nu'} (U^{-1})_{\mu' \nu'} (\nu' | a_q + a_{-q} | \nu) U_{\nu \mu} \quad (8.15)$$

which can also be written, using operator notation, as

$$(\mu' | \sum_j z_j | \mu) = \sum_q R(q) (\mu' | a_q + a_{-q} | \mu). \quad (8.16)$$

Since the radial integrals  $R(q)$  are regarded as known by the method of Sec. 4, the problem consists of determining the matrix elements of  $a_q$  and  $a_{-q}$  corresponding to the (unknown) states  $\Psi_\mu$  and  $\Psi_{\mu'}$  without necessarily calculating the complete matrices  $U$  and  $U^{-1}$ .

The Schrödinger equation for the eigenstates  $\mu$  and  $\mu'$  can be applied to the matrix elements of  $a_q$  and  $a_{-q}$  to yield

$$\begin{aligned} (E_{\mu'} - E_\mu) (\mu' | a_q | \mu) &= (\mu' | H a_q - a_q H | \mu) \\ (E_{\mu'} - E_\mu) (\mu' | a_{-q} | \mu) &= (\mu' | H a_{-q} - a_{-q} H | \mu). \end{aligned} \quad (8.17)$$

Without loss of generality we separate  $H$  into two terms  $H_{\text{mod}}$ , given by (5.1), and  $H_1 = H - H_{\text{mod}}$  so that owing to (5.3)

$$\begin{aligned} H_{\text{mod}} a_q - a_q H_{\text{mod}} &= (E_{n'l'} - E_{nl}) a_q = E_q a_q \\ H_{\text{mod}} a_{-q} - a_{-q} H_{\text{mod}} &= (E_{nl} - E_{n'l'}) a_{-q} = -E_{-q} a_{-q}. \end{aligned} \quad (8.18)$$

Substituting in (8.17) yields

$$\begin{aligned} (E_{\mu'} - E_\mu - E_q) (\mu' | a_q | \mu) &= (\mu' | H_1 a_q - a_q H_1 | \mu) \\ (E_{\mu'} - E_\mu + E_q) (\mu' | a_{-q} | \mu) &= (\mu' | H_1 a_{-q} - a_{-q} H_1 | \mu). \end{aligned} \quad (8.19)$$

All portions of the matrix  $(\nu' | H | \nu)$  that involve no transitions in or out of  $(nlms)$  or  $(n'l'm's')$  commute with  $a_q$  and  $a_{-q}$  and hence do not contribute to (8.19); this simplification—which results from the notation utilized here rather than from any physical consideration—was anticipated at the outset of this section. Equation (8.19) is still general and exact and is to be regarded as a convenient point of departure for approximation treatments.

The objective of the approximations considered here is to expand the right-hand side of (8.19) into a linear combination of matrix elements  $(\mu' | a_r | \mu)$ , whereby (8.19) becomes a linear algebraic system amenable to numerical solution, perhaps with the help of some truncation. In the  $(v', v)$  representation this would amount to representing the matrix

$$(v' | [H_1, a_q] | v) \quad (8.20)$$

as a superposition of  $(v' | a_r | v)$ . In view of the definition of  $a_q$  this representation would imply that non-vanishing elements (8.20) exist only for pairs  $(v', v)$  that differ by a single set of quantum numbers (*nlms*). Now, the operator  $H_1$  replaces in general *two* of these sets with *two* others and  $a_q$  *one* with *another*. Non-vanishing of the commutator  $[H_1, a_q]$  requires only that two of these six sets coincide. Therefore  $[H_1, a_q]$  can be represented in general as a superposition of *bilinear* terms  $a_r a_s$  in addition to linear ones. The RPA-type treatments disregard the bilinear terms.

Basically, the linearization of (8.20) in *extended systems*—as distinguished from atoms, which are small—corresponds to the assumption that the system as a whole is modified weakly by virtual excitations even though many excitations are present on the average in the whole system. Formally, however, the argument generally advanced is substantially the following (BS67). A matrix element of a product, such as

$$(v' | a_q H_1 | v) = \sum_{v''} (v' | a_q | v'') (v'' | H_1 | v),$$

results from the sum over  $v''$  of a large number of terms which tend to cancel out (hence the name of RPA) so as to yield a negligible contribution. A significant contribution stems, however, from those terms of  $H_1$  which cause a transition  $-q$ , exactly reciprocal to  $q$ .

This contribution is then evaluated—for extended systems—utilizing two further elements of the RPA which are also quite plausible for these systems, namely: (a) the relevant transitions  $q$  occur between an orbital (*nlms*) which is normally occupied in the atomic ground state and one ( $n'l'm's'$ ) which is normally unoccupied; (b) the transition operators  $a_q$  and their reciprocals  $a_{-q}$  can be treated as boson creation and annihilation operators, respectively, (to within the normalization constant  $t(q)$  introduced in our notation). Since the portions of  $H_1$  which contribute to the two equations (8.19) are proportional to  $a_{-q}$  and  $a_q$ , respectively, according to the RPA, the commutators  $[H_1, a_q]$  and  $[H_1, a_{-q}]$  can now be represented by a superposition of  $a_r$ , as desired. The coefficients of  $a_r$  and  $a_{-r}$  in this superposition are identical, as noted

below. Thereby (8.19) becomes

$$\begin{aligned} (E_{\mu'} - E_{\mu} - E_q) (\mu' | a_q | \mu) &= - \sum_r h_{qr} (\mu' | a_r + a_{-r} | \mu) \\ (E_{\mu'} - E_{\mu} + E_q) (\mu' | a_{-q} | \mu) &= \sum_r h_{qr} (\mu' | a_r + a_{-r} | \mu). \end{aligned} \quad (8.21)$$

The coefficients  $h_{qr}$  are suitably normalized matrix elements of  $H_1$ . Because the transitions  $q$  involve a change of parity and of one unit of angular momentum, while  $H_1$  is invariant as a whole, the transitions  $r$  must also involve a compensating change of parity and angular momentum. Therefore (8.21) constitutes a system of equations among matrix elements of a single class of transition operators. It also follows that the matrix elements  $h_{qr}$  coincide with the  $\mathcal{G}_1$  of (6.3) to within a proportionality factor. [More specifically, however,  $h_{qr}$  may be properly labeled as a  $\mathcal{G}_1$  when it multiplies  $a_q a_{-r}$  or  $a_{-q} a_r$  in the expansion of  $H_1$ , that is, when  $H_1$  replaces one excitation with another one, but no such label seems appropriate when it multiplies  $a_q a_r$  or  $a_{-q} a_{-r}$  in the creation or annihilation of a pair of excitations.]

The remaining problem of solving (8.21) would reduce exactly to the intrachannel problem of Sec. 6.2 if one were to disregard the matrix elements of  $a_{-q}$  and  $a_{-r}$  and to restrict the  $q$  and  $r$  to a single channel. The contribution of the matrix element of  $a_{-q}$  to the “exact” dipole matrix element (8.16) stems from improvements of the ground state wave function represented by virtual excitations which were ignored in Sec. 6. An indication of the relative magnitude of the matrix elements of  $a_{-q}$  and  $a_q$  is obtained by taking the ratio of the two equations (8.21), which gives

$$\frac{(\mu' | a_{-q} | \mu)}{(\mu' | a_q | \mu)} = \frac{E_{\mu'} - E_{\mu} - E_q}{E_{\mu'} - E_{\mu} + E_q}. \quad (8.22)$$

The denominator on the right is the sum of two non-negative terms,  $E_{\mu'} - E_{\mu}$  and  $E_q$ , and therefore non-negative whereas the numerator can be of either sign and is small whenever  $E_q$  lies close to  $E_{\mu'} - E_{\mu}$ . Therefore the ratio (8.22) has a small absolute value unless  $E_q$  is either much smaller or much larger than  $E_{\mu'} - E_{\mu}$ . The largest among the  $(\mu' | a_{-q} | \mu)$  will be *much smaller* than the largest  $(\mu' | a_q | \mu)$  unless the large  $(\mu' | a_q | \mu)$  occur for values of  $E_q / (E_{\mu'} - E_{\mu})$  much different from unity. This situation, which implies a very large effect of interactions, does occur for plasmas; it is uncertain whether it is ever significantly met for atoms.

Here we do not disregard  $a_{-q}$  but combine the two equations (8.22) into a single one for the variable  $(\mu' | a_q + a_{-q} | \mu)$  to be entered in (8.16). Straight-

forward algebra yields

$$\begin{aligned} & [(E_{\mu'} - E_{\mu})^2 - E_q^2] (\mu' | a_q + a_{-q} | \mu) \\ & = 2E_q \sum_r h_{qr} (\mu' | a_r + a_{-r} | \mu), \quad (8.23) \end{aligned}$$

which has the familiar form of the equation for the normal modes of classical coupled oscillators and for the corresponding frequencies,  $(E_{\mu'} - E_{\mu})$  in our case. Notice that it is no more difficult or laborious to solve (8.23) than the equations of the intrachannel problem of Sec. 6.2; therefore one might wish to solve it merely for heuristic purposes.

The differences between atoms and extended systems make a direct application of the RPA to atoms unrealistic. Therefore (AG64) started from a general formula equivalent to (8.19), introduced in its a complete expansion of  $H_1$  in terms of transition operators and proceeded to simplify the equations utilizing a sequence of assumptions appropriate to atoms. A main, realistic assumption was that virtual excitations in the exact ground state have a small probability amplitude whose square can be disregarded. The (AG64) treatment applies from the outset only to atoms with a complete outer subshell; its final step of simplification is further restricted to outer subshells with  $l=0$ , that is, to atoms of the alkaline earths. The role of this further restriction has not been clarified. Eventually the system (8.19) is reduced to a form that differs from (8.21) only by the substitution of a modified value  $E'_p$  in place of  $E_p$ . An equation analogous to (8.23) is then also obtained.

The quantitative applications carried out in (AG64) yielded results analogous to those obtained in Sec. 6.2 concerning the effect of intrachannel interaction on the Ar spectrum. The spectra of oscillator strength calculated by (AG64) are less sharply peaked at the first discrete excitation ("resonance line") than is predicted by the single-electron model of Sec. 4, and decay more gradually toward the deep minimum discussed in Sec. 4.5, which lies a little above the ionization threshold. However, even a comparatively minor shift of the gross spectral distribution near this minimum changes the strength of individual lines by large factors. Good agreement with experimental data was not obtained or expected, in view of various limitations of the treatment. It might be interesting to compare these results with those of an analogous calculation that takes into account the intrachannel interaction in the manner of Sec. 6.2 but disregards any improvement of the ground-state wave function.

In conclusion, calculations of oscillator strengths utilizing RPA-type formulations may well be of potential interest. The work done thus far has produced reasonable results, though not obviously superior to those obtained by the more straightforward approach of Sec. 6.2 or 8.3. Additional efforts will be required to

evaluate the relevant differences of the various approaches and to extend the applicability of (AG64), before the RPA can be established as a general method of atomic calculations.

## 9. UNSOLVED PROBLEMS

This concluding section has two related goals. It draws attention to some major outstanding problems and it attempts a summary assessment of the information surveyed in the whole article.

(a) The survey of the spectral distribution of oscillator strengths for neutral atoms, presented briefly in Sec. 4, is likely to prove a useful but hardly dependable guide for the semiquantitative prediction of absorption coefficients that have not yet been measured. No extensive attempt has been made to interpolate and extrapolate available data to other elements or other frequency ranges. A systematic attempt in this direction, coupled with experimental spotchecks, might provide a realistic assessment of present capabilities. The description and theoretical interpretation of major features of the spectra in Sec. 4 might prove to be reasonably complete and accurate, but additional unexpected features might also emerge from further experimental exploration. Notice that hardly any data exist for elements of groups IV-VII of the periodic system and very few for groups I-III except near threshold. Also the theoretical model of Sec. 4 is particularly inaccurate for predicting photoabsorption near the thresholds of successive shells and subshells.

(b) The survey performed in this article for neutral atoms might well be extended to ions, particularly by comparing the photoabsorption by neutral atoms and ions along each isoelectronic sequence. A substantial amount of data exists for discrete spectra but in the continuum only for  $H^-$ . The spectra should become progressively more hydrogenic with increasing degree of positive ionization. Preliminary steps have been taken recently in this direction (HR67, Wi68).

(c) A major shortcoming of theory is the lack of a consistent formula for the calculation of oscillator strengths by successive approximations, as discussed particularly in Sec. 5.4.

(d) As a corollary, no consistent method exists for determining theoretically the contribution of each subshell to the total integrated oscillator strength of each atom. Experimental determination of such contributions seems feasible (Sec. 3.5) but the necessary techniques are still in early development.

(e) The methods of theoretical analysis and improved calculation of oscillator strengths outlined in Secs. 6.2, 7.1, and 8 seem open to extensive application. However, present experience with these methods is quite limited and might prove misleading. Furthermore, this experience has been confined to situations with no more than two or three electrons (or vacancies) outside

closed shells. More complex situations would certainly require initial exploration.

(f) In particular, only a few steps have been taken in the experimental and theoretical studies of multiple excitations (Secs. 7.2 and 8.4), of the effects of spectral repulsion (Sec. 8.2) and of strong interchannel coupling (Sec. 8.3). The assessment of these effects in the present article is extremely tentative.

This list has excluded problems, such as the angular distribution of photoelectrons, which have been touched upon in Sec. 3.5 and occasionally in Secs. 7 and 8 and which are of importance to atomic mechanics but lie somewhat outside the main scope of the present article.

### ACKNOWLEDGMENT

This work has been helped greatly by countless, generous and informal contributions of information and unpublished data by so many colleagues in different countries that we can only thank them as a group.

### BIBLIOGRAPHY

- |       |   |        |  |
|-------|---|--------|--|
| ACS67 | M. Ya. Amusia, N. A. Cherepkov, and S. I. Sheftel, Phys. Letters <b>24A</b> , 541, (1967); also M. Ya. Amusia <i>Fifth International Conference on the Physics of Electronic and Atomic Collisions</i> (Nauka, Leningrad, USSR, 1967) Abstracts Volume, p. 90.                              | BJ67   | F. W. Byron and C. J. Joachain, Phys. Letters <b>24A</b> , 616 (1967); Phys. Rev. <b>164</b> , 1 (1967).   |
| AG64  | P. L. Altick and A. E. Glassgold, Phys. Rev. <b>133</b> , A632 (1964).  | BK67   | K. L. Bell and A. E. Kingston, Proc. Phys. Soc. (London) <b>90</b> , 31 (1967).  |
| Al68  | P. L. Altick, Phys. Rev. <b>169</b> , 21 (1968).  | BL63   | W. Brandt and S. Lundqvist, Phys. Rev. <b>132</b> , 2135 (1963).   |
| Am65  | M. Ya. Amusia, Phys. Letters <b>14</b> , 1, 36 (1965).  | BL65   | W. Brandt and S. Lundqvist, Arkiv Fysik <b>28</b> , 399 (1965).  |
| AM65  | P. L. Altick and E. N. Moore, Phys. Rev. Letters <b>15</b> , 100 (1965).  | BMcV65 | P. G. Burke and D. D. McVicar, Proc. Phys. Soc. (London) <b>86</b> , 989 (1965).   |
| AM66  | P. L. Altick and E. N. Moore, Phys. Rev. <b>147</b> , 59 (1966).  | BN67   | L. M. Biberman and G. E. Norman, Usp. Fiz. Nauk <b>91</b> , 193 (1967) [English transl.: Soviet Phys.—Usp. <b>10</b> , 52 (1967)].   |
| AP48  | A. Akhiezer and I. Pomeranchuk, J. Phys. (USSR) <b>11</b> , 167 (1948).   | Bo64   | A. E. Boyd, Planetary Space Sci. <b>12</b> , 729 (1964).   |
| Ba46  | D. R. Bates, Monthly Notices Roy. Astron. Soc. <b>106</b> , 432 (1946).   | Br58   | W. Brandt, Phys. Rev. <b>111</b> , 1042 (1958).  |
| Ba59  | A. I. Baz, Zh. Experim. i Teor. Fiz. <b>36</b> , 1762 (1959) [English transl.: Soviet Phys.—JETP <b>9</b> , 1256 (1959)].   | BRV61  | G. Balloufet, J. Romand, and B. Vodar, Compt. Rend. <b>252</b> , 4139 (1961).  |
| Ba59a | R. L. Barinskii, Izv. Akad. Nauk SSSR Ser. Fiz. <b>25</b> , 947 (1959) [English transl.: Bull. Acad. Sci. USSR, Phys. Ser. <b>25</b> , 958 (1961)]; see also R. L. Barinskii and V. I. Nefelov, <i>Rentgenospektralnoe Opredelenye Zaradiatomov v Molekulakh</i> (Izd. Nauka, Moscow 1966). | BS49   | D. R. Bates and M. J. Seaton, Monthly Notices Roy. Astron. Soc. <b>109</b> , 608 (1949).   |
| Ba64  | P. S. Bagus, Argonne National Lab Report No. ANL 6959 (1964).   | BS57   | H. A. Bethe and E. E. Salpeter, <i>Quantum Mechanics of One and Two-Electron Atoms</i> (Springer-Verlag, Berlin, 1957).  |
| BB67  | J. A. Bearden and A. F. Burr, Rev. Mod. Phys. <b>39</b> , 78 (1967).  | BS60   | A. Burgess and M. J. Seaton, Monthly Notices Roy. Astron. Soc. <b>120</b> , 121 (1960).  |
| BD49  | D. R. Bates and A. Damgaard, Phil. Trans. Roy. Soc. London <b>A242</b> , 101 (1949).  | BS67   | D. Bohm and B. Salt, Rev. Mod. Phys. <b>39</b> , 894 (1967).   |
| BD65  | R. J. Bell and A. Dalgarro, Proc. Phys. Soc. (London) <b>86</b> , 375 (1965).   | BTP67  | A. K. Bhatia, A. Temkin, and J. M. Perkins, Phys. Rev. <b>153</b> , 177 (1967).  |
| Be58  | A. J. Bearden, thesis, Johns Hopkins University, 1958 (unpublished).  | Bu65   | P. G. Burke, Advan. Phys. <b>14</b> , 521 (1965).  |
| Be64  | H. A. Bethe, <i>Intermediate Quantum Mechanics</i> (W. A. Benjamin, Inc., New York, 1964).  | BW63   | C. Bonnelle and F. Wuilleumier, Compt. Rend. <b>256</b> , 5106 (1963).   |
| Be65  | R. J. Bell, National Physical Laboratory (Teddington, England) Report Ma52 (Oct. 1965).   | Ca67   | T. A. Carlson, Phys. Rev. <b>156</b> , 142 (1967).   |
| Be66  | O. Bely, Proc. Phys. Soc. (London) <b>88</b> , 833 (1966).  | CE64   | J. F. Comes and A. Elzer, Z. Naturforsch <b>19a</b> , 721 (1964).  |
| BEL67 | W. Brandt, L. Eder, and S. Lundqvist, J. Quant. Spectry. and Radiative Transfer <b>7</b> , 185 (1967).  | CE67   | J. F. Comes and A. Elzer, Phys. Letters <b>25A</b> , 334 (1967).   |
| BET67 | J. Berkowitz, H. Ehrhardt, and T. Tekaat, Z. Physik <b>200</b> , 69 (1967).   | CF66   | H. D. Cohen and U. Fano, Phys. Rev. <b>150</b> , 30 (1966).  |
|       |   | CF67   | F. Combet-Farnoux, Compt. Rend. <b>264</b> , 1728 (1967).  |
|       |   | CF67a  | D. P. Chock and U. Fano, Informal Report entitled "An Analysis of Data on Double Transitions in He," Department of Physics, University of Chicago, Chicago, Ill. (unpublished).                          |
|       |   | CFH67  | F. Combet-Farnoux and Y. Heno, Compt. Rend. <b>264</b> , 138 (1967).   |
|       |   | CFP63  | J. W. Cooper, U. Fano, and F. Prats, Phys. Rev. Letters <b>10</b> , 518 (1963).  |
|       |   | Ch45   | S. Chandrasekhar, Astrophys. J. <b>102</b> , 223 (1945).   |
|       |   | CHH64  | L. R. Canfield, G. Hass, and W. R. Hunter, J. Physique <b>25</b> , 124 (1964).   |
|       |   | CHK66  | T. A. Carlson, W. E. Hunt, and M. O. Krause, Phys. Rev. <b>151</b> , 41 (1966).  |
|       |   | CHLT66 | P. K. Carroll, R. E. Huffman, J. C. Larrabee, and Y. Tanaka, Astrophys. J. <b>146</b> , 553 (1966).  |
|       |   | CK65   | T. Carlson and M. Krause, Phys. Rev. <b>140</b> , A1057 (1965).  |
|       |   | CLS67  | M. Connely, L. Lipsky, and K. Smith, <i>Proceedings of the Fifth International Conference on Electronic and Atomic Collisions</i> (Nauka, Leningrad, USSR, 1967) Abstracts Volume, p. 619.               |
|       |   | CM64   | K. Codling and R. P. Madden, Phys. Rev. Letters <b>12</b> , 106 (1964).  |
|       |   | CM65   | K. Codling and R. P. Madden, J. Appl. Phys. <b>36</b> , 380 (1965).  |
|       |   | CM65a  | K. Codling and R. P. Madden, Appl. Opt. <b>4</b> , 1431 (1965).  |
|       |   | CM68   | J. W. Cooper and S. T. Manson (to be published).   |
|       |   | CME67  | K. Codling, R. P. Madden, and D. L. Ederer, Phys. Rev. <b>155</b> , 26 (1967).   |
|       |   | CME68  | K. Codling, R. P. Madden, and D. L. Ederer (to be published).  |
|       |   | CMHA66 | K. Codling, R. P. Madden, W. R. Hunter, and D. W. Angel, J. Opt. Soc. Am. <b>56</b> , 189 (1966).  |
|       |   | Co61   | J. W. Cooper, <i>Proceedings of the Second International Conference on the Physics of Electronic and Atomic Collisions</i> , Boulder, Colorado, June, 1961 (W. A. Benjamin, Inc., New York, 1961), p. 7. |

- Co62 J. W. Cooper, Phys. Rev. **128**, 681 (1962).  
 Co64 J. W. Cooper, Phys. Rev. Letters **13**, 762 (1964).  
 CS35 E. U. Condon and G. Shortley, *The Theory of Atomic Spectra* (Cambridge University Press, London, 1935).  
 CS66 F. J. Comes and H. G. Salzer, Phys. Rev. **152**, 29 (1966).  
 CZ67 J. Cooper and R. N. Zare, Bull. Am. Phys. Soc. **12**, 1147 (1967).  
 Da60 A. Dalgarno, Proc. Phys. Soc. (London) **76**, 422 (1960).  
 De68 R. D. Deslattes (to be published).  
 Dc68a R. D. Deslattes, Phys. Rev. Letters **20**, 483 (1968).  
 DH60 R. W. Ditchburn and R. D. Hudson, Proc. Roy. Soc. (London) **A256**, 53 (1960).  
 DHS64 A. Dalgarno, R. J. W. Henry and A. L. Stewart, Planetary Space Sci. **12**, 235 (1964).  
 DJM53 R. W. Ditchburn, P. J. Jutsum, and G. V. Marr, Proc. Roy. Soc. (London) **A219**, 89 (1953).  
 DL57 A. Dalgarno and N. Lynn, Proc. Phys. Soc. (London) **A70**, 802 (1957).  
 DNST67 S. Dworetzky, R. Novick, W. W. Smith, and N. Tolk, Phys. Rev. Letters **18**, 939 (1967).  
 DS31 E. Desrhem and M. Schein, Phys. Rev. **37**, 1238 (1931).  
 DS60 A. Dalgarno and A. L. Stewart, Proc. Phys. Soc. (London) **A70**, 49 (1960).  
 Ed64 D. L. Ederer, Phys. Rev. Letters **13**, 760 (1964).  
 Ed67 D. L. Ederer (private communication).  
 ET64 D. L. Ederer and D. H. Tomboulian, Phys. Rev. **133**, A1525 (1964).  
 Fa60 U. Fano, Phys. Rev. **118**, 451 (1960).  
 Fa61 U. Fano, *Proceedings of the Second International Conference on the Physics of Electronic and Atomic Collisions, Boulder, Colorado, June, 1961* (W. A. Benjamin, Inc., New York, 1961), p. 10.  
 Fa61a U. Fano, Phys. Rev. **124**, 1866 (1961).  
 Fa63 U. Fano, Ann. Rev. Nucl. Sci. **13**, 1 (1963).  
 Fa64 U. Fano, in *Lectures on the Many-Body Problem*, E. R. Caianiello, Ed. (Academic Press Inc., New York, 1964).  
 Fa66 U. Fano, Science **153**, 522 (1966).  
 FC65 U. Fano and J. W. Cooper, Phys. Rev. **137**, A1364 (1965).  
 Fe28 E. Fermi, in *Quantentheorie und Chemie, Leipziger Vortraege*, H. Falkenhagen, Ed. (S. Hirzel-Verlag, Leipzig, 1928), p. 95; also in *Collected Papers of Enrico Fermi* (The University of Chicago Press, Chicago, Ill., 1962), p. 291.  
 Fe31 E. Fermi, Nuovo Cimento **8**, 7 (1931); also in *Collected Papers of Enrico Fermi* (The University of Chicago Press, Chicago, Ill., 1962), p. 379.  
 Fe51 R. P. Feynman, Phys. Rev. **84**, 108 (1951).  
 Fi31 A. N. Filippov, Z. Physik **69**, 526 (1931).  
 FMC26 P. D. Foote, F. Mohler, and R. L. Cherhault, Phys. Rev. **27**, 37 (1926).  
 FMcDV67 D. C. Frost, C. A. McDowell, and D. A. Vroom, Proc. Roy. Soc. (London) **A296**, 566 (1967).  
 FN59 L. Fonda and R. Newton, Ann. Phys. (U.S.) **7**, 133 (1959); also, R. Newton and L. Fonda, Ann. Phys. (U.S.) **9**, 416 (1960); L. Fonda, Nuovo Cimento Suppl. **20**, 116 (1961).  
 FN67 P. Feldman and R. Novick, Phys. Rev. **160**, 143 (1967).  
 Fo34 V. Fock, Z. Physik **89**, 744 (1934).  
 FP64 U. Fano and F. Prats, J. Natl. Acad. Sci. India **33**, Part IV, 553 (1964).  
 FZGZh67 V. A. Fomichev, T. M. Zimkina, S. A. Gribovskii, and I. I. Zhukova, Fiz. Tverd. Tela **9**, 1490 (1967) [English transl.: Soviet Phys.—Solid State **9**, 1163 (1967)].  
 Ga63 M. Gailitis, Zh. Eksperim. i. Teor. Fiz. **44**, 1974 (1963) [English transl.: Soviet Phys.—JETP **17**, 328 (1963)].  
 Ga66 W. R. S. Garton, Advan. Atomic Mol. Phys. **2**, 93 (1966).  
 Ga66a R. H. Garstang, Publ. Astron. Soc. Pacific **78**, 399 (1966).  
 GC60 W. R. S. Garton and K. Codling, Proc. Phys. Soc. (London) **75**, 87 (1960).  
 GJK66 L. C. Green, N. C. Johnston, and E. K. Kolchin, Astrophys. J. **144**, 369 (1966).  
 GM41 M. Goeppert-Mayer, Phys. Rev. **60**, 184 (1941).  
 Go29 W. Gordon, Ann. Phys. (Leipzig) **2**, 1031 (1929).  
 Gr64 H. R. Griem, *Plasma Spectroscopy* (McGraw-Hill Book Co., New York, 1964).  
 GVB65 R. H. Garstang and J. Van Blerkom, J. Opt. Soc. Am. **55**, 1054 (1965).  
 GW64 M. L. Goldberger and K. M. Watson, *Collision Theory* (John Wiley & Sons, Inc., New York, 1964).  
 Ha57 D. R. Hartree, *The Calculation of Atomic Structures* (John Wiley & Sons, Inc., New York 1957).  
 HAT65 W. R. Hunter, D. W. Angel, and R. Tousey, Appl. Opt. **4**, 891 (1965).  
 HB66 J. H. Hubbell and M. J. Berger, U.S. National Bureau of Standards Report 8681, 1966 (unpublished).  
 HC65 R. D. Hudson, Phys. Rev. **135**, A1212 (1964); R. D. Hudson and V. L. Carter, Phys. Rev. **137**, A1648 (1965); and **139**, A1426 (1965).  
 HC67 R. D. Hudson and V. L. Carter, J. Opt. Soc. Am. **57**, 651, 1471 (1967).  
 HC67a R. D. Hudson and V. L. Carter (private communication).  
 He66 R. J. W. Henry, J. Chem. Phys. **44**, 4357 (1966).  
 HJH67 G. Hass, G. F. Jacobus, and W. R. Hunter, J. Opt. Soc. Am. **57**, 758 (1967).  
 HK66 D. Haidt and H. Kleinpoppen, Z. Physik **146**, 72 (1966).  
 HK67 R. Haensel and C. Kunz, Z. Angew. Physik **23**, 276 (1967).  
 HKSS68 R. Haensel, C. Kunz, T. Sasaki, and B. Sonntag, Appl. Opt. **7**, 301 (1968).  
 HL67 R. J. W. Henry and L. Lipsky, Phys. Rev. **153**, 51 (1967).  
 HR67 R. Heffler and L. Rascon, J. Opt. Soc. Am. **57**, 964 (1967).  
 HS63 F. Herman and S. Skillman, *Atomic Structure Calculations* (Prentice-Hall, Inc., Englewood Cliffs, N. J., 1963).  
 Hu48 S. Huang, Astrophys. J. **108**, 54 (1948).  
 HW63 R. H. Hughes and L. D. Weaver, Phys. Rev. **132**, 710 (1963).  
 HY63 R. D. Hudson and P. A. Young, Sci. Rept. Space Tech. Lab. Rept. No. 9803-6004-RU000, 1963 (unpublished).  
 IKP67 M. Inokuti, Y. Kim, and R. L. Platzman, Phys. Rev. **164**, 55 (1967).  
 In67 M. Inokuti (private communication).  
 JM66 P. Jaegle and G. Missoni, Compt. Rend. **262**, 71 (1966).  
 JMD67 P. Jaegle, G. Missoni, and P. Dhez, Phys. Rev. Letters **18**, 887 (1967).  
 KC67 M. O. Krause and T. A. Carlson, Phys. Rev. **158**, 18 (1967).  
 Ke64 P. S. Kelly, J. Quant. Spectry. Radiative Transfer **4**, 117 (1964).  
 Ki63 C. Kittel, *Quantum Theory of Solids* (John Wiley & Sons, Inc., New York, 1963), p. 369.  
 Kn57 R. S. Knox, *Solid State Physics*, F. Seitz and D. Turnbull, Eds. (Academic Press, Inc. New York, 1957), Vol. 4, p. 413.  
 Kr68 M. O. Krause (to be published).  
 KS57 P. K. Kabir and E. E. Salpeter, Phys. Rev. **108**, 1256 (1957).  
 KS67 M. G. Koslov and G. P. Startsev, Opt. i Spektroskopija (USSR) **22**, 670 (1967) [English transl.: Opt. Spectr. (USSR) **22**, 366 (1967)].  
 Ku68 C. E. Kuyatt in *Methods of Experimental Physics*, L. L. Marton, Ed. (Academic Press Inc., New York, 1968), Vol. 7.  
 La30 R. Langer, Phys. Rev. **35**, 649 (1930).  
 LBG66 A. P. Lukirskii, I. A. Brytov, and S. A. Gribovskii, Opt. i Spektroskopija **20**, 368 (1966).  
 LBSK64 E. N. Lassettre, A. S. Berman, S. M. Silverman,

- and M. E. Krasnow, *J. Chem. Phys.* **40**, 1232 (1964).
- LBZ64** A. P. Lukirskii, I. A. Brytov, and T. M. Zimkina, *Opt. i Spektroskopiya* **17**, 438 (1964) [English transl.: *Opt. Spectry. (USSR)* **17**, 234 (1964)].
- LC67** L. Lipsky and J. W. Cooper, *Proceedings of the Fifth International Conference on Electronic and Atomic Collisions* (Nauka, Leningrad, USSR, 1967), Abstracts Volume, p. 126.
- LC68** L. Lipsky and J. W. Cooper (to be published).
- Le53** J. S. Levinger, *Phys. Rev.* **90**, 11 (1953).
- Le53a** M. N. Lewis, "Oscillator Strength of Ionizing Transitions; Data Calculated in the Hydrogen-Like Approximation," U.S. National Bureau of Standards Report No. 2457 (1953) (unpublished).
- Le60** J. S. Levinger, *Nuclear Photodisintegration* (Oxford University Press, Oxford, England, 1960).
- Li54** J. Lindhard, *Kgl. Danske Videnskab. Selskab, Mat. Fys. Medd.* **28**, 8 (1954).
- Li67** L. Lipsky, *Proceedings of Fifth International Conference on Electronic and Atomic Collisions* (Nauka, Leningrad, USSR, 1967), Abstracts Volume, p. 617.
- LKS64** E. N. Lassettre, M. E. Krasnow, and S. M. Silverman, *J. Chem. Phys.* **40**, 1242 (1964).
- LL65** E. T. P. Lee and C. C. Lin, *Phys. Rev.* **138**, A301 (1965).
- LNT65** M. Lipeles, R. Novick, and N. Tolk, *Phys. Rev. Letters* **15**, 815 (1965).
- LR66** R. Lipsky and A. Russek, *Phys. Rev.* **142**, 57 (1966).
- LRS60** A. P. Lukirskii, M. A. Rumsh, and L. A. Smirnov, *Opt. i Spektroskopiya* **11**, 505 (1960) [English transl.: *Opt. Spectry. (USSR)* **11**, 262 (1960)].
- LS53** J. Lindhard and M. Scharff, *Kgl. Danske Videnskab. Mat. Fys. Medd.* **27**, 15 (1953).
- LTE65** J. F. Lowry, D. H. Tomboulian, and D. E. Ederer, *Phys. Rev.* **137**, A1054 (1965).
- Lu61** A. P. Lukirskii, *Izv. Akad. Nauk SSSR, Ser. Fiz.* **25**, 913 (1961) [English transl.: *Bull. Acad. Sci. USSR, Phys. Ser.* **25**, 926 (1961)].
- Lu68** K. T. Lu, *Bull. Am. Phys. Soc.* **13**, 37 (1968).
- LZ63** A. P. Lukirskii and T. M. Zimkina, *Izv. Akad. Nauk SSSR, Ser. Fiz.* **27**, 327 and 817 (1963) [English transl.: *Bull. Acad. Sci. USSR, Phys. Ser.* **27**, 333 and 808 (1963)].
- LZB64** A. P. Lukirskii, T. M. Zimkina, and I. A. Brytov, *Izv. Akad. Nauk SSSR, Ser. Fiz.* **28**, 772 (1964) [English transl.: *Bull. Acad. Sci. USSR, Phys. Ser.* **28**, 681 (1965)].
- Ma54** G. V. Marr, *Proc. Roy. Soc. (London)* **A224**, 83 (1954).
- Ma66** J. H. Macek, *Phys. Rev.* **146**, 50 (1966).
- Ma67** J. H. Macek, *Phys. Rev.* **160**, 170 (1967).
- Ma67a** J. H. Macek, *Proc. Phys. Soc. (London)* **92**, 265 (1967).
- Ma67b** G. V. Marr, *Photoionization Processes in Gases* (Academic Press Inc., New York, 1967).
- MC63** R. P. Madden and K. Codling, *Phys. Rev. Letters* **10**, 516 (1963).
- MC64** R. P. Madden and K. Codling, *J. Opt. Soc. Am.* **54**, 268 (1964).
- MC65** R. P. Madden and K. Codling, *Astrophys. J.* **141**, 364 (1965).
- MC68** S. T. Manson and J. W. Cooper, *Phys. Rev.* **165**, 126 (1968).
- McC53** G. W. McClure, *Phys. Rev.* **90**, 796 (1953).
- McG59** R. T. McGinnies, Supplement to U.S. National Bureau of Standards Circular 583 (1959).
- McG67** E. J. McGuire, *Phys. Rev.* **161**, 51 (1967); also Ph.D. thesis, Cornell University, Ithaca, N.Y., 1965 (unpublished).
- MdH67** H. R. Moustafa and F. J. de Heer, *Physica* **36**, 646 (1967); H. R. Moustafa, Ph.D. thesis, Amsterdam, 1967 (unpublished).
- Me66** H. Mendowitz, *Astrophys. J.* **141**, 573 (1966).
- MEC67** R. P. Madden, D. L. Ederer, and K. Codling, *Appl. Opt.* **6**, 31 (1967).
- Mi41** A. Migdal, *J. Phys. (USSR)* **4**, 449 (1941).
- ML65** R. Migneron and J. S. Levinger, *Phys. Rev.* **139**, A646 (1965).
- Mo66** D. L. Moores, *Proc. Phys. Soc. (London)* **88**, 843 (1966).
- Mo67** D. L. Moores, *Proc. Phys. Soc. (London)* **91**, 830 (1967).
- MP57** W. F. Miller and R. L. Platzman, *Proc. Phys. Soc. (London)* **70**, 299 (1957).
- MS48** N. F. Mott and I. N. Sneddon, *Wave Mechanics and Its Applications* (Clarendon Press, Oxford, England, 1958), Sec. 32.2.
- Mu67** G. Musa, *Studii Cercetări Fiz.* **19**, 215 (1967).
- NHH62** R. G. Newburgh, L. Heroux, and H. E. Hinteregger, *Appl. Opt.* **1**, 733 (1962).
- NS62** R. W. Nicholls and A. L. Stewart, in *Atomic and Molecular Processes*, D. R. Bates, Ed. (Academic, Press Inc., New York, 1962).
- NTC66** C. W. Nestor, T. C. Tucker, T. A. Carlson, L. D. Roberts, F. B. Malik, and C. Froese, ORNL Report 4027, December 1966 (unpublished).
- OMG65** T. F. O'Malley and S. Geltman, *Phys. Rev.* **137**, A1344 (1965).
- Pe59** C. L. Pekeris, *Phys. Rev.* **115**, 1216 (1959).
- PL64** K. R. Piech and J. S. Levinger, *Phys. Rev.* **135**, A332 (1964).
- PS62** N. P. Penkin and L. N. Shabanova, *Opt. i Spektroskopiya* **12**, 3 (1962) [English transl.: *Opt. Spectry. (USSR)* **12**, 1 (1962)].
- Ra55** G. Racah, *Lunds Univ. Årsskr. Avd. 2* **50**, No. 21, 31 (1955).
- RF67** A. R. P. Rau and U. Fano, *Phys. Rev.* **162**, 68 (1967).
- RF68** MA. R. P. Rau and U. Fano, *Phys. Rev.* **167**, 7 (1968).
- Ri67** J. C. Rich, *Astrophys. J.* **148**, 275 (1967).
- Ro36** M. E. Rose, *Phys. Rev.* **49**, 727 (1936).
- Ro65** A. Ron, Ph.D. thesis, University of Jerusalem, 1965 (unpublished).
- RP68** F. F. Rieke and W. Pepreichal (to be published).
- Sa57** A. E. Sandstrom, *Encyclopedia of Physics*, S. Flügge, Ed. (Springer-Verlag, Berlin, 1957), Vol. 30, p. 205 ff.
- Sa64** J. A. R. Samson, *J. Opt. Soc. Am.* **54**, 6, 876 (1964).
- Sa66** J. A. R. Samson, *Advan. Atomic Mol. Phys.* **2**, 178 (1966).
- Sa66a** T. Sagawa *et al.*, *J. Phys. Soc. Japan* **21**, 2587, 2602 (1966).
- Sa67** J. A. R. Samson, *Proc. 16th Intern. Conf. on Mass Spectry.*, ASTM Committee E14 Denver, 1967 (unpublished).
- Sc61** C. Schwartz, *Phys. Rev.* **123**, 1700 (1961).
- Sc63** K. Schnopper, *Phys. Rev.* **131**, 2558 (1963) and Report No. 29, Material Science Center, Cornell University, Ithaca, New York (1962) (unpublished).
- Sc65** B. L. Schram, F. J. de Heer, M. J. van der Wiel, and J. Kistemaker, *Physica* **31**, 94 (1965); also, B. L. Schram, Ph.D. thesis, University of Leiden, 1965 (unpublished).
- Sc49** L. Schiff, *Quantum Mechanics* (McGraw-Hill Book Co., New York, 1949).
- SC65** J. A. R. Samson and R. B. Cairns, *J. Opt. Soc. Am.* **55**, 1035 (1965).
- Se51** M. J. Seaton, *Proc. Roy. Soc. (London)* **A208**, 418 (1951).
- Se53** M. J. Seaton, *Phil. Trans. Roy. Soc. (London)* **A245**, 469 (1953).
- Se58** M. J. Seaton, *Monthly Notices Roy. Astron. Soc.* **118**, 504 (1958).
- Se65** K. G. Sewell, *Phys. Rev.* **138**, A418 (1965).
- Se66** M. J. Seaton, *Proc. Phys. Soc. (London)* **88**, 801, 815 (1966).
- Se67** K. G. Sewell, *J. Opt. Soc. Am.* **57**, 1058 (1967).
- Sh67** B. W. Shore, *Rev. Mod. Phys.* **39**, 439 (1967); also, *J. Opt. Soc. Am.* **57**, 881 (1967).
- SHB67** K. Smith, R. J. W. Henry, and P. G. Burke, *Phys. Rev.* **157**, 51 (1967).
- Sl30** J. C. Slater, *Phys. Rev.* **36**, 57 (1930).

- Sl51 J. C. Slater, *Quantum Theory of Matter* (McGraw-Hill Book Co., New York, 1951).  
 Sl60 J. C. Slater, *Quantum Theory of Atomic Structure* (McGraw-Hill Book Co., New York, 1960).  
 Sl63 C. P. Slichter, *Principles of Magnetic Resonance* (Harper and Row Publishers, New York, 1963), Appendix B.  
 SL64 S. M. Silverman and E. N. Lassettre, *J. Chem. Phys.* **40**, 1265 (1964).  
 SL64a A. M. Skerbele and E. N. Lassettre, *J. Chem. Phys.* **40**, 1271 (1964).  
 Sm60 F. T. Smith, *Phys. Rev.* **118**, 349 (1960).  
 SP62 M. J. Seaton and G. Peach, *Proc. Phys. Soc. (London)* **79**, 1296 (1962).  
 SP64 B. Schiff and C. L. Pekeris, *Phys. Rev.* **134**, A638 (1964).  
 SP67 R. D. Schmickley and R. H. Pratt, *Phys. Rev.* **164**, 104 (1967).  
 St54 A. L. Stewart, *Proc. Phys. Soc. (London)* **A67**, 917 (1954).  
 StJL64 R. M. St. John and C. C. Lin, *J. Chem. Phys.* **41**, 195 (1964).  
 Su29 Y. Sugiura, *Sci. Papers Inst. Phys. Chem. Res. (Tokyo)* **11**, 1 (1929).  
 SW63 A. L. Stewart and T. G. Webb, *Proc. Phys. Soc. (London)* **82**, 532 (1963).  
 SZ62 E. E. Salpeter and M. H. Zaidi, *Phys. Rev.* **125**, 248 (1962).  
 Ta64 J. H. Tait, in *Atomic Collision Processes*, M. R. C. McDowell, Ed. (North-Holland Publ. Co., Amsterdam, 1964), p. 586.  
 TH56 D. H. Tomboulian and P. L. Hartman, *Phys. Rev.* **102**, 1423 (1956).  
 TJL58 Y. Tanaka, A. S. Jursa, and F. J. LeBlanc, *J. Opt. Soc. Am.* **48**, 304 (1958).  
 TL61 A. Temkin and J. Lamkin, *Phys. Rev.* **121**, 788 (1961).  
 TM66 D. W. Turner and D. P. May, *J. Chem. Phys.* **45**, 471 (1966).  
 To57 D. H. Tomboulian, *Encyclopedia of Physics*, S.
- To62 Flügge, Ed. (Springer-Verlag, Berlin, 1957), Vol. 30, p. 246.  
 To67 R. Tousey, *Appl. Opt.* **1**, 679 (1962).  
 TSDJ57 F. Tomkins (private communication).  
 Vi32 E. Trefftz, E. Schlueter, K. H. Dettman, and K. Z. Jorgens, *Astrophysik* **44**, 1 (1957).  
 Vi48 J. P. Vinti, *Phys. Rev.* **41**, 432 (1932).  
 Vi49 J. Victoreen, *J. Appl. Phys.* **19**, 855 (1948); **20**, 1141 (1949).  
 Wa65 T. Watanabe, *Phys. Rev.* **139**, A1747 (1965).  
 We63 A. W. Weiss, *Astrophys. J.* **138**, 1262 (1962).  
 We67 A. W. Weiss, *Phys. Rev.* **162**, 171 (1967).  
 We67a A. W. Weiss, *J. Res. Natl. Bur. Std.* **71A**, 163 (1967).  
 We67b A. W. Weiss, *J. Chem. Phys.* **47**, 353 (1967).  
 We68 A. W. Weiss (private communication).  
 WG55 R. W. Woodruff and M. P. Givens, *Phys. Rev.* **97**, 52 (1955).  
 WG57 G. White-Grodstein, "X-Ray Attenuation coefficients from 10 keV to 100 MeV," U.S. National Bureau of Standards Circular 583 (1957).  
 WHW67 M. J. Van der Wiel, F. J. de Heer, and G. Wiebes, *Phys. Letters* **24A**, 423 (1967).  
 Wi52 A. Winther, *Kgl. Danske Videnskab. Selskab, Mat. Fys. Medd.* **27**, 3 (1952).  
 Wi55 E. P. Wigner, *Phys. Rev.* **98**, 145 (1955).  
 Wi68 W. L. Wiese, in *Proceedings of the Beam-Foil Spectroscopy Conference*, University of Arizona, Tucson, Arizona, 20-22 November 1967 (to be published).  
 WSG66 W. L. Wiese, M. W. Smith, and B. M. Glennon *Atomic Transition Probabilities*, NSRDS-NBS 4 (U.S. National Bureau of Standards, Washington, D.C., 1966).  
 WWW55 W. Wainfan, W. C. Walker, and G. L. Weissler, *Phys. Rev.* **99**, 942 (1955).  
 Za67 R. N. Zare, *J. Chem. Phys.* **47**, 3561 (1967).  
 ZFGZh67 T. M. Zimkina, V. A. Fomichev, S. A. Gribovskii, and I. I. Zhukova, *Fiz. Tverd. Tela* **9**, 1447 (1967) [English transl.: Soviet Phys.—Solid State **9**, 1128 (1967)].